LBL-23665 c.2

Lawrence Berkeley Laboratory

UNIVERSITY OF CALIFORNIA

Materials & Chemical Sciences Division

JUL 31 1987

DOCUMENTS SECTION

ACID-BASE REACTIONS OF TRANSITION METAL ALLOYS: THERMOCHEMISTRY OF THE BASE-RICH END

J.H. Bularzik
(Ph.D. Thesis)

June 1987

TWO-WEEK LOAN COPY

This is a Library Circulating Copy which may be borrowed for two weeks.

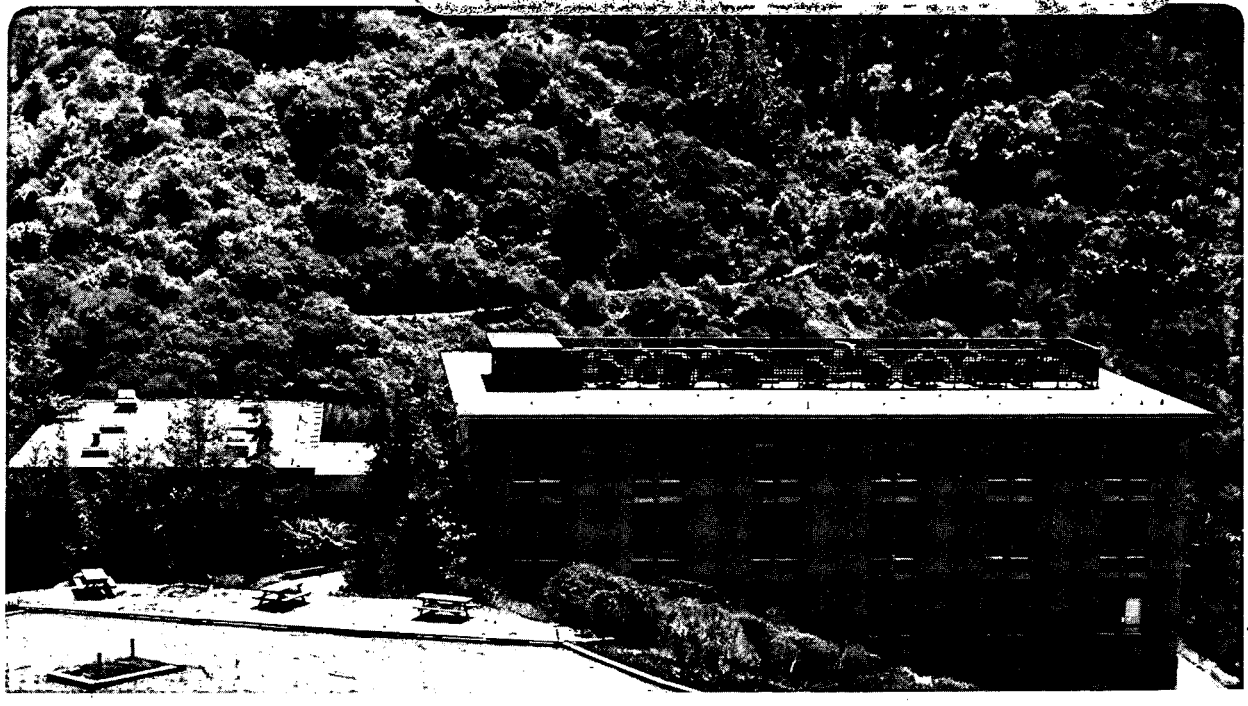

LBL-23665 c.2

Prepared for the U.S. Department of Energy under Contract DE-AC03-76SF00098

DISCLAIMER

This document was prepared as an account of work sponsored by the United States Government. While this document is believed to contain correct information, neither the United States Government nor any agency thereof, nor the Regents of the University of California, nor any of their employees, makes any warranty, express or implied, or assumes any legal responsibility for the accuracy, completeness, or usefulness of any information, apparatus, product, or process disclosed, or represents that its use would not infringe privately owned rights. Reference herein to any specific commercial product, process, or service by its trade name, trademark, manufacturer, or otherwise, does not necessarily constitute or imply its endorsement, recommendation, or favoring by the United States Government or any agency thereof, or the Regents of the University of California. The views and opinions of authors expressed herein do not necessarily state or reflect those of the United States Government or any agency thereof or the Regents of the University of California.

Acid-Base Reactions of Transition Metal Alloys:

Thermochemistry of the Base-Rich End

Joseph Henry Bularzik

Ph.D. Thesis

Lawrence Berkeley Laboratory
University of California
Berkeley, California 94720

June 1987

Acid-Base Reactions of Transition Metal Alloys: Thermochemistry of the Base-Rich End

Joseph Henry Bularzik

Abstract

The thermodynamics of binary transition metal alloys, stabilized by generalized Lewis acid-base reactions, were studied within the context of the Engel-Brewer Theory.

The activity of the base metals was determined from the vapor pressure measurements of the Pd or Rh in the base-rich end of TiPd, VPd, NbPd and VRh alloys. The vapor pressures were determined by thermally induced atomic emission spectroscopy. The composition of the alloys in equilibrium with carbon were determined. From the known thermodynamics of the metal carbides, the activity was calculated for the acid metals. Titration curves from the pure base metal to the compositions in equilibrium with carbon were developed.

The data confirmed the general qualitative properties of the acid-base reaction. The 4d metals are better acids than the 3d metals. The effectiveness of the acid-base reaction across a transition series is determined by the number of d electron pairs available for donation, the number of empty d orbitals available to accept electron pairs, the nuclear charge and a crystal field effect.

The data was compared to the regular solution model in an attempt to represent the solution behavior. More data is needed to determine the bonding behavior throughout the whole compositional range.

Because of the refractory properties of these alloys, the methods of thermodynamic investigation are limited and challenging. The data from this study is important to confirm the results of thermodynamic investigations of the Engel-Brewer alloys obtained by different techniques.

To Leonora

ACKNOWLEDGEMENT

I want to thank Dr. Leo Brewer for his guidance and friendship over these years. His ever-present optimism, enthusiasm for science and continual search for new ways to view a problem will always be remembered.

The opportunity given to me by the faculty members at Berkeley to see the state of the art in chemical research is greatly appreciated. I especially want to thank Dr. Sumner Davis for the loan of his equipment and the advice he willingly shared, and Dr. Samuel Markowitz who always gladly discussed the many aspects of my graduate school career.

The help of the many skilled people at both the Univ. of California Chemistry Department and the Materials and Molecular Research Division at Lawrence Berkeley Labs made my research possible. The discussions, encouragement and friendship of my co-workers, M. Cima, B. Ebbinghaus, E. Faizi, J. Gibson, J. Kouvetakis, K. Krushwitz and S. Leonard are greatly appreciated and helped make the time at Berkeley much more pleasant.

I thank my wife, Leonora, for all the love and help she has given me over these years, and for putting up with everything that a "graduate-student spouse" entails. And to Nicholas who has added joy and fun, especially on our days at "daddy's school".

Finally, I thank my loving parents who have given me more than I can ever thank them for.

This work was supported by the Director, Office of Energy Research, Office of Basic Energy Sciences, Materials Science Division of the U. S. Department of Energy under contract number DE-AC03-76SF00098.

TABLE OF CONTENTS

DEDICATION i

ACKNOWLEDGEMENT ii

I INTRODUCTION

A. Engel-Brewer Theory 1

B. Generalized Lewis Acid-Base Reaction 5

C. Literature Search 7

D. References 11

E. Tables and Figures 13

II THEORY

A. Vapor Pressure Measurements 18

B. Carbide Equilibration 24

C. References 26

D. Tables and Figures 27

III EXPERIMENTAL EQUIPMENT AND PROCEDURE

A. The King Furnace 32

B. The Optical Set-up 33

C. Temperature Measurements 37

D. Alloy Production 39

E. Alloy Analysis 40

F. Vapor Pressure Measurements 42

G. Carbide Equilibration 45

H. References 48

I. Tables and Figures 49

IV RESULTS

A. Melting Points 72

B. Vapor Pressure Measurements 77

C. Carbide Equilibration 82

D. Activity Measurements 83

E. A Solution Model 88

F. Discussion of Results 91

G. References 95

H. Tables and Figures 97

INTRODUCTION

Engel-Brewer Theory

Over fifty percent of the elements are classified as transition metals. These metals and their alloys are important in an industrialized technological society. The bonding within these alloys is not well understood, especially with the additional bonding contributions of d and f shell electrons. "Ab Initio" calculations have not as yet approached the sophistication to provide this information, and with so many alloy combinations, enough data can not be collected to yield a purely empirical model. A model with a theoretical chemical basis needs to be developed to understand the transition metal alloy behavior. The Engel-Brewer theory is a valence-bond approach to bonding in transition metals. This study concentrates on some extraordinary stability of transition metal alloys, as predicted by the Engel-Brewer theory.

The valence bond theory is an accepted way to look at bonding in non-metallic elements.[1] In the valence bond theory, the elements keep their atomic orbitals upon bonding. Unpaired electrons in the separate atoms form pairs with each other, which creates an electron pair bond. For example, Cl has the ground state valence electron configuration s^2p^5, and the bonding in Cl_2 is formed by the electron pair bond of the lone unpaired p electron of each Cl. Besides bonding of the unpaired

electrons in the ground state valence electron configuration, electrons may be promoted to make more electrons available for bonding. Carbon, with a ground state configuration s^2p^2 promotes one s electron to a p orbital. The promotion energy is more than compensated by the availability of four electons for bonding in the excited state, compared to two in the ground state.

The Engel-Brewer theory applies the valence bond approach to the transition metals.[2] From spectroscopic data, the ground state configurations and promotion energies to excited states are known.[3] Examination of the promotion energies to excited states, and their corresponding electron configurations in regards to the number of electrons made available for bonding determines the electron configuration of the condensed phases for the elemental metals.[4] A correlation, first noted by Engel, exists between the number of valence electrons and the crystal structure of metals.[5] Engel's correlation states that the body-centered cubic, hexagonal close-packed and face-centered cubic structures, respectively, correspond to the configurations $d^{n-1}s$, $d^{n-2}sp$, and $d^{n-3}sp^2$. The number of s and p electrons determine the structure, while the number of d bonds have a secondary effect by stabilizing the electron configuration. This is a reasonable assumption because s and p electrons extend over a long range while d electons are much more localized, having a less significant effect on the structure. The correlation has been refined to include the correct prediction for most of the structures of the binary intermetallic phases.[6] The configurational ranges of $d^{n-1}s$ to $d^{n-1.5}sp^{0.5}$, $d^{n-1.7}sp^{0.7}$ to $d^{n-2.1}sp^{1.1}$ and $d^{n-2.5}sp^{1.5}$ to $d^{n-3}sp^2$

correspond to bcc, hcp and fcc structures, respectively. The correspondance of the transition metals' crystal structures at their melting points with their electron distibution is shown in Figure 1-1.

The structure of metallic tungsten can be used as an example. The ground state of W gas is $5d^4 6s^2$, allowing for the bonding of only four electrons per atom. The promotion of one electron to $5d^5 6s^1$ allows for six electon pair bonds. The further promotion to $5d^4 6sp$ or $5d^3 6sp^2$ does not increase the number of bonding electrons, so does not further stabilize those corresponding structures. Therefore, the bcc structure of W, found at all temperatures, is correctly predicted.[7]

The valence states utilized in the Engel-Brewer theory are not single states. Even in gaseous atoms the states described by an electron configuration correspond to a band of energies resulting from the various combinations of spin and orbital angular momenta of the electrons. As long as the band maintains the essential characteristics of the atomic valence state, such as its d character or p character, it can well be described by that atomic valence state.

Electric and magnetic properties of metals rely on the density-of-states at the Fermi level. The understanding of these properties depend on the detailed knowledge of the density of states at various energy levels, so that a molecular orbital approach using an electron band model is necessary. Fortunately the bonding energy relies on the integration over all the occupied states within the band. Therefore, the valence bond approach described by the Engel-Brewer theory is useful

in understanding the structures and thermodynamic stabilities of the phases of metallic systems.[8]

The Engel-Brewer correlation has been used to estimate the bonding energies of the s, p and d orbitals. The experimental promotion energies and enthalpies of sublimation were used in a Born-Haber type calculation to determine the bonding energies. The bonding energies of the 5s and 5p electrons were determined from the known bonding energies of Sr and Cd, which have no d electron contribution. The bonding energies of the 5s and 5p electrons for the 4d metals were then estimated by assuming a non-linear yet smooth variation through the transition series. The bonding energy of the d orbitals was determined for each structure by subtracting the s and p contributions. The characteristic curve is shown in Figure 1-2. The curve can be used to predict the bonding in yet unobserved phases of a metal with either the hcp or bcc structure.[8]

The average d electron bonding energy decreases with an increase of the number of d electrons, up to five, then increases again as the d orbitals are further filled. The decrease is due to the interference between the d bonds as the number of bonds increase. The average bonding energy is also decreased due to a crystal field effect. In a non-spherically symmetric field, the d orbitals split in energy, with the higher energy orbitals more extended in space. At the start of the transition series the d electrons will go into the orbitals most extended in space, and with the highest bonding energy. The next electrons fill orbitals with lower bonding energies. Past five

electrons, where some of the electrons are internally paired, the number of d bonds decreases while the average energy increases. The paired electrons will occupy the most contracted orbitals, increasing the average bonding energy of the remaining orbitals.

Generalized Lewis Acid-Base Reaction

An additional interaction should be considered when describing the bonding in binary alloys of an early and late transition metal. Extraordinary thermodynamic stability has been observed for many of these alloys.[9] Within the context of the Engel-Brewer theory, these results have been explained by a generalized Lewis acid-base reaction between the metals.

The Lewis acid definition is an accepted way to view an acid-base reaction.[10] The defined characteristics of an acid and base are, respectively, the ability to accept and donate an electron pair during bond formation. An example is the reaction between ammonia, a base, and boron trifluoride, an acid. Upon bonding, an unshared pair of electrons of the ammonia is accepted by an empty orbital of the boron to form a covalent bond. This reaction is illustrated below.

The Lewis definition can be applied to the bond formation in transition metal alloys. The reaction of Pd with Zr, shown in Figure 1-3, is given as an example. Zr has a $5s^1 4d^3$ electron configuration in the solid state corresponding to the bcc structure. One s electron and three unpaired d electrons are available for bonding. The Pd has a $5s^1 5p^2 4d^7$ electron configuration in the solid state corresponding to the fcc structure. For Pd only the three s and p and three d electrons are available for bonding because the other d electrons are internally paired. The bonding between the Zr and Pd, such as in a ZrPd alloy, consists of two s and p electrons and three d electrons on average per atom. A total of ten electrons are used in bonding in a ZrPd alloy pair.

If an acid-base reaction occurs between metals, the bonding will change. Two pairs of d electrons of the Pd are donated to the Zr empty d orbitals. The excess stability of these alloys can be seen by an increase in the number of electrons forming bonds. After the acid-base reaction, the ZrPd alloy has two s and p electrons per atom bonding, which is the same in the alloy when no acid-base reaction occurs. The number of d electrons forming bonds increases to five per atom on average, counting the donated Pd electrons. A total of fourteen electrons are used in bonding in a ZrPd pair that has undergone a Lewis acid-base reaction. The donation of the electron pairs to form bonds is not meant to suggest a large negative formal charge on the acidic metal. Within the context of a Lewis acid definition, no ions are ever formed. The excess electron density on the acidic metal can be compensated by back-bonding, a mechanism observed in the bonding of

electron donating ligands with transition metals.[11]

Many unanswered questions remain before this interaction is understood well enough to derive a theory to quantitatively predict the thermodynamic properties in the various alloys. What is the energy contribution of the acid-base bonds compared to the bonding of the unpaired electrons? What are the major factors determining the differences among these donated bonds: energy levels, number of possible donating pairs, number of empty accepting orbitals, atomic number and shielding effects of other electrons, or even a crystal field effect?

Literature Search

There is not much literature information. The present data contributes to qualitatively determine the important aspects of the thermodynamics of transition metal acid-base reactions. Gibson gives a good review over most of the available literature.[12]

The qualitative trends across a transition series have been investigated. Wengert has shown with various Zr alloys that the platinum group metals are the most effective bases. Figure 1-4 shows the excess partial Gibbs free energy at infinite dilution of Zr with a range of base metals, depicting the maximum stability occuring with the platinum metals.[13]

Cima[14] compared the effectiveness of Pd and Rh as bases with Nb by electrochemical cell measurements. The activity of Nb is lower in the

Pd base-rich alloy due to the presence of the extra pair of d electrons of Pd. This orbital's enhanced basicity is attributed to crystal field splitting. The crystal field effect splits the degenerate d orbitals. The second set of paired d electrons of the Pd is in a more extended orbital than its first set of paired d electrons or the only pair of d electrons of the Rh. The further extension makes the Pd electron pair more available for donation, increasing the basicity of Pd over Rh. At higher acid concentration the Nb activity was lower in the Rh alloy. The greater nuclear charge on the Pd contracts its orbitals more than those of Rh. The further extension of the pair of d electrons of the Rh enhances its effectiveness in acid-base bonding as compared to the most contracted pair of the Pd. The competing effects of crystal field splitting and nuclear charge are demonstrated by the crossing of the activity of Nb with various concentrations of Pd and Rh.

Qualitative trends have also been determined going down an elemental family. The interaction becomes greater as the energy level of the electrons increase from the 3d to 5d level. Table 1-1 shows comparisons of the activities of some alloys within the same families. The 5d alloys consistantly demonstrate equal or higher stability than the 4d or 3d alloys. This result is explained by the difference in the real space extension of the orbitals. The 5d orbitals extend further out from the closed shell than 4d orbitals and thus allow for greater overlap to form more stable bonds. Additionally, the 3d orbitals are so contracted, illustrated by the 3d metals' magnetic properties, that they do not undergo significant acid-base reaction.

Some of the alloys of Ti, V, and Nb with Pd and Rh are investigated in this study. Besides the work already cited by Cima and Gibson, Choudary et al. have investigated the thermodynamics of TiPd alloys by Knudson cell vapor pressure measurements using a mass spectrometer.[17] This work will be compared to the present study later in the discussion section.

Kleppa has recently developed a new experimental method, high temperature mixing calorimetry, suitable for thermochemical studies of many refractories, originally used to determine enthalpies of formation of transition metal borides and silicides.[18] The method is also applicable to highly refractory metal alloys. The heat of formation of the stoichiometric intermetallic compounds of Ti, Zr and Hf with Pd and Rh have given further insight into the bonding relationships of these alloys. The equiatomic Rh compounds have a larger negative enthalpy of formation than the Pd compounds. In both families there are increasing negative enthalpies of formation in the sequence TiX < ZrX < HfX.[19]

X-ray photoemission spectroscopy may be another way to probe the bonding in these alloys. Many of the transition metals,[20] their carbides[21] and intermetallic compounds[22,23] have been investigated. In $YbPd_x$, alloys with possible acid-base interactions, a strong band narrowing is observed with decreasing Pd content, leading to a large reduction in the bandwidth compared to pure Pd metal.[24] Band narrowing justifies a more atomic-like description of the bonding within these alloys.

Theoretical linear-combination-of-atomic-orbital calculations have been performed for the YPd molecule.[25] The calculations attributed the chemical bonds to donation of charge from the filled $d\sigma$ and $d\Pi$ orbitals of the Pd atom into the empty or partly filled $d\sigma$ and $s\Pi$ orbitals of the Y atom, and a back-donation of charge from the filled 5s orbital of the Y atom into the empty 5s orbital of the Pd atom. This bonding description is the same accorded to the generalized Lewis acid-base reaction.

Because of the refractory properties of the Engel-Brewer alloys, the methods of thermodynamic investigation are limited and challenging. Special calorimetric techniques are needed because of the difficulty in burning or dissolving the alloys. The oxide and carbide equilibrations are difficult because of the long equilibration time and the limit of possible data points. Emf measurements, which give the most precise information, often have systematic errors. The thermodynamics should be investigated by several methods to insure the accuracy of the data.

Information on the thermodynamics of extraordinary stable alloys by vapor pressure measurements and carbide equilibration methods will be determined in this study. With more data, hopefully, the bonding mechanism will be clarified and a theory formulated to predict the thermodynamics of other acid-base reactions.

References

1 Huheey J., "Inorganic Chemistry", ed. 2, 112, Harper and Row, NY (1978)

Coulson, C. A., "Valence", ed. 2, Oxford Univ. Press, Oxford (1963)

2 Brewer, L., J. Mat. Ed., 6, (5), 733 (1984)

3 Moore, C. E., "Atomic Energy Levels", [Government Printing Office, Washington, D.C. Vol. 1 (1949), Vol. 2 (1952), Vol. 3 (1958)]

4 Brewer, L., In "Phase Stability in Metals and Alloys", (Rudman, P., Stringer, J., and Jaffee, R. I., eds.), 39, McGraw-Hill, NY (1967)

5 Engels, N., Ingenioeren, N101 (1939), M1 (1940); Acta Met., 15, 557 (1967)

6 Brewer, L., Acta Met., 15, 553 (1967)

7 Donohue, J., "The Structures of the Elements", 187, John Wiley & Sons, NY (1974)

8 Brewer, L., Science, 161, (3837), 115 (1968)

9 Brewer, L. and Wengert, P., Met. Trans., 4, 83 (1973)

10 Douglas B. and McDaniel D., "Concepts and Models of Inorganic Chemistry", 211, Blaisdell Pub. Co., NY (1965)

11 Pauling, L., Proc. Natl. Acad. Sci. U. S., 36, 533 (1950)

12 Gibson, J., Ph.D. Thesis, Univ. of Cal., Berkeley (1983)

13 Wengert, P., Ph.D. Thesis, Univ. of Cal., Berkeley (1969)

14 Cima, M., Ph.D. Thesis, Univ. of Cal., Berkeley (1986)

15 Meschter, P. J. and Worrell, W. L., Met. Trans. A, 7A, 299 (1976)

16 Meschter, P. J. and Worrell, W. L., Met. Trans. A, 8A, 503 (1977)

17 Choudary, U. V., et al., Met. Trans. A, 8A, 1487 (1977)

18 Topor, L. and Kleppa, O. J., J. Chem Therm., 16, 993 (1984); Met. Trans., 17, 1217 (1986)

19 Topor, L. and Kleppa, O. J., Z. Metalk., 77, (10), 633 (1986); J. Less Com. Metals, (in Press); Met. Trans., (in Press)

20 Smith, N. et al., Phys. Rev. B, 10, (8), 3197 (1974)

21 Silberbach, H. and Merz, H., Z. Phys. B, 59, 143 (1985)

22 Hedman, J. et al., Phys. Scripta, 4, 195 (1971)

23 Lapka, R. et al., Phys. Rev. B, 31, (12), 7734 (1985)

24 Donke, M. et al., Phys. Rev. B, 32, (12), 8002 (1985)

25 Shim, J. and Gingerich, A., Chem Phys. Let., 101, (6), 528 (1983)

TABLE 1-1

The variation of the strength of a base within a family of compounds

Alloy	d Levels	T (K)	Base Activity	Reference
TiPt (20%Ti)	3 - 5	1300	$\alpha_{Pt} = 2.6 \times 10^{-12}$	15
ZrPt (23%Zr)	4 - 5	1300	$\alpha_{Pt} = 6.5 \times 10^{-16}$	16
HfPt (23%Hf)	5 - 5	1300	$\alpha_{Pt} = 7.9 \times 10^{-17}$	16
$TiPd_3$	3 - 4	1873	$\alpha_{Pd} = 1.9 \times 10^{-1}$	17
$ZrPd_3$	4 - 4	1955	$\alpha_{Pd} = 3.0 \times 10^{-2}$	12
$HfPd_3$	5 - 4	1955	$\alpha_{Pd} = 3.0 \times 10^{-2}$	12
$NbPd_3$	4 - 4	1761	$\alpha_{Pd} = 1.0 \times 10^{-1}$	12
$TaPd_3$	5 - 4	1808	$\alpha_{Pd} = 4.0 \times 10^{-2}$	12

Sc $3d^2$ $4s^1$ bcc	Ti $3d^3$ $4s^1$ bcc	V $3d^4$ $4s^1$ bcc	Cr $3d^5$ $4s^1$ bcc	Mn $3d^6$ $4s^1$ bcc	Fe $3d^7$ $4s^1$ bcc	Co $3d^6$ $4s^1 4p^2$ fcc	Ni $3d^7$ $4s^1 4p^2$ fcc	Cu $3d^8$ $4s^1 4p^2$ fcc
Y $4d^2$ $5s^1$ bcc	Zr $4d^3$ $5s^1$ bcc	Nb $4d^4$ $5s^1$ bcc	Mo $4d^5$ $5s^1$ bcc	Tc $4d^5$ $5s^1 5p^1$ hcp	Ru $4d^6$ $5s^1 5p^1$ hcp	Rh $4d^6$ $5s^1 5p^2$ fcc	Pd $4d^7$ $5s^1 5p^2$ fcc	Ag $4d^8$ $5s^1 5p^2$ fcc
La $5d^2$ $6s^1$ bcc	Hf $5d^3$ $6s^1$ bcc	Ta $5d^4$ $6s^1$ bcc	W $5d^5$ $6s^1$ bcc	Re $5d^5$ $6s^1 6p^1$ hcp	Os $5d^6$ $6s^1 6p^1$ hcp	Ir $5d^6$ $6s^1 6p^2$ fcc	Pt $5d^7$ $6s^1 6p^2$ fcc	Au $5d^8$ $6s^1 6p^2$ fcc

Figure 1-1

The transition metals are shown along with their electron configurations and corresponding structures near their melting points.

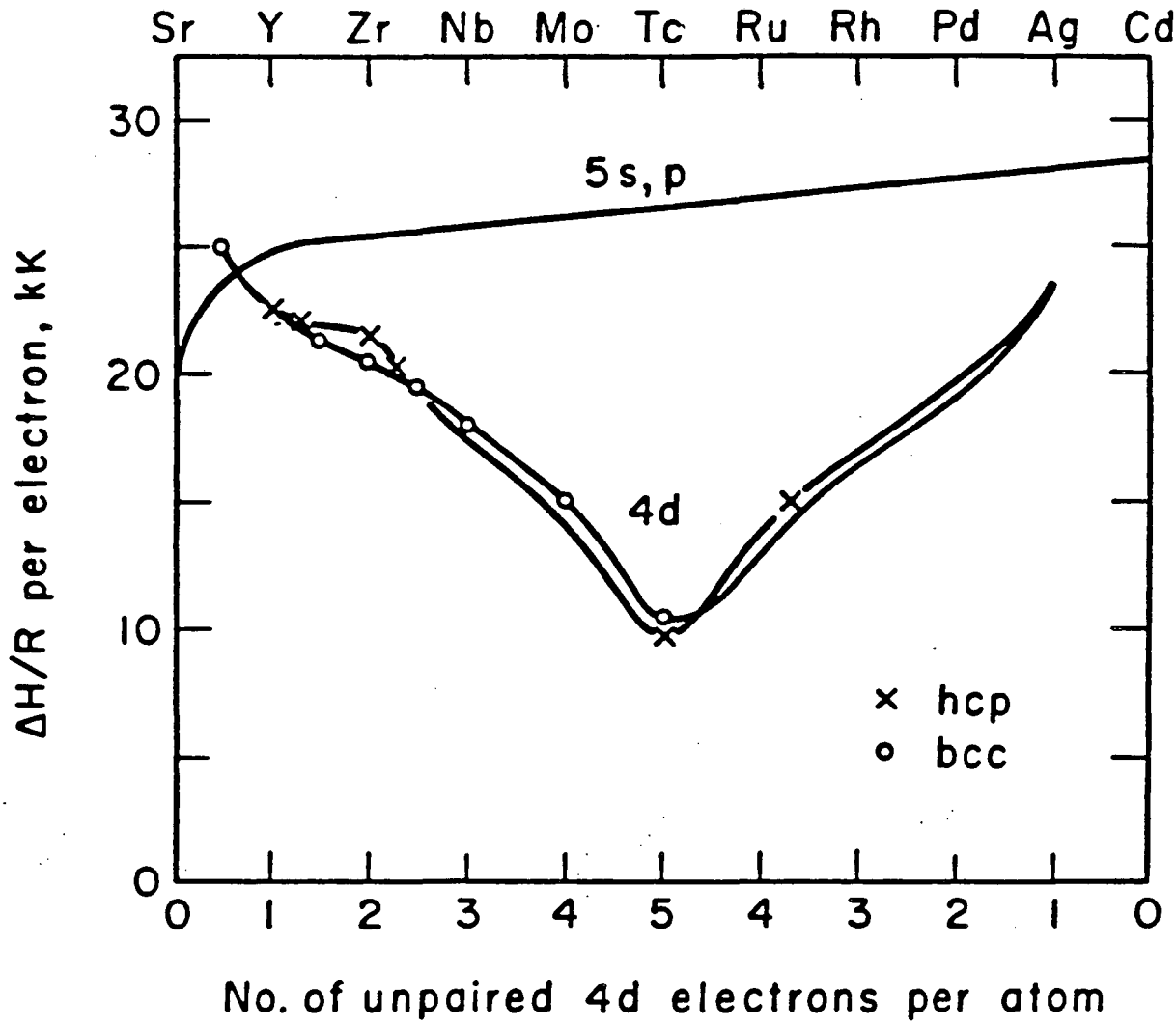

Figure 1-2

The top curve shows the bonding energy in kilokelvin per mole per electron of the 5s and 5p electrons for the elements in the 4d row. The lower curve shows the average energy due to bonding of the 4d electrons for the elements in the 4d row also as a function of the number of unpaired d electrons. This diagram was provided by L. Brewer

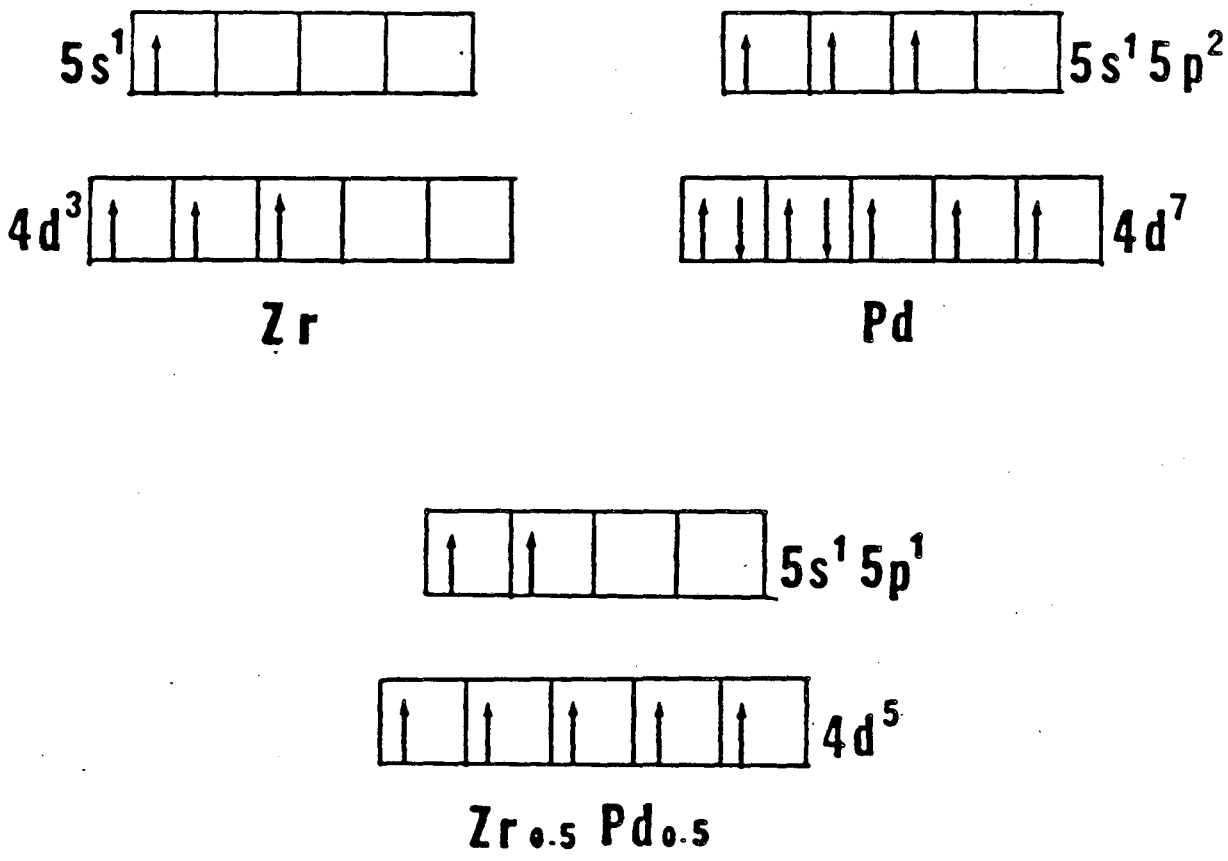

Figure 1-3

Representations of the electron configurations of Zr, Pd and the average configuration of an atom in the ZrPd alloy are shown. On each atom the upper four boxes represent one 5s and three 5p orbitals, and the lower boxes represent five 4d orbitals. Electrons are shown as arrows with their relative spins depicted by the arrow's direction.

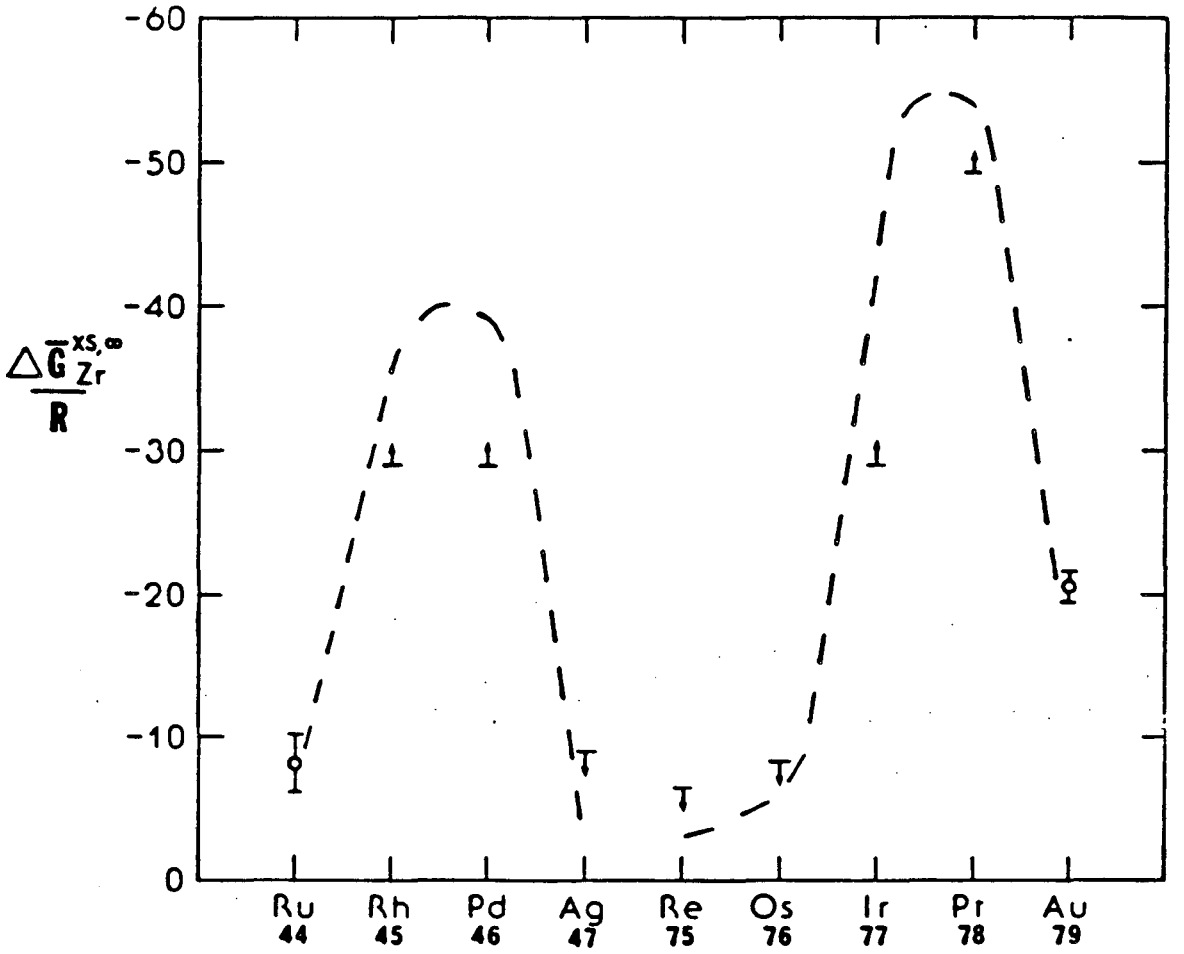

Figure 1-4

A lower limit of the excess partial molar free energy in kilokelvin per gm-atom of Zr at infinite dilution with the basic 4d and 5d transition metals are shown at 1800 K. This diagram was provided by L. Brewer.

THEORY

Vapor Pressure Measurements

This investigation of the thermodymanics of generalized Lewis acid-base transition metal alloys mainly consists of vapor pressure measurements. The vapor pressures of the base components of the binary alloys have been determined by thermally induced emission spectroscopy. The vapor pressure measurements were performed in a King furnace, a closed system with a constant temperature region, to allow for the equilibration of a condensed alloy with its vapor. The ratio of the partial pressure over the alloy compared with the vapor pressure over the pure element gives the activity of that component in the alloy, thus providing a measurement of their relative bonding.

The chemical potential of a species A is identical in all phases that are in equilibrium.

$$\mu_A \text{ (phase I)} = \mu_A \text{ (phase II)} \qquad (2\text{-}1)$$

This relationship allows for the measurement of the chemical potential of species A in a condensed phase by measuring the chemical potential in its equilibrated gaseous phase. The chemical potential of a gas is related to its fugacity and can be well approximated by its partial pressure at low pressures.

$$\mu_{A(gas)} = RT \ln f_A \cong RT \ln P_A \qquad (2\text{-}2)$$

The difference in chemical potentials in two phases is calculated by the ratio of the partial pressures of component A in an alloy over its standard state phase.

$$\mu_A^{alloy} - \mu_A^{o} = RT \ln (f_A^{alloy} / f_A^{o}) \simeq RT \ln (P_A^{alloy} / P_A^{o}) \qquad (2\text{-}3)$$

μ = chemical potential

R = gas constant

T = Temperature (K)

f = fugacity

P = partial pressure

The activity (α) of the component is calculated from the difference of the chemical potentials.

$$RT \ln \alpha_A = \mu_A^{alloy} - \mu_A^{o} \qquad (2\text{-}4)$$

A simpler calculation of the activity, assuming the gas behaves as a perfect gas, is from the ratio of partial pressures.

$$\alpha_A \simeq P_A^{alloy} / P_A^{o} \qquad (2\text{-}5)$$

The standard state chosen for this study is Raoult Law standard state where P^{o}_A is the partial pressure of A in equilibrium with the pure condensed phase A.[1]

The partial pressures were measured by thermally induced emission spectroscopy. The intensity (I) of the recorded spectra in mV is determined by the number of photons hitting the photomultiplier, proportional to the number (n_i) of atoms in the excited state emitting at the recording wavelength.

$$I \propto n_i \qquad (2\text{-}6)$$

Several factors prevented the measurement of the absolute vapor pressure, limiting the measurements to relative pressures. The measured pressure is dependent on the geometry of the optical system and length of the emitting vapors. These factors were kept constant, but were not exactly known. The intensity is also dependent on other factors such as the oscillator strength of the emission lines.[2] The Einstein - Boltzmann equation for the intensity of a spectral line can be written in the following form.

$$I = \frac{N\, 8\pi^2\, e^2\, h\, g\, f}{Q\, M\, \lambda^3}\, e^{-(\varepsilon/KT)} \qquad (2\text{-}7)$$

N = particle density

Q = partition function

h = Planck's constant

K = Boltzmann's constant

g = statistical weight of upper state

e/m = specific charge of the electron

λ = wavelength of the spectral line

f = oscillator strength

The oscillator strengths of the Pd emission lines are not well known, with only one source for many of the Pd oscillator strengths.[2] Other studies have determined different oscillator strengths for some of the Pd transitions,[3] and the main study has been shown to give erroneous values for other elements.[4] Yet because the activity is a ratio of the partial pressures, as long as both the alloy and pure element are measured under the same conditions, relative pressures will yield information as useful as absolute pressures.

The emission line intensity gives the relative number of atoms emitting from the excited state corresponding to that wavelength. The total population, which varies from the individual state populations at different temperatures is needed, not just the population of one state. The corresponding total number of atoms (N) can be found from the population of one state by the use of the partition function (Q) and the Boltzmann principle.[5]

$$N = \frac{n_i \; Q}{g_i \; e^{(\varepsilon_i/KT)}} \qquad (2\text{-}8)$$

where

$$Q = \sum_i g_i \; e^{(\varepsilon_i \; / \; KT)} \qquad (2\text{-}9)$$

N = total population

i = number of the state

n_i = population of the state i

g_i = number of quantum states of equal energy

$g = (2J + 1)$

ε_i = energy level of state i

The spectral data of Pd up to the energy of 3000 cm^{-1} is given in Table 2-1.[6] The contribution to the partition function of each energy level is shown in Table 2-2. The values are tabulated from 1900 K to 2500 K in 100 degree intervals, covering the useful temperature range of this study. Table 2-2 indicates that the contribution of all the levels above 11721.7 cm^{-1} are insignificant for this temperature range. The partition function can then be calculated over the limited sum of levels from 11721.7 cm^{-1} down to the ground state. To obtain the partition function for any temperature in this range the values were fit with a quadratic equation.

$$Q = 1.343 - 4.701 \times 10^{-4}\, T + 1.702 \times 10^{-7}\, T^2 \qquad (2\text{-}10)$$

Both the calculated and fitted values are shown in Table 2-3

With the value of the partition function the relative gas population can be found from the population of one state. Assuming at the experimental pressures that the metallic vapors act like an ideal gas, relative pressures are found using the ideal gas law.

$$P \propto N\, T \qquad (2\text{-}11)$$

Substituting equation (2-6) into (2-8) and then into equation (2-11), the relationship of the measured intensity to the relative pressure is found.

$$P \propto \frac{I \; Q \; T}{g_i \; e^{(\varepsilon_i / KT)}} \qquad (2\text{-}12)$$

The partial pressure measurements are the basis of the thermodynamic values, giving the activity of the alloys. Since each experiment is not run at the same temperature but within a range, the Clausius Clapeyron equation.[7]

$$\frac{dP}{dT} = \frac{\Delta H}{T \Delta V} \qquad (2\text{-}13)$$

is used. Assuming the enthalpy does not vary with temperature over a small temperature range, the equation can be written as a linear relation.

$$\log P = \text{Constant} - \frac{\Delta H}{RT} \qquad (2\text{-}14)$$

Plotting log P versus 1/T gives a straight line with the slope equal to the enthalpy of vaporization. The difference between the line for the log of the pressure over the elemental metal compared to the line for the pressure over the alloy directly gives the log of the activity of that compound in the alloy. This relationship can be seen by taking the log of equation (2-5).

$$\log \alpha_A = \log P_A^{alloy} - \text{Log } P_A^{o} \qquad (2\text{-}15)$$

Carbide Equilibration

Another method of investigation used to calculate the activity of the metals within highly stable binary alloys is carbide equilibration. This method consists of equilibrating an alloy with graphite to form a carbide phase with one of the metals.

The Phase Rule[8] states that with three components at a fixed temperature and pressure, three phases of fixed composition can be in equilibrium. By use of equation (2-1) the chemical potential of a component in any phase is identical to the chemical potential of that component in any other phase. Because of the relationship between the chemical potential and the activity, as shown in equation (2-4), the activity of any component is also equal in all equilibrated phases. Therefore, the activity in the alloy can be found by calculating the activity of that metal in the carbide phase.

$$\alpha_A^{carbide} = \alpha_A^{alloy} \qquad (2\text{-}16)$$

The equilibration of a TiPd alloy with carbon is used as an example. A representative ternary phase diagram, Figure 2-1, shows the relationship among Ti, Pd and C at 2100 K. The complete solution between the molten metals Ti and Pd is indicated along the binary edge, also the stable TiC phase is shown. No stable phases occur along the C - Pd binary. The ternary tie lines outline a possible ternary phase region of C, TiC and a soluton of Ti and Pd with a composition X.

From equation (2-16) the activity of Ti in the TiPd alloy of composition X is equal to the activity of the Ti in TiC at 2100 K. For the formation of TiC:

$$Ti + C = TiC \qquad (2\text{-}17)$$

the Gibbs free energy of formation is:

$$\Delta G_f^0 \ (TiC) = - R\ T \ln (\alpha_{TiC}\ \alpha_C^{-1}\ \alpha_{Ti}^{-1}) \qquad (2\text{-}18)$$

Both the pure C and TiC are present in equilibrium with the alloy of composition X, defining their activities as essentially unity. The activity of the Ti in the carbide phase is directly found from the energy of formation of the carbide

$$\alpha_{Ti} = e^{\left(\frac{\Delta G_F^{\circ}\ (TiC)}{R\ \ T}\right)} \qquad (2\text{-}19)$$

The literature values for the $\Delta G^{\circ}{}_f$ for the carbides of V, Ti and Nb are given in Table 2-4, along with references.

References

1 Raoult, F. M., Compt. rend., 104, 1430 (1887); Z. Physik. Chem., 2, 353 (1888)

2 Coliss, C. and Bozman, W., NBS Monograph, #53 (1963)

3 Lawrence, G. et al., Astrophys. J., 141, 293 (1965)

4 Bremont, E. et al., Astron. Astrophys., 108, 127 (1982)

5 Pitzer K. S. and Brewer, L., "Thermodynamics", 422, McGraw-Hill, NY (1961)

6 Moore, C. E., "Atomic Energy Levels", [Government Printing Office, Washington, D.C., Vol. 3 (1958)]

7 Clapeyron, E., J. ecole polytech (Paris), 14, (23), 153 (1834)

8 Gibbs, J. W., Trans. Conn. Acad. Sci., 3, 228 (1876)

9 "JANAF Thermochemical Data", compiled and calculated by The Dow Chemical Company, Midland, MI

10 Hultgren, R., et al., "Selected Values of the Thermodynamic Properties of Binary Alloys", American Society for Metals (1973)

TABLE 2-1

Pd - Electronic Energy Levels

Configuration	Designation	J	Level (cm^{-1})
$4d^{10}$	^1S	0	0.00
$4d^9 5s$	^3D	3	6564.11
		2	7754.99
		1	10093.94
$4d^9 5s$	^1D	2	11721.77
$4d^8 5s^2$	^3F	4	25101.1
		3	28213.5
		2	29711.0

TABLE 2-2

Energy Level Partition Function Contributions

Level (cm^{-1})	g (2J+1)	Partition Function Contributions $ge^{-(E/KT)}$ Temperatures K						
		1900	2000	2100	2200	2300	2400	2500
0.00	1	1	1	1	1	1	1	1
6564.1	7	.0486	.0623	.0779	.0957	.1153	.1367	.1601
7755.0	5	.0141	.0189	.0246	.0314	.0391	.0478	.0576
10093.9	3	.0014	.0021	.0030	.0041	.0054	.0071	.0090
11721.8	5	.0007	.0011	.0016	.0023	.0033	.0044	.0059
25101.1	9	all less than 4.79×10^{-6}						
28213.5	7	all less than 6.12×10^{-7}						
29711.0	5	all less than 1.88×10^{-7}						

TABLE 2-3

Variation of Partition Function with Temperature

Temperature K	Q calculated	Q fitted
1900	1.0647	1.0650
2000	1.0844	1.0840
2100	1.1071	1.1070
2200	1.1335	1.1330
2300	1.1631	1.1630
2400	1.1960	1.1960
2500	1.2326	1.2320

TABLE 2-4

ΔG°_f For The Metal Carbides

2200 K

Carbide	ΔG°_f Kcal/Mole	Reference
TiC	-36.6	9
	-36.7	10
NbC	-31.7	9
	-32.0	10
VC	-22.4	10

Carbide Equilibration

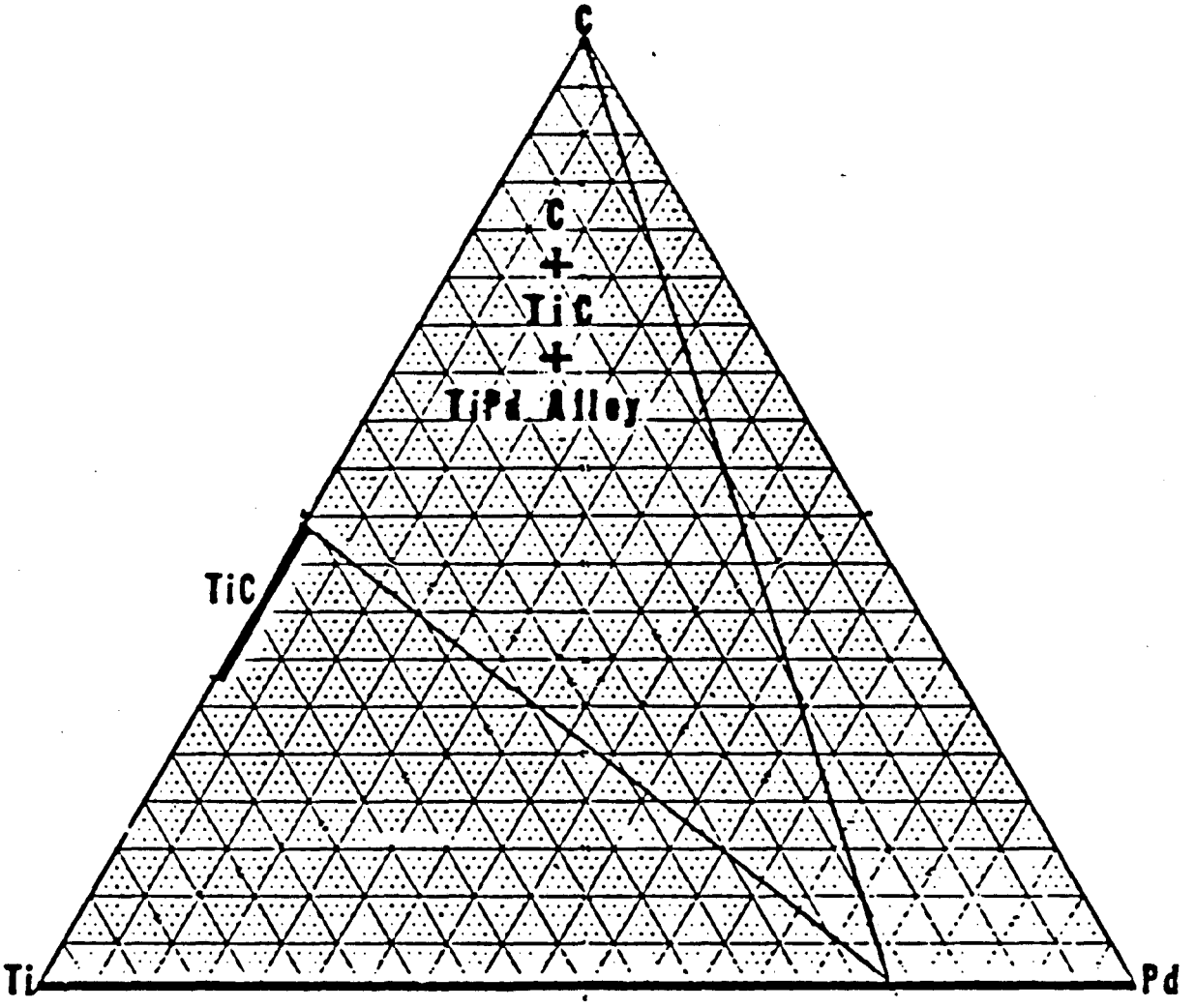

Figure 2-1

The partial ternary phase diagram of Ti, Pd and C is shown. Tie lines are drawn to represent a possible three phase region, where the activity of the Ti is equal in all three phases.

EXPERIMENTAL EQUIPMENT AND PROCEDURE

The King Furnace

A 'King' graphite resistance furnace originally described by Jenkins, Gilles and Brewer,[1] with modifications over the years described by Hicks[2] and Hagan,[3] shown in Figure 3-1, was used for the vapor pressure measurements. A 30.48 cm long graphite tube with a 1.27 cm bore was used as a heating element, see Figure 3-2. The tube was tapered from an outer diameter of 2.197 ± .013 cm in the center, to a minimum of 1.905 ± .013 cm at 7.62 cm from each end, resulting in a 15.24 cm constant temperature hot zone. The 7.62 cm ends had an outer diameter of 2.223 ± .013 cm.

The tube is supported by split graphite brushings held by massive copper electrodes, all encased in a vaccuum tight brass chamber. The furnace is cooled by four water lines; one through the copper electrodes, one covering the outer barrel, and one at each end encircling the windows.

The heating tube is surrounded by a graphite heat shield, which is enclosed in five concentric heat shields held on a graphite spool. The outer shields were machined from porous graphite, with each shield having a 0.159 cm ridge at each end. Each set of ridges is offset from the previous shield by 1.27 cm. The ridges minimize the physical

contact and heat transfer between the shields.

The windows made of quartz glass are 0.159 cm thick and 4.128 cm in diameter, held in place by viton O-rings. Shutters consisting of a copper holder and a thin steel door were positioned directly inside each window. The doors could be opened or closed by manipulating magnets outside the furnace. The shutters were kept closed, except when recording an emission spectra or taking a temperature reading, to prevent vapor deposition on the windows.

The heating tubes, sample boats and baffles, shown in Figure 3-2, were all made of very dense ECV grade graphite[4] to ensure good thermal and electrical conduction. The boat, either 1.26 or 2.00 cm long, was placed in the middle of the hot zone and used as the primary source of temperature measurements. To define the cut-off end of the hot zone, a baffle was located at the end of the hot zone at the side of the tube nearest to the spectometer. No baffle was placed at the other end of the tube because of its reduction of the viewing area for temperature readings. A second baffle was put at the very end of the tube to cut down on extraneous light emitted by the walls of the tube.

The Optical Set-up

The optical setup can be seen in Figure 3-3. The system consists of a furnace as the emission light source, a set of lenses and pinhole

stop, a spectometer, and a photomultiplier to analyse the spectra. The focal lengths of the lenses were determined by measuring the focal distances of illuminated cross hairs through the lenses. The furnace, lenses and pinhole stop were aligned with a HeNe laser. The laser beam was directed backwards through the spectrometer, then the furnace and lens track were adjusted to lie along the beam.

Lens A focuses the light from the tube on to the stop. At the stop a circle of light is visible representing the emission from the walls of the furnace. Half of the inside of the circle is also bright from the emission from the sample boat. The other half is dark, only transmitting the light from the vapors in the tube. The stop has a 0.05 cm pinhole positioned in the darkened half of the circle to transmit the light. Lens B focuses the light allowed through the pinhole onto the entrance slit of the spectrometer.

The spectrometer used is a Jarrell-Ash 1.5 meter Fastie two mirror spectrogragh - (series 75-100).[5] The useful wavelength range is 1900 Å to 11000 Å, with a f/14 aperature ratio, and an optimal resolution of 0.3 Å. The entrance and exit slits are set at 230 μ and 170 μ respectively, large enough to encompass the whole emission line of a metallic vapor. Under these conditions the total area of the emission peak is recorded within the height of the measured spectral line. The choice of the slit widths were decided upon after observing the variation of the peak response to the variation of the slit widths.[6]

The grating is driven by an electric gear box with readings of 0° to 40° with a readout of 0.01°. The grating angle had to be calibrated with spectra of known wavelength to determine the relationship between the angle reading and recorded wavelength. One reference wavelength was the HeNe laser with a wavelength of 6328 Å at a grating angle of 22.45°. Initially the other reference was a Hg lamp. The wavelengths and corresponding grating angles are given in Table 3-1 along with the best fit least square quadratic and its calculated wavelengths. This relationship was used to identify the various peaks of the spectra of the metal vapor.

Since the best reading with the quadratic formula over the range of 12° to 22° does not give an estimation better than 1 Å, a linear equation:

$$\lambda = 283.31\ \theta + 35.06 \qquad (3\text{-}1)$$

was used in the range $\theta = 12°$ to $\theta = 16°$ to identify the peaks, giving a fit good enough for peak identification. Over the three years of taking spectra, the relationship between the grating angle and wavelength slightly changed by a constant value. This occurred because of a slight change in the angle reading gear on the grating shaft, consequently the linear equation was periodically checked and adjusted.

An EMI (9789QB)[7] end-on window photomultiplier tube was used to measure the spectral intensity. The photomultiplier tube has 13 CsSb dynodes in a venetian blind configuration. The cathode has an effective

diameter of 1.0 cm with a sensitivity to 'white light' of 50 μA/lm and a typical maximum quantum effeciency of 27%. The tube has quartz windows and follows the spectral response curve shown in Figure 3-4. This response limits the selection of measureable wavelengths to a range of 3000 Å to 5000 Å. The effect of the spectral response is noted by the measurement of the blackbody emission off of the walls in the furnace. Due to a combination of the natural emission curve of a blackbody and the sensitivity of the photomultiplier, the maximum emission intensity of a black graphite plug in the King furnace at 2250 K is recorded at about 5100 Å not at the natural peak of about 13000 Å for a blackbody. A comparison of the natural blackbody emission and the recorded emission of a blackbody using the experimental set-up is shown in Figure 3-5.

The photomultiplier tube has a typical gain of 1×10^8 A/lm and an EMI VA.01 amplifier[7] was used, increasing the recorded intensity by a voltage gain of 100X. An EMI MFA magnetic lense assembly[7] was employed to reduce the dark current through a defocusing of photoelectrons emitted from areas of the photocathode which are extraneous to the signal area. The whole photomultiplier tube assembly was enclosed in an EMI RF1/B-289F PMT housing unit,[7] providing electrostatic and magnetic shielding at the cathode potential. The housing unit was light-tight sealed at the end-on position around the exit slit of the spectrometer. A Houston Instrument series 4500 Microscribe[8] strip chart recorder was used to display the spectra.

Temperature Measurements

Temperature measurement is a very critical factor in the vapor pressure determinations. The temperature was measured with a Leeds Northrup optical pyrometer.[9] The pyrometer was calibrated against another Leeds and Northrup optical pyrometer which was calibrated by the National Bureau of Standards using the 1968 Temperature Scale, see Table 3-2.

For both the low and high ranges, the pyrometer gave the same readings as the NBS standard and are given uncertainties of ±5° and ±8° respectively by the manufacturer. The X-high range had consistantly high readings compared to the standard. This was confirmed by internal comparisons with the overlapping temperatures of the high and X-high ranges. The X-high readings were consistantly about 10° to 15° higher than at the high setting. Consequently, all readings from the X-high range were decreased by 10°. The uncertainty given by the manufacturer was ±15° for the X-high setting.

The temperature readings were taken from the ends of the graphite boats during the vapor pressure measurements because the focus was much simpler than on the sides of the tube. Many heating runs were taken to obtain the temperature profile of the tubes. Several different sized pieces of graphite were inserted in a graphite tube, arranged so they each could be viewed from one end of the tube. As the temperature was increased or decreased, the temperature was recorded from each graphite

piece. Initially a temperature difference could be detected due to the different heating rates along the tube. Once a steady state temperature profile was reached, all the pieces within the central portion of the tube gave the same temperature readings within the pyrometer's uncertainty. Any piece in the thicker-walled ends of the tube gave drastically lower temperatures. These readings confirmed that the tubes have a good constant temperature region in which vapor pressures can reach equilibrium with a sample placed within the region.

The temperature of the side of a boat was compared to a graphite plug with a 2.54 cm deep 0.300 cm diameter hole. No difference could be detected between the temperature of the hole and the boat, showing that the readings are good blackbody approximations and that no corrections are needed for the emissivity of the boats. Further evidence of the accuracy of the temperature measurements is given by the melting point determinations of the metals as seen in the results.

A correction had to be calculated for the transmission of the quartz window. The intensity of a tungsten filament lamp was measured through the furnace and optical set-up. A comparison between when a quartz window was on or off the furnace gave the percent transmission of the quartz window at various wavelengths, see Table 3-3. This data agrees with Olson.[10,11] A temperature correction is calculated using Wien's Law.[12]

$$1/T - 1/T_B = \lambda/C_2 \ln\tau \qquad (3\text{-}2)$$

T = true temperature

T_B = measured brightness temperature (at λ)

λ = wavlength

C_2 = second radiation constant

τ = transmittance

With the transmittance a relative constant value of approximately 0.922 throughout the experimental wavelength range, the correction on the measured temperature for the quartz window is:

$$1/T = 1/T_B - 4.78 \times 10^{-6} \qquad (3\text{-}3)$$

Alloy Production

A list of all the starting material is given in Table 3-4. All of the alloys were arc-melted in a water-cooled copper hearth with a tungsten electrode under a Ti-gettered argon atmosphere. Each pellet was flipped several times to insure good mixing. After arc-melting the alloys were usually annealed at 100° - 300° below their melting points for several hours.

Some of the alloys were made during this study, while others were made by previous co-workers. Therefore the annealing time varies for the samples. As long as the samples were sufficiently flipped while arc-melting, annealing is not important for good homogeneity. Annealing

is important in crystal formation of the equilibrium phases, but did not effect the bulk homogeneity in this study. The list of alloys, when they were produced, their annealing time and weight loss during the arc-melting and annealing process are presented in Table 3-5.

Alloy Analysis

The samples, small arc-melted buttons, were sectioned with a diamond saw. Because of their hardness and long cutting time required some samples were sectioned using an EDM. Sometimes during the annealing process a thin oxide coating would form on the acid-rich alloys, which was removed by sanding.

The samples were all checked for homogeneity both optically and by energy dispersive X-ray analysis (EDAX). A scanning electron microscope made by the AMR corporation[13] with a drifted lithium silicon X-ray detector made by Kevex Corporation[14] was used for the analysis. Quantitative analysis of the compositions of the alloys were obtained by comparing the characteristic emission peaks from each element. Spectra were obtained from 0.0 to 10.24 KeV with a resolution of 10eV/ch. The silicon escape peaks and background Bremstrahlung radiation emitted from the alloy were removed from the X-ray spectra using Quantex Ray software.[14] The Quantex Ray analysis did not give reliable quantitative results for the composition of the alloys. Cima[15] has developed a method for obtaining reliable results from the relative X-ray emission intensities of the components in the alloys.

Cima's method involves making a series of standard alloys of known composition to be used as a reference for analysing unknown alloys. The relative intensity of the characteristic lines of each component in the binary alloy is measured. The relative intensity is defined

$$R_A = \frac{I_{A,alloy}}{I_{A,alloy} + I_{B,alloy}} \qquad (3\text{-}4)$$

The relative intensities of a component are plotted as a function of the atomic percent of that element. This curve is then used to determine unknown compositions from the measurements of their relative intensities.

A one parameter equation based on Ogilvie's[16] quasi-empirical technique for determining calibration curves for multicomponent alloys was developed to model the relationship between the relative intensity and mole fraction.

$$R_A = \frac{X_A\ (a_{BA}\ X_A + X_B)}{X_A\ (a_{BA}\ X_A + X_B) + \lambda\ X_B (a_{AB}\ X_B + X_A)} \qquad (3\text{-}5)$$

X_N is the mole fraction of component N. a_{NM} is a constant dependent on the effects of electron loss per unit depth of penetration and back scattering efficiency of the species, the molecular weight, the take off angle of the spectrophotometer, the beam voltage and the mass absorption coefficient of the X-ray line of one species dissolved in the other. See Cima's thesis for a detailed derivation. All of these values are available except for the one parameter, λ, which is obtained from the standards.

For this study the samples made for the vapor pressure measurements were used to develope the standard curve. While measuring the relative intensities of each sample, the homogeneity was was checked by measuring the intensities from different sites on the prepared alloy section. The relative intensities of the standard samples for the binaries TiPd, VPd, NbPd, and VRh are shown in Tables 3-6 through 3-9, respectively. A graphical presentation of the data is shown in Figures 3-6 through 3-9.

EDAX was used to analyse the samples after a vapor pressure run. Any variation due to loss by vaporization or to a reaction with the crucible was detected by the change in relative intensities as compared to the standards.

Vapor Pressure Measurements

Vapor pressure measurements were carried out in the King furnace. For each measurement (run) a sample was weighed along with a carbon (graphite) boat, then placed in the center of a heating tube. The baffles were then inserted in the tube. The furnace and tube were placed under dynamic vacuum overnight, keeping the pressure at < 20 microns. A mechanical pump and thermocouple pressure gauge were sufficient throughout the experiments.

Each sample was put through a heating cycle to degas the tube. The furnace was filled with approximately 100 torr of Ar and the temperature

was raised to about 1300 K over a 15 minute interval. The furnace was evacuated for 5 minutes while the furnace power was still on. When the power was turned off the vacuum was kept on until the furnace cooled off and the pressure again fell to < 20 microns.

For each vapor pressure run the same proceedure was always followed. The system was backfilled with about 100 torr of Ar. The furnace was then heated to 1300 K within 15 to 20 minutes, then raised slowly. When the temperature approach the suspected melting point of the sample, the temperature was allowed to equilibrate, then very slowly raised while being recorded with a pyrometer. The melting temperature, or a small temperature range in which the metal melted, was recorded by observing the phase change of the part of the metal that was positioned sticking above the sides of the boat.

Once the melting point was recorded, the temperature was again increased more rapidly until it approached near the value of the vapor pressure measurements. At the designated temperature, the power was kept steady to allow the temperature to equilibrate. During the time the temperature was leveling off, several emission measurements were taken of one spectral line. The temperature usually reached a constant value before the emissions reached a maximum. The temperature and intensity readings each became constant within 15 to 20 minutes, indicating the system had reached equilibrium. All relevant spectral line intensities were recorded by scanning over the wavelength interval of interest. The temperature was checked after the intensity measurements to insure no deviation from the constant temperature.

Again the temperature was raised to a new value for another vapor pressure measurement.

Only three to four measurements were run for each sample. The samples were kept above their melting points for a maximum of about 100 minutes, and generally not more than an hour. If the alloys were allowed to remain at high temperatures for an extended period, a significant amount of vapor would tend to condense in the cooler parts of the furnace, and the amount of that metal in the sample would be depleted. This sample loss would be most crucial if one component had a much larger vapor pressure, so the loss would be primarily from one component and change the composition of the alloy.

When the intensity measurements were completed, the power was abruptly discontinued, quenching the samples. The temperature would fall from the high temperature range of 2150 - 2300 K down to 1000 K within five minutes, preserving the high temperature composition for analysis after the run. Between each run the tubes were cleaned out. First the tubes were physically cleaned to detect and remove any large alloy deposits. Then the empty tubes were heated in the furnace to vaporize and condense out any small amount of metals left in the tube. The tubes were heated to 2500 - 2600 K for several hours. Each tube was then checked for any characteristic emission of the alloyed metals. If any emission was observed in the experimental temperature range, the tube was further heated.

This cleaning method removed all traces of the base metals Pd and Rh. This is important because the measured intensities were from the base metal emissions. When the tubes were new as well as after all cleanings, a small emission could always be detected from the acidic metals Ti and V. These metals form refractory compounds with carbon. The tubes were never sufficiently heated to remove all traces of the carbides. The measurements of the Ti and V above an alloy were often smaller than within an empty tube. The intensity readings were so small that they did not represent any real data. Throughout the experiments only the intensity measurements from the base metals were recorded and reported here.

Carbide Equilibration

The carbide equilibration experiments were run as an off-shoot of the vapor pressure measurements, yet gave very valuable data about the activity of the acid metals. During the vapor pressure runs sometimes the alloys would react with the graphite boat. The reaction depended on the concentration of the acid metal. The base metals used, Pd and Rh, do not react with graphite to form a carbide phase, only dissolving a small amount of carbon at these temperatures.[17] All of the acid metals used, Ti, V, and Nb form carbide phases. Due to the excess of the carbon of the boat, the carbide phases that formed are the MC phases, the most carbon-rich stable phase with each of the metals. The carbide phase would form when the concentration of the acid metal in the alloy

increased enough for its activity in the metal to be greater than in the MC phase in equilibrium with graphite.

The formation of the carbide phase was very obvious. The vapor pressure of the base metal is greater than expected whenever a carbide phase formed. The alloy is depleted of the acid metal forming the carbide, leaving a greater base metal concentration in the alloy. Also the alloys with a high base metal concentration did not greatly wet the graphite boats. When a reaction did occur, the alloy drastically wetted the boat, spreading all over the bottom and walls of the container. A quick observation of the form of the alloy after a run indicated whether a carbide phase formed.

The samples were cut, polished and analysed after each run. With a high base metal concentration the alloys optically looked very homogeneous with only some dendritic growths of carbon in the alloy, due to the lowering of the solubility of the carbon upon cooling the sample. The base-poor alloys showed two phases present. The second phase, mostly concentrated at the metal-boat interface, was the carbide.

All the alloys were analysed by EDAX. Besides checking the homogeneity and compositional changes of the alloys which had no carbide phases, the analysis determined the composition of the alloy in equilibrium with a carbide phase. The relative intensity measurements of the alloy phase provide the composition by use of the relationship given by the standard curves. The X-ray intensities of the carbide phase showed an analysis of almost pure acid metal, because of the

exclusion of the base metal in the carbide phase and the inability to detect carbon with the available equipment. The analysis of the bulk alloy phase varied due to the intermixing of small carbide crystals. Many locations on the sample were examined, with the most base-rich atomic percent chosen as the correct composition for the alloy in equilibrium with the carbide phase. Results giving higher acid metal atomic percents were due to having some carbide in the area chosen to examine.

References

1 Brewer, L., Gilles, P. W. and Jenkins, F. A., J. Chem. Phys., 16, 797 (1948)

2 Hicks, Ph.D. Thesis, Univ. of Cal., Berkeley, (1957)

3 Hagan, L., Ph.D. Thesis, Univ. of Cal., Berkeley, (1963)

4 Union Carbide Corp., Carbon Products Division, Chicago, IL

5 Jarell-Ash Co., Waltham, MA

6 Clark, G. L., ed., "Encylopedia of Spectroscopy", 138, Van Nostrand Reinhold, NY (1960)

7 EMI Gencom Inc., Plainview, NY

8 Houston Instrument, Austin, TX

9 Leeds and Northrup Co., Philadelphia, PA

10 Olson, O. H. and Morris J. C., "Determination of Emissivity and Reflectivity Data on Aircraft Structural Materials Pt. 3: Techniques for Measurement", WADC-TR-56-222, (Pt 3), 1 (1959)

11 Touloukian, Y. S., ed., "Thermophysical Properties of Matter, Vol. 7: Thermal Radiative Properties of Non-Metallic Elements and Alloys", 1577, IFI/Plenum, NY (1972)

12 Wien, W., Ann. der Phys., 3, (58), 662 (1896)

13 AMRay Corp., Bedford, MA

14 Kevex and Quantex-Ray Software, Foster City, CA

15 Cima, M., Ph.D. Thesis, Univ. of Cal., Berkeley, (1986)

15 Ziebold, T. O. and Olgilvie, R. E., Anal. Chem., 35, 621 (1963)

17 Selman, G. L., et al., Plat. Met. Rev., 14, (1), 14 (1970)

TABLE 3-1

Calibration of Grating Angle

	λ (Å) Hg Spectra	ν	λ (Å) Calculated
	3650.15	12.814	3650.0
	3654.83	12.831	6354.8
	3663.28	12.860	3663.1
	4046.60	14.210	4046.7
	4077.80	14.329	4076.3
	4339.23	15.245	4339.0
	4347.50	15.276	4347.7
	4358.35	15.315	4358.7
	5460.74	19.271	5460.6
	5769.59	20.392	5769.0
	5790.65	20.474	5790.3
HeNe	6328.00	22.445	6330.8

$$\lambda = -0.742\ \theta^2 + 304.3\ \theta - 126.9$$

With a variation of ± 0.005 in θ, the best reading allows a deviation of 1.5 Å in λ.

TABLE 3-2

Calibration of Pyrometer

Range	Standard NBS Calibrated	AGC #721 Pyrometer This Study
	800	800
Low	1000	1000
	1200	1200
	1100	1100
	1200	1205
	1300	1300
High	1400	1397
	1500	1498
	1600	1595
	1700	1700
	1500	1508
	1600	1609
X-high	1700	1710
	1800	1805
	1900	1902
	2000	2008

TABLE 3-3

Transmittance of Quartz

	λ (Å)	Transmittance
Olson	2870	0.888
	3970	0.918
	4560	0.920
	6010	0.921
	6950	0.926
This Study	3435	0.908
		0.885
	3886	0.910
		0.918
		0.932
	4001	0.905
		0.920
	4568	0.925
		0.928
		0.932
	5135	0.916
		0.920
		0.922
	5946	0.918
		0.920
		0.922

TABLE 3-4

Starting Materials

Material		% Purity	Source
Pd	1/2" Rod	99.9	LBL Stock
Rh	Sheet	99.99	LBL Stock
Ti	1/16" Rod	99.9	Orion Chemical Co.
	1/4" Ingots	99.8	Cerac
V	1/2" Ingots	99.5	United Min. & Chem. Corp
Nb	1/8" Rod	99.95	Material Research Corp.
Zr	1/8" Rod	99.95	Material Research Corp.

TABLE 3-5

TiPd Arcmelted Samples

Sample ID	a/o Pd	a/o Ti	Original Weight	Annealing Conditions [1]	% Loss
			TiPd Arcmelted 1982		
F-2*	93.94	6.06	7.12015		0.43
F-4*	87.24	12.76	3.29987		1.05
F-5*	81.52	18.48	2.33038		0.32
F-6	76.42	23.58	1.86266		-
F-7	71.81	28.19	1.51819		0.52
			TiPd Arcmelted 1984		
J-2*	79.97	20.03	5.53883		0.10
J-3*	75.00	25.00	4.97733		0.35
J-4*	70.03	29.97	5.03670		0.18
J-5	64.96	35.04	5.02542		0.29
J-6	60.03	39.97	4.45256		0.05
J-7*	54.99	45.01	4.99172		0.06
J-8	49.93	50.07	4.98589		0.02
J-9	44.93	55.07	4.98345		0.33
J-10	40.04	59.96	4.99822		0.05

All values used in the calibration curve

* Used in vapor pressure study

[1] All samples annealed for several hours at 1000° C

TABLE 3-5 continued

VPd Arcmelted 1986

	Sample ID	a/o Pd	a/o V	Original Weight	Annealing Condition	% Loss
1	V-1	90.17	9.83	1.51262	1100°C 14 hrs	19.84
	V-2*	84.61	15.39	1.32772	1100°C 2 hrs	0.96
	V-3*	79.66	20.34	1.67232	1100°C 2 hrs	1.06
2	V-4	74.92	25.08	1.16556	1100°C 14 Hrs	7.54
	V-5*	69.81	30.19	1.70137	1100°C 2 hrs	0.78
	V-6	59.96	40.04	1.06794	1100°C 2 hrs	0.13
3	V-7	50.02	49.98	1.10683	1100°C 14 hrs	-0.59
	V-8	35.00	65.00	0.94957	1100°C 2 hrs	0.22
4	V-9	25.12	74.88	1.15937	1100°C 14hrs	-1.64
5	V-10	10.04	89.96	1.08665	1100°C 14 hrs	-4.42

Because of the obvious reaction of the five samples (labeled) annealed at 14 hours the first sample was arc-melted a second time, and another Pd rich sample was also made. The composition of the first sample was determined by dispersive X-ray analysis.

V-1*			0.88902	830°C 2 hrs	1.28
V-11*	93.06	6.94	1.40181	830°C 2 hrs	1.73

* Used in vapor pressure study

TABLE 3-5 continued

ZrPd Arcmelted Samples

Sample ID	a/o Pd	a/o Zr	Original Weight	Annealing Condition	% Loss
Z-1	95.32	4.68	1.98176	1100°C 5 hrs	4.02
Z-2	89.62	10.38	2.01572	1100°C 5 hrs	3.20
Z-3	81.56	18.44	1.38971	800°C 2 hrs	1.81
Z-4	75.00	25.00	-	-	-
Z-5	49.77	50.23	1.31584	800°C 2 hrs	0.43
Z-6	25.07	74.93	1.36125	800°C 2 hrs	-0.11

Samples Z-1 and Z-2 made by Mike Cima UCB (1985)

Sample Z-4 made by John Gibson UCB (1983)

Samples Z-3, Z-5 and Z-6 made for this study (1986)

All the samples were used in calibration curve

TABLE 3-5 continued

NbPd Arcmelted Samples

Sample ID	a/o Pd	a/o Nb	Original Weight	Annealing Condition	% Loss
N-1*	93.9	6.1			
N-2*	89.6	10.4			
N-3	87.8	12.2	All samples made by M. Cima		
N-4[1]*	86.3	13.7	Annealed several hours at 1000° C		
N-5*	82.8	17.2	All samples used in calibration curve		
N-6	82.0	18.0	See Cima's Thesis (1986)		
N-7*	77.3	26.7			
N-8	35.0	65.0			
N-9	15.2	84.8			
N-10	8.2	91.8			
N-11	2.8	97.2			

[1] Was made for this study

* Used in vapor pressure study

TABLE 3-5 continued

VRh Arcmelted 1986

Sample ID	a/o Rh	a/o V	Original Weight	Annealing[1] Conditions	% Loss
VR-1*	94.67	5.33	0.99880		-
VR-2	89.93	10.07	1.47486		0.94
VR-3*	84.15	15.85	1.20512		0.91
VR-4*	79.93	20.07	1.5005		-
VR-5*	74.64	25.36	1.19318		0.72
VR-6*	70.26	29.74	1.00900		-
VR-7*	54.78	45.22	1.00836		0.55
VR-8	40.49	59.91	1.01054		0.45
VR-9	25.81	74.19	1.00567		-
VR-10	10.46	89.46	1.00652		-

All values used in the calibration curve

* Used in vapor pressure study

[1] All samples annealed for several hours at 1000° C

TABLE 3-6

EDAX Results for Standard Curves

TiPd

Sample	X_{Ti}	Ti (Lα)	Pd (Lα)	R_{Ti}
F-2	0.061	3.270	67.52	0.046
		2.267	55.62	0.039
		2.757	65.71	0.040
F-4	0.128	6.523	72.88	0.082
		6.417	73.41	0.080
		6.313	74.01	0.079
F-5	0.185	7.507	57.23	0.116
		8.177	61.48	0.117
		8.880	69.33	0.114
J-2	0.200	26.43	191.0	0.122
		24.66	177.4	0.122
J-3	0.250	42.47	235.9	0.153
		37.11	203.3	0.154
F-6	0.236	15.17	85.22	0.151
		15.79	90.50	0.149
		16.09	90.78	0.151
F-7	0.282	12.26	50.81	0.194
		10.28	45.11	0.186
		12.29	53.54	0.187
J-4	0.300	57.82	257.5	0.183
		50.57	214.1	0.191
J-5	0.350	73.58	260.4	0.220
		58.19	204.8	0.221
J-6	0.400	70.46	193.7	0.267
		83.65	235.9	0.262
J-7	0.450	90.43	204.4	0.307
		61.08	138.8	0.306
J-8	0.501	123.3	240.8	0.339
		128.4	249.6	0.340

TABLE 3-6 continued

EDAX Results for Standard Curves

TiPd

Sample	X_{Ti}	Ti (Kα)	Pd (Lα)	R_{Ti}
J-9	0.551	152.0	232.5	0.395
		138.8	215.5	0.392
J-10	0.600	174.8	216.9	0.446
		157.6	200.8	0.440

TABLE 3-7

EDAX Results for Standard Curves

VPd

Sample	X_V	V (Kα)	Pd (Lα)	R_V
V-2	0.150	8.667	88.40	0.089
		9.477	100.30	0.086
		10.57	112.5	0.086
V-3	0.200	5.080	36.52	0.122
		5.263	38.54	0.120
		5.840	40.70	0.125
V-5	0.300	23.16	99.07	0.189
		15.95	69.30	0.187
		15.27	67.17	0.185
		12.10	49.76	0.196
V-6	0.400	24.78	68.34	0.266
		24.96	72.25	0.257
		17.53	47.45	0.270
V-8	0.650	51.17	48.11	0.515
		64.39	60.14	0.517
		69.26	66.21	0.511
V-11	(0.070)	3.237	76.40	0.041
		3.020	75.59	0.041
		3.753	82.91	0.043
V-1	(0.100)	5.413	75.00	0.067
		4.933	65.09	0.071
		5.837	79.75	0.068

TABLE 3-8

EDAX Results for Standard Curves

NbPd

Sample	X_{Nb}	Nb (Lα)	Pd (Lα)	R_{Nb}
N-1	0.061	5.75	102.5	0.053
N-2	0.104	11.31	111.6	0.092
		10.26	107.1	0.087
		10.97	111.8	0.089
		26.46	245.3	0.097
		19.75	183.0	0.097
		31.92	332.3	0.088
		28.38	309.6	0.084
		26.84	270.1	0.090
N-3	0.122	8.50	71090	0.106
		8.74	68.98	0.112
		11.73	96.13	0.109
		35.24	311.1	0.102
		41.25	328.4	0.112
		36.70	300.0	0.109
N-5	0.172	16.80	86.29	0.163
N-6	0.180	16.29	85.65	0.160
N-7	0.227	26.53	74.37	0.263
		22.85	63.18	0.264
		20.19	58.81	0.256
		11.24	32.32	0.258
		66.84	201.5	0.249
		72.93	215.7	0.253
		68.14	208.4	0.246
N-8	0.650	82.41	35.36	0.700
N-9	0.848	124.8	15.15	0.892
		129.8	13.79	0.904
		122.2	13.02	0.904
N-10	0.918	241.8	13.52	0.947
		238.9	14.03	0.0945
		290.8	16.86	0.945
N-11	0.972	235.6	4.57	0.981
		221.8	3.93	0.983
		216.1	3.36	0.985

TABLE 3-9

EDAX Results for Standard Curves

VRh

Sample	X_V	V (Kα)	Rh (Lα)	R_V
VR-1	0.053	1.157	29.40	0.038
		1.367	33.78	0.039
		1.507	38.55	0.038
VR-2	0.101	3.927	51.72	0.071
		4.987	61.37	0.075
		5.720	72.03	0.074
VR-3	0.159	3.190	24.42	0.116
		3.833	30.82	0.111
		4.953	36.11	0.121
VR-4	0.201	2.400	13.30	0.153
		3.737	20.90	0.152
VR-5	0.254	40.34	178.5	0.184
		40.59	178.3	0.185
		34.52	155.7	0.182
VR-6	0.298	47.19	167.7	0.220
		42.19	149.8	0.220
		47.25	169.3	0.218
VR-7	0.452	94.10	170.3	0.356
		68.64	121.2	0.362
		67.43	120.0	0.360
VR-8	0.599	167.6	158.6	0.514
		171.9	165.3	0.510
		167.1	160.2	0.511
VR-9	0.742	95.91	45.42	0.679
		274.4	134.6	0.671
		274.9	131.1	0.677
		280.3	136.0	0.673
VR-10	0.895	265.0	40.99	0.866
		272.1	40.58	0.870
		267.1	39.56	0.871

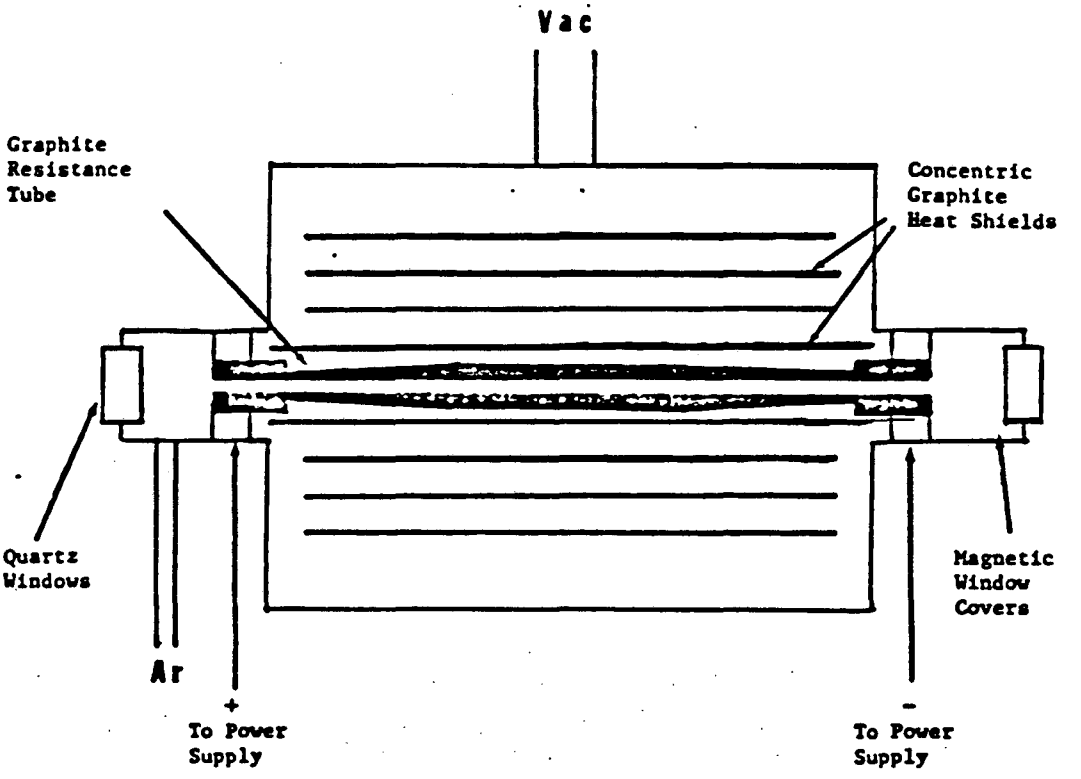

Figure 3-1

A schematic representation of the King furnace is shown. The center of the heating tube is visible from both ends, allowing for the simultaneous measurement of temperature and emission spectra.

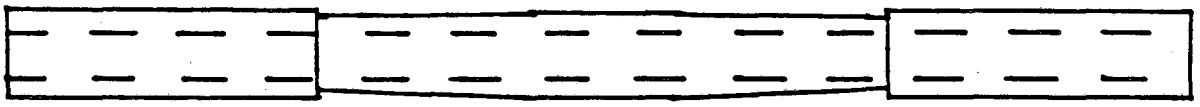

A Graphite Heating Tube -- The middle is bowed to give a constant temperature hot zone.

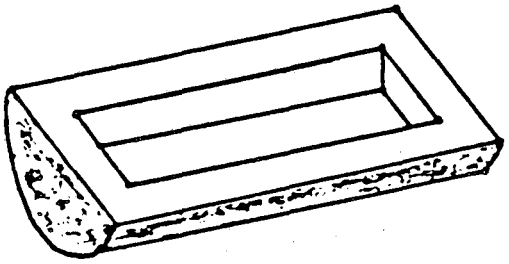

A Sample Boat

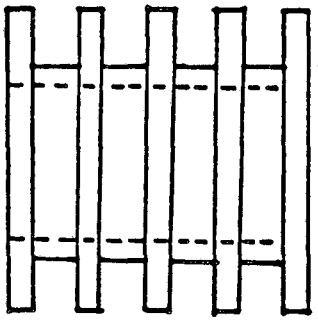

A Graphite Baffle

Figure 3-2

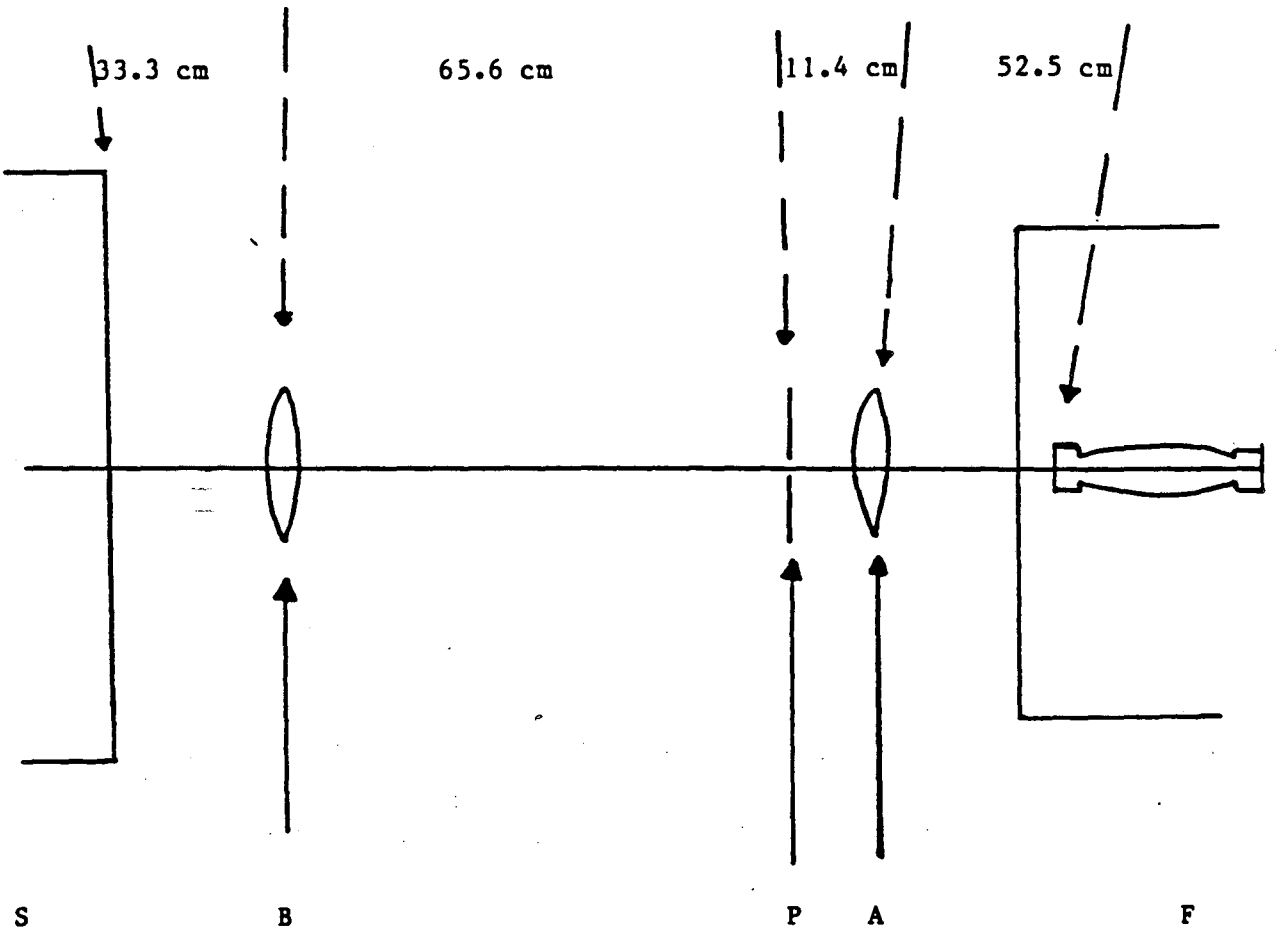

Figure 3-3

F - The King Furnace

P - Stop with 0.5 cm pinhole

S - Spectrometer

A - Lens A with focal length of 9.5 cm

B - Lens B with focal length of 22.1 cm

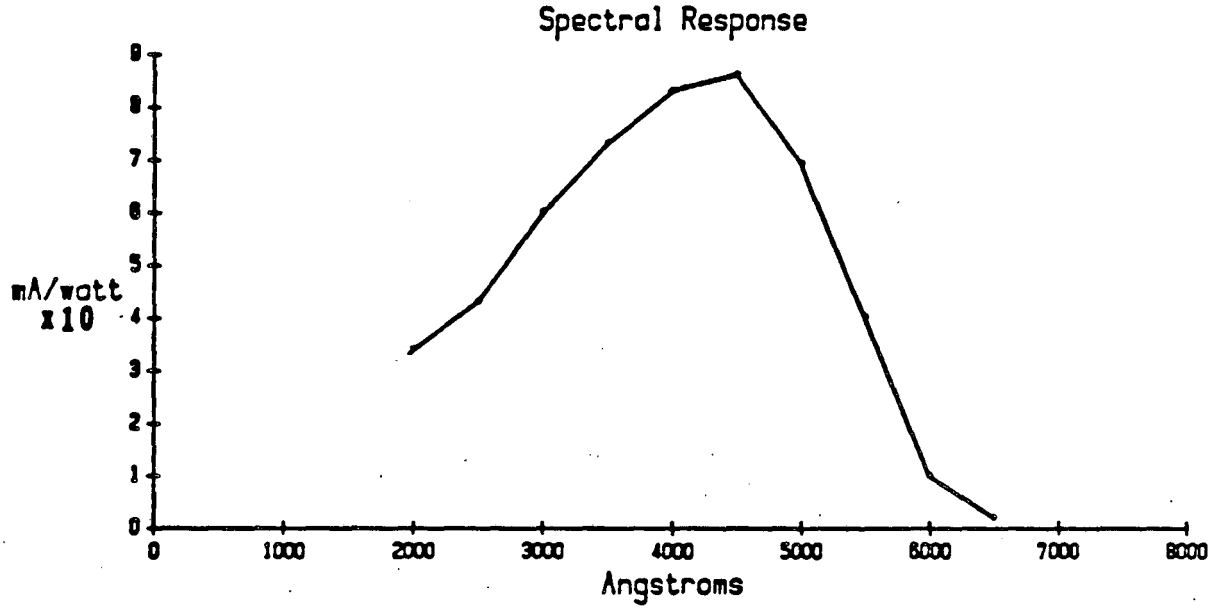

Figure 3-4

The radiant energy spectral coverage for the PMT is shown for a wavelength range to 1000 Angstroms. The absolute intensity scale in milliamperes per watt is on the left margin.

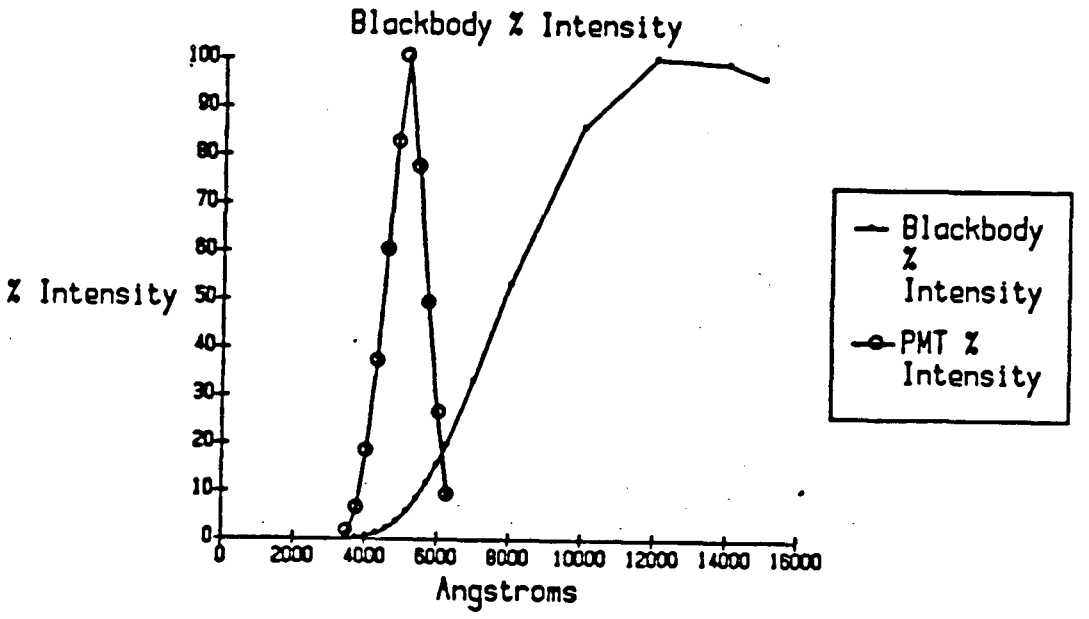

Figure 3-5

The broad peak with a maximum around 13000 Å is the true blackbody emission. The narrow peak with a maximum around 5100 Å is the measured spectra obtained from blackbody emission under the limitation of the PMT spectral response.

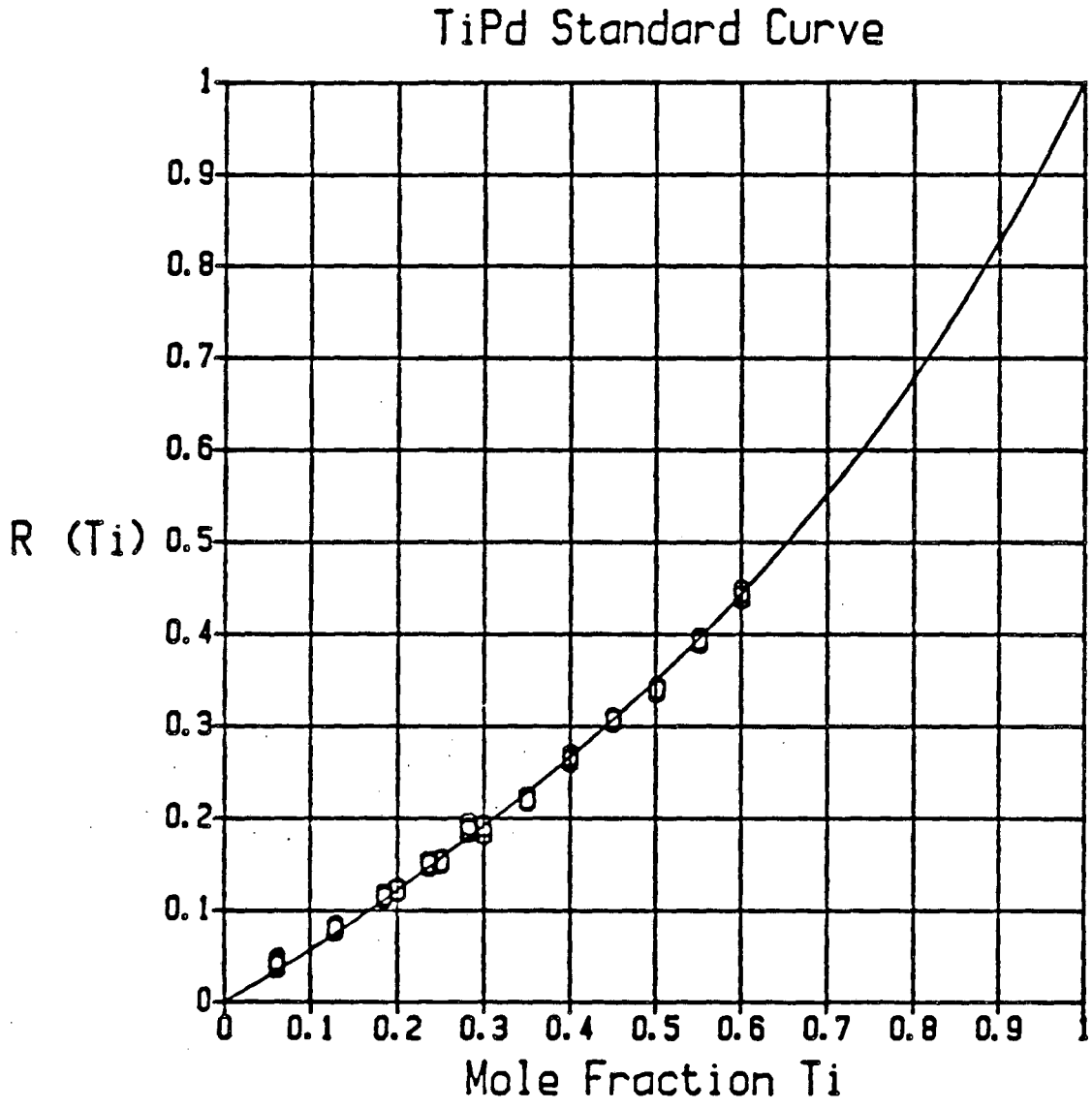

Figure 3-6

The relative intensity of the Ti(Kα) and Pd(Lα) peaks as a function of X_{Ti} in TiPd alloys.

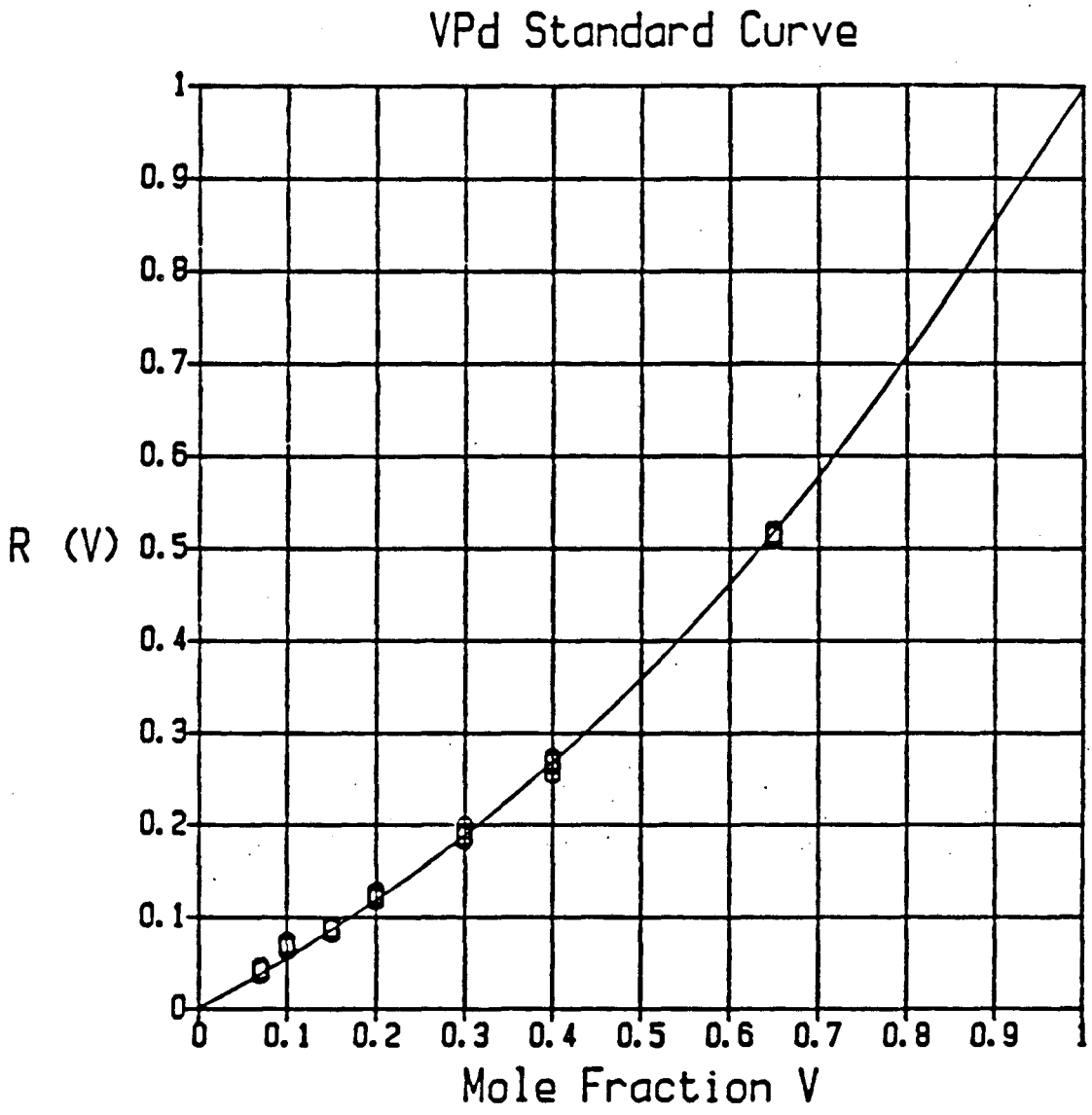

Figure 3-7

The relative intensity of the V(Kα) and Pd (Lα) peaks as a function of X_V in VPd alloys.

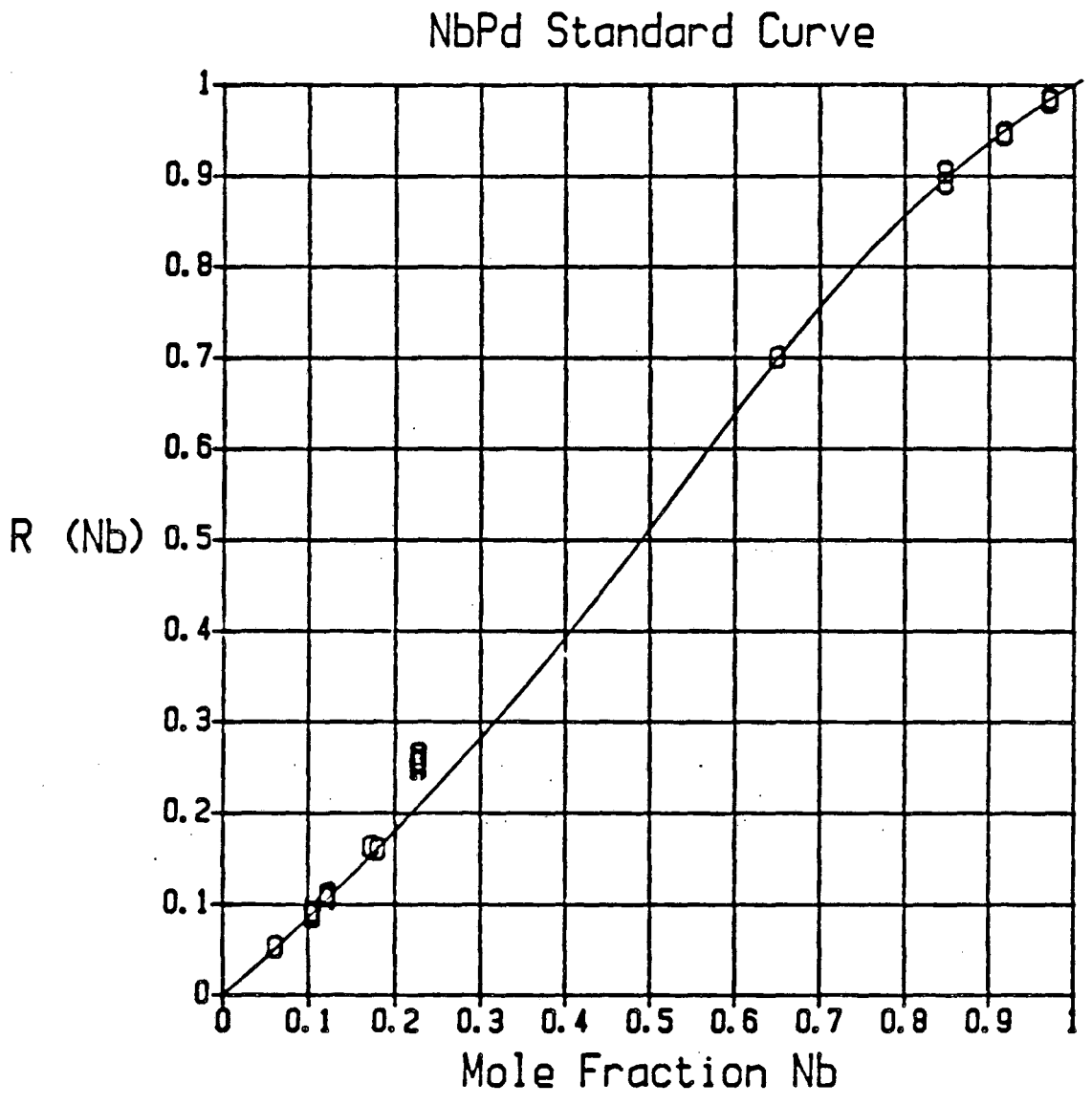

Figure 3-8

The relative intensity of the Nb(Lα) and Pd(Lα) peaks as a function of X_{Nb} in NbPd alloys.

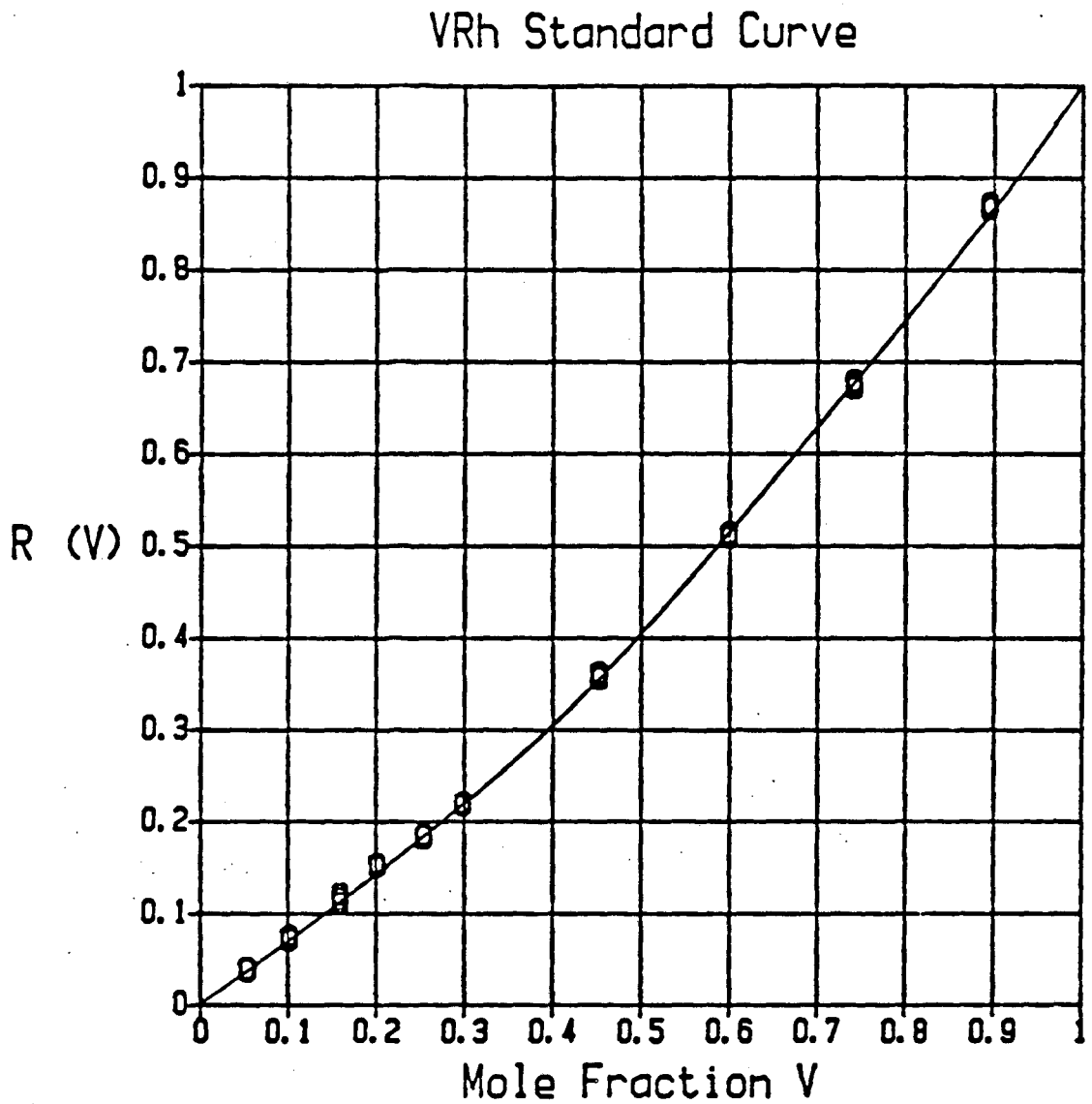

Figure 3-9

The relative intensity of the V(Kα) and Rh(Lα) peaks as a function of X_V in VRh alloys.

RESULTS

Melting Points

The Elements

The accuracy of the temperature measurements are checked by observing the melting points of the samples. Not all the samples were observable because they could not be positioned visibly through the end of the furnace. The melting points of the pure elements are used to determine the accuracy of the temperature measurements. The temperatures were measured with a Leeds and Northrup optical pyrometer. The calibration of the pyrometer and subsequent corrections due to the emissivity of the sighting source and transmittance of the furnace windows are described in the Temperature Measurements section of Chapter Three. The intermetallic alloys' melting points not only help verify the accuracy of the temperature measurements, but yield information about the solubility of carbon in these alloys and help verify the phase diagrams.

The melting points were determined by observing the rounding and collapsing of the samples. The temperatures were easily measured simultaneously because all the observations were taken through the optical pyrometer. Some of the observed temperatures are not specific values, but temperature ranges. Temperature ranges are reported when the melting process, from the time the sample started to round until it was not visible, lasted long enough to record an increase in the

temperature. Sometimes the melting was not observed. Then the highest temperature recorded before the sample melted and the lowest temperature after the sample melted are reported.

The most data was collected on the melting point of Palladium. Many runs were performed with elemental Pd because it is used to determine the Raoult Standard State to which many of the alloys are compared. Table 4-1 shows the observed melting temperatures of the Pd samples over a two year period. The temperature was increasing, usually about 5° per minute, during the measurements. The values probably are slightly higher and have a larger uncertainty than if melting point determinations were performed with a very slow temperature increase. The average observed melting temperature for Pd is 1780 K, with all of the values except one falling within ±12°. This small range of temperatures demonstrated the reproducibility of the temperature measurements throughout the time of the experiments and with the different heating tubes.

The reported melting point of pure Pd is 1825 K. The melting temperature is lowered to 1777 ±16 K[1,2,3] in contact with carbon because of the carbon solubility in the Pd. An eutectic is present in the binary phase diagram between Pd and C. The lower melting point of Pd represents the eutectic temperature found at the composition of the Pd having the greatest C solubility. This eutectic temperature agrees with the experimental results of this study.

Only one melting point determination was run for each of the other

elemental metals, also shown in Table 4-1. Rhodium melts at 2236 K. The melting point of Rh is lowered to 1967 ±17 K[1,2,3] in the presence of carbon. An eutectic is also present in the Rh - C binary phase diagram, similar to the Pd - C phase diagram. The measured temperature of 1930 to 1940 K is much lower than the melting point of pure Rh and close to the eutectic temperature.

Vanadium and Titanium both react with the graphite boat to form an intermediate carbide. The temperature observed for the disappearance of the alloy reflects the eutectic temperature of the reaction, and not the metal's melting point. The melting points of Ti and V are 1941 K and 2183 K, respectively.

The eutectic temperature in the V - C system is reported at 1903 K[4] and 1923 K[5,6]. The measured temperature range of 1940 to 1960 K is much lower than the melting point of V, and near the eutectic temperature. A higher temperature than the eutectic temperature, and an elapse of time between the onset (rounding of the sample) and the completion (collapsing of the sample) of melting are observed for V. These discrepancies are explained by the following argument. The V was still visible after part of it had begun to form a carbide layer. Due to the slower diffusion of the carbon through the carbide layer, part of the V does not react until after the furnace temperature has risen above the eutectic temperature, the temperature at which the reaction began. If the temperature could be held constant, lower readings agreeing with the literature values could be observed.

The eutectic temperature in the Ti - C system has been reported at 1918 K[7] and 1923 K[8], with an uncertainty of about 5°. There have been some reports of a possible peritectic,[9,10] instead of the eutectic, between the Ti and TiC phases, with an extrapolated peritectic temperature of 1973 K. The observed melting at 1956 K does not support the peritectic model even though it is slightly higher than the melting point of pure Ti. Systematic error in the temperature measurement should give a higher reading because of the time involved in the diffusion during the reaction and the constant increasing of the furnace temperature. An error of the same magnitude as seen with the V - C system would place the recorded Ti - C eutectic value close to the literature values of the eutectic temperature.

Overall, the temperature measurements of the elemental metals confirmed the accuracy and reliability of the pyrometric measurements.

Transition Metal Alloys

Melting point measurements were also taken for the intermetallic alloys. Because the accuracy of the pyrometric measurements are demonstrated with the elemental metals, the alloy data is used to check the reported binary phase diagrams. Table 4-2 gives the observed temperatures for the melting of the samples. Most of the alloys are not congruent melting phases. The temperature range between the reported solidus and liquidus or eutectic reaction and liquidus are listed for the non-congruent melting phases.

There is disagreement about the TiPd phase diagram. The Pd_4Ti phase which has been reported by some studies, is not found by others. Murray[11] gives a review of the many problems of the phase diagram. Table 4-2 lists the melting ranges for the TiPd alloys based on the phase diagram proposed by Murray[11] and another by Kubaschewski.[12,13]

The data from this study fits with the diagram proposed by Murray. The uncertainty of the temperatures should give experimental temperatures slightly higher than the true temperatures. The high Pd alloys (94% and 88% Pd - all alloy percents given in this report are atomic percents) melted at, or slightly above, the temperatures shown by Murray. The values reported by Kubaschewski were higher than the observed temperatures.. The agreement with Murray indicates that the Pd_4Ti phase is not present. A further complication that should be studied is the effect of the carbon solubility in these samples. The measured melting temperatures could have been lowered by the solubility of the carbon in the alloy, as in the pure Pd, and not reflect the true melting point of the TiPd alloy.

The data listed for VPd is the temperature range of the solidus to the liquidus between Pd and V_2Pd.[14] The experimental data matches the literature values. All the melting points are only a few degrees above the literature values, showing no lowering effect by the carbon present.

The data listed for NbPd is the temperature range of the solidus to the liquidus between Pd and $NbPd_3$.[15] All the data fits the phase diagram. The experimental temperatures fit within the given range or

are slightly higher. With neither the VPd or NbPd alloys showing any temperature-lowering effects from carbon solubility, the same is probably true for the TiPd system. The lower alloy temperatures are probably not caused by the carbon solubility in the alloy, but confirms the phase diagram by Murray. Less carbon solubility is expected for the alloys than for the pure Pd because of the strong acid-base reaction in the alloys.

The data listed for VRh is from Rh to $V_{0.44}Rh_{0.56}$ from the phase diagram by Waterstrat.[16] All the measured temperatures are significantly lower than those reported. The melting point of Rh is lowered by 250° by its solubility of carbon. This solubility effect is still apparant in the VRh alloys, lowering the melting points by at least 200° to 50° from the 90% Rh to the 70% Rh, respectively. The solubility of carbon is still significant in these alloys.

Vapor Pressure Measurements

Palladium

The emission intensities of Pd in the pure metal and the alloys were measured at 4087.34 Å and 4212.95 Å. The emission lines at 4087.34 Å and 4212.95 Å will be refered to as wavelength 1 and 2 throughout this paper. These lines were chosen because they are within the optimal range for the instrumentation, see Figure 3-4. Emission lines from C_2, C_3 and CN molecules were always present in the emission

spectra, interfering with the intensity of some of the Pd lines. The Pd lines that fell within the ranges of these coincidental emissions were not used. The relative pressures of the Pd vapor was calculated from the intensities by equation (2-12). A list of the temperatures, intensities and log of the calculated relative pressures of both Pd lines are given in Table 4-3 for over a two year period. The relationship between the log of the relative pressure and 1/T of each emission line is shown in Figures 4-1 and 4-2. The enthalpy of vaporization can be calculated from the slope.

There have been many vapor pressure studies made to determine the enthalpy of vaporization of Pd.[17] Many of the literature values for ΔH_{298} are 90 ±2 Kcal/mole with a spread from 80 to 103 Kcal/mole. The variation of ΔH_{vap} with temperature has given lower enthalpies at higher temperatures for most of these studies. All but two of the previously reported experiments have measured ΔH_{vap} over solid Pd, not determining the enthalpy for the liquid state. Only two reported studies were run with liquid Pd,[18] giving enthalpies of 96.43 and 83.96 Kcal/mole for the temperature ranges 1273 to 2223 K and 1828 to 2023 K, respectively.

The slope from the data for wavelength 1 gives an ΔH_{vap} of 90 Kcal/mole over the experimental temperature range. At a given temperature the data points have a scatter of ±0.1 for the log (P), allowing for an uncertainty of up to 20 Kcal/mole for the enthalpy. Even with this uncertainty, the calculated ΔH_{vap} is within the range of the other studies and provides confidence in the vapor pressure measurements of this study.

The vapor pressure measurements of wavelength 2 does not yield a linear line. The slope of the data points up to 2100 K are represented by a line with the same slope as the data of wavelength 1. After 2100 K the data points deviate from linearity decreasing the slope. The change in the data is assumed to be caused by self-absorption of the Pd emission.

Under self-absorbing conditions, emitted photons from some atoms of the emitting source are absorbed by other atoms. The self-absorbing conditions can occur when the vapor pressure of the emitting atoms are increased or the emission travels through a cold region of the vapors.[19] The emission from a self-absorbing source is less than would be measured if none of the photons were absorbed.

Because the emission intensity is greater for wavelength 2, the wavelength 2 emission undergos self-absorption while the wavelength 1 emission does not. Even though the absolute oscillator strengths of these emissions are not know, their relative strengths are known.[20] The oscillator strength of wavelength 2 is an order of magnitude greater, increasing its capacity for self-absorption.

Pd Alloys

Vapor pressure measurements were run for several Pd-rich intermetallic alloys. The emission intensity data and the log of the calculated relative pressures are shown in Tables 4-4, 4-5 and 4-6 for

TiPd, VPd and NbPd alloys, respectively. The relative pressures of each alloy are compared to pure Pd. The activity of the alloy is calculated by the relative difference in the log of the vapor pressure between the alloy and pure Pd. Representative plots of the log of the relative pressures for some alloys are shown in Figures 4-3 through 4-6.

The slope of the line for the alloys is not calculated from fitting the data of the log (P) vs 1/T graph. The slope is kept constant for all of the alloys, equal to the slope of the many data points of pure Pd. The scatter of the few data points run for each alloy does not yield a meaningful slope. Many more runs are needed to validate assigning a slope to the pressure data of the alloys. The main source of error is the uncertainty of the temperature measurements. A difference of 20° relates to a difference in the log of the pressure of 0.5. The lines for the alloys are made by estimating the best fit of a line with the same slope as Pd through the data points.

The vapor pressure data of the alloys does not always fit along the defined slope. Most often the data tended towards a less steep slope, indicating a lower value for ΔH_{vap} of the alloys than for Pd. Because of the acid-base reactions in the alloys, the ΔH_{vap} is expected to increase for the alloys. Additional self-absorption of the alloy emissions as compared to the pure Pd emissions may be the reason for the lower slope, as described below. The values of the relative pressure for the temperature range 2100 to 2300 K were more heavily weighted in determining placement of the line for wavelength 1. The emission intensity is low at temperatures less than 2100 K, introducing a large

uncertainty in the emission intensity measurements. The uncertainty of the temperature increases at higher temperatures (above 2300), along with the added possibilities of self-absorption. The self absorption of the Pd vapors at the cooler ends of the furnace would have a greater effect on the recorded intensities of the alloys than on the pure Pd. Because the pressure of the Pd vapor in the cooler ends of the furnace is independent of the composition of the alloy in the hot zone for a given temperature, the absorption would be a greater percent of the smaller alloy emmissions. The temperature range most heavily weighted for wavelength 2 is from 2000 to 2200 K, due to the higher intensity of the emission.

Rhodium

Vapor pressure measurements were also run with Rhodium metal. The emission intensities and log of relative pressures are shown in Table 4-7 for the 3700.91 Å and 4374.80 Å emission lines. The relative pressures calculated are not for the total Rh vapor population, but just for one excited state of the emission. A partition function was not calculated nor used to relate the pressure of the excited state to the whole population. The calculation of the activity of a Rh alloy is not affected. The Boltzmann distribution of all states of the Rh is constant for each temperature whether the Rh is a pure metal or alloy. The relative pressures of each state compared to the total vapor pressure at a constant temperature is therefore the same. Yet with the measurement of the population of only one state, the slope of the log (P) vs 1/T seen in Figure 4-7 is not the standard ΔH_{vap}.

VRh Alloys

Several vapor pressure measurements were made for the VRh alloy series. The values of the emission intensities and relative vapor pressures are shown in Table 4-8. Figure 4-8 shows the log of the relative pressures of alloys V-6 and V-7 compared to pure Rd. As in the case of Pd, the slope chosen to fit the alloy data is the best slope through the pure Rh measurements.

Carbide Equilibration

The composition of the alloys was analysed with a scanning electron microscope after the vapor pressure measurements. The compositions are determined by the relative intensities of characteristic X-ray emissions (R_A - defined in equation (3-4)) of the alloys' components. The relative X-ray intensities of the TiPd, VPd, NbPd and VRh alloys are shown in Tables 4-9 through 4-12, respectively.

Compositional changes are shown by a comparison of the relative X-ray intensities from the alloys after the vapor pressure run to the alloys before the run. Below the acid metal concentration which permits carbide formation, no changes were detected greater than ±1 atomic percent.

In alloys with carbide formation, the analytical results widely varied. The value of the relative X-ray intensities depended on whether the analysed area contained any carbide. The composition of the alloy in equilibrium with the carbide is determined by the lowest acid metal concentration measured. Figures 4-9 through 4-12 graphically demonstrate the determination of the equilibrium concentration.

The results of the carbide equilibration, along with previous determinations are shown in Table 4-13. The equilibration temperature used in this study varied near 2300 K. The exact value for each run can be found by noting the highest temperature used for that alloy's vapor pressure measurements. Gibson's[21] results show that within his uncertainty, the composition of the NbPd alloy in equilibrium with carbon does not change over a 100° range. Previous work[22] shows that the composition of the alloys do not vary more than four atomic percent from 1300 to 2300 K.

Activity Measurements

The activity of the base metal in an alloy is directly taken from the difference in the log of the pressures, as seen in equation (2-15). The activity coefficient is calculated using the equation,

$$\gamma_A = \alpha_A / X_A \qquad (4\text{-}1)$$

The activity and activity coefficient of the acid metal are also listed for the alloys in equilibrium with the carbide phase, from the data given in Table 2-4. Once the activity of the acid metal has been established for the cabide equilibration composition, the activity of the acid metal, from the equilibration compostion to infinite dilution of the acid metal, can be calculated with the Gibbs-Duhem relationship, using the base metal's activity data. The uncertainty in the log of the activity is large, about 0.05, due to the inherent uncertainties of this experimental method. Comparisons can still be made about the relative effectiveness of the acid-base reactions of the alloy combinations. Figure 4-13 shows the comparative effectiveness of TiPd and VPd alloys, Figure 4-14 shows the comparison of NbPd and VPd and Figure 4-15 shows V with the base metals Pd and Rh.

TiPd

Five samples are used in the titration curve of Ti with Pd. The data for the high Pd alloys (94% and 88% Pd) fell within the uncertainty of the pure Pd, having an activity close to unity. The activity of Pd dramatically decreases in the other samples. The sample originally starting at 75% Pd equilibrated with TiC to give the activity of Pd at 78.5% Pd.

Several vapor pressure measurements were taken with samples having a greater atomic percent of Ti. The data from these runs was used to confirm the composition of the alloy in equilibrium with the carbide, see Table 4-9. The maximum atomic emission intensity measurements from

these samples were the same as the 75% Pd sample, which is expected as these samples all reached the same equilibrium point. The data of the much higher Ti samples are not always reliable. Some of the vapor pressure measurements have low values, slowly increasing with time toward the 75% Pd value. This time dependent variation of the pressure is an effect of the compositional change of the sample towards the TiC equilibrated alloy.

Choudary et al.[23] have investigated the TiPd system by Knudsen cell mass spectrometry. Their temperature of investigation was 1875 K and the log of the activities of Pd were -0.42, -0.72, -1.81 and -2.31 for 85%, 75%, 60%, and 50% Pd, respectively. The extrapolated value for the log of the activity of Pd at 85% Pd in this study is about -0.35. This value is close to Choudary's value, especially considering the large uncertainty of the extrapolation due to the steep rise of the slope. The extrapolation of the log of the activity of Pd from this study to 75% Pd would be a value more negative than -1.0, much different from Choudary's reported value. The higher Pd activity measurements of Choudary could be from the reaction of the alloy with the graphite Knudsen cells in which the alloys were measured. A reaction between the alloy or sample vapor with the Knudsen cell would decrease the amount of Ti. The compositional increase in Pd gives higher Pd activity measurements. The Pd activity of the 75% Pd sample from the Knudsen cell experiments is still higher than the Pd activity from the alloy in equilibrium with the carbon from this study, but the agreement is closer.

VPd

Four samples are used to develope the VPd titration curve. The 90% Pd sample gave vapor pressure measurements very similar to pure Pd. The pressure of the Pd slowly decreased as the percent of Pd decreased in the samples. The titration curve of VPd has a much flatter variation than TiPd.

The extrapolation of the activity of Pd, assuming no drastic changes in the Ti and V titration curves, to $TiPd_3$ and VPd_3, gives a lower activity of Pd in the $TiPd_3$ alloy. Previous investigations have similarly shown the activity of Pd is lower in $ZrPd_3$ than $NbPd_3$ and in $HfPd_3$ than $TaPd_3$, see Table 1-1.

NbPd

Five samples were used in the vapor pressure studies of NbPd, yet only three gave reliable results used in the titration curve. The two samples with a Nb concentration large enough to form NbC wet the sample boat and crept over the sides coating the outside walls. NbC has a lower emissivity than carbon, giving lower temperature readings than the true temperature. Because of the uncertainty of trying to estimate the emissivity of the NbC coating formed within the center of the carbon heating tube, the results of the high Nb alloys were discarded. The alloys gave higher vapor pressure readings, which would be the appropriate direction for reading lower temperatures than the true temperatures.

The activity values are much lower in the Nb alloys than in the V alloys. This comparison is agreeable with the previous results that show a greater acid-base reaction in 4d elements than 3d elements, see Table 1-1. The Pd activities of the NbPd alloys show a general decrease with decreasing percent of Pd, without any drastic slope changes. This trend is similar to the V alloys, unlike the drastic Pd activity change in the Ti alloys.

Cima[24] and Gibson[21] have determined the activity of NbPd alloys by emf measurements and Knudsen cell vapor pressure measurements, respectively. Gibson directly measured the vapor pressure of Pd, while Cima measured the emf of Nb and used the Gibbs-Duhem relationship to calculate the activity of the Pd. They both measured the activity of the Pd in an alloy of 82% Pd, with Cima measuring an activity of 0.13 at 1000 K, and Gibson measuring an activity of 0.40 at 1515 K. The lowest Pd content that was measured in this study was 86% Pd with an activity of 0.18 at 2300 K. The extrapolated activity at 82% Pd would be around 0.1, well within the range of Cima's value, especially if a small positive entropy was assumed. Cima chose an excess entropy of -3 to -5 cal/deg/mole as a reasonable value. This choice fit his data with Gibson's data. A negative entropy would calculate the activity at the temperature of this study far greater than the measured activity. To fit his calorimetric results of TiPd with Choudary's mass spectrometric measurements, Kleppa[25] has suggested a small positive excess entropy of mixing for these intermetallic alloys.

VRh

Five alloy vapor pressure measurements are used to determine the VRh titration curve. The vapor pressure of the alloys from Rh down to 80% Rh are within the range of pure Rh. A slight decrease is noticed for 70% Rh. The sample starting at 55% Rh and equilibrating with carbon at 68% Rh has a much lower vapor pressure. The resultant titration curve of the VRh is much different than VPd, with having a high Rh section of very slight change in the Rh activity followed by a sharp decrease at 68% Rh.

A Solution Model

The regular solution model is a method to thermodynamically represent solutions that do not follow ideal behavior.[26] Solutions with large deviations due to acid-base reactions often are not well represented by a regular solution model. The regular solution model only accounts for positive deviations from ideality.

The excess partial molar Gibbs energy of a component in a solution can be represented by:

$$\Delta \overline{G}_A^{xs} = \Delta \overline{G}_A - RT \ln x_A \qquad (4\text{-}2)$$

where the partial molar Gibbs energy is related to the activity and the

activity coefficient.

$$\Delta \overline{G}_A = RT \ln \alpha_A = RT \ln \gamma_A x_A \qquad (4\text{-}3)$$

The substitution of equation (4-3) into (4-2) defines the excess partial molar Gibbs energy in terms of the activity coefficient.

$$\Delta \overline{G}_A^{xs} = RT \ln \gamma_A \qquad (4\text{-}4)$$

The regular solution model describes the excess partial molar Gibbs energy in terms of an interaction parameter, W, and the volume fraction of the second component. The interaction parameter is constant under the assumptions of a regular solution equation where the molal volumes are nearly equal for the two components and the volume fraction therefore equals the mole fraction: (1) the molecules of both components have equal volume, (2) the number of mearest molecules surrounding any molecule is the same in the pure components and in the solution, (3) the solution is random so that S^e is zero, and (4) ΔH of mixing is independent of temperature. To compensate for different molal volumes of the components, the regular solution equation has a cubic term.

$$\Delta \overline{G}_A^{xs} = W x_B^2 = bx_B^2 + cx_B^3 \qquad (4\text{-}5)$$

W is a function of X_B due to the different molal volumes of the components in these alloys. The square and cubic coefficients b and c can be calculated from the linear relation of W with composition as $W = b + cx_B$. From equations (4-4) and (4-5), the interaction parameter is

related to the activity coefficient.

$$RT \ln \gamma_A = W x_B^2 \qquad (4\text{-}6)$$

The data from this vapor pressure study determined log γ_A of the base metals of several Engel-Brewer alloys. The log γ_A is used to fit the data to the regular solution model.

$$\frac{\log_A \gamma}{x_B^2} = w \qquad (4\text{-}7)$$

where the interaction parameter is redefined as:

$$w = \frac{W}{RT\ 2.303} \qquad (4\text{-}8)$$

The interaction parameter w calculated for the data from TiPd, VPd and NbPd is shown in Table 4-15. The values of log γ_{Pd} less than 0.1 is not used to calculate w because of the relative high uncertainty compared to the absolute value.

A linear relation of the interaction parameter is calculated with respect to the composition of the alloys. A linear fit of the interaction parameter and coefficients b and c, are shown in Table 4-15. The calculated log γ_{Pd} from the estimated interaction parameter derived from the linear fit is also shown in Table 4-15.

The VPd and NbPd alloys behave similarly. In both cases the interaction parameter fit with a positive slope. All of the calculated

log γ_{Pd} fit within the uncertainty of the experimental values.

The fit of the interaction parameter for the TiPd alloys has a negative slope. The fit of the calculated log γ_{Pd} values is not as good as for the V or Nb alloys. The linear approximation especially overestimates the log γ_{Pd} for the alloy at 88% Pd. No fit is attempted with the VRh data, with only one log γ_{Pd} value over 0.1. A negative slope for the interaction parameter approximation would be expected because of the great change in the slope similar to the TiPd alloys.

Discussion of Results

The comparisons of the thermodynamics of binary Engel-Brewer alloys at the base-rich end give insight into the major factors controlling the acid-base reaction. The comparison of VPd and VRh express the same relationship Cima found between NbPd and NbRh. Pd has two electron pairs to donate. Due to the crystal field effect the pairs are not equally extended from the closed shell. The further extended pair of electrons of Pd is easily donated to V. The activity of Pd in the V alloys is lowered compared to the Rh activity in the base-rich alloys because of this donation. In the very Rh-rich alloys, the lone electron pair is held tighter than the most extended Pd electron pair. At lower base concentrations, the Rh activity dramatically decreases. Because of a larger nuclear charge, the most contracted electron pair of the Pd is held tighter than the most contracted pair on the Rh. The most

contracted pair of electrons of the Pd is therefore not very effective for acid-base donation. The Rh is a better base than the Pd at these concentrations where only one electron pair is donated.

The greater acidity of Ti than V with Pd is explained by the number of empty d orbitals available for bonding and the difference in nuclear charges. Ti has two empty d orbitals available for accepting electrons, compared to the one empty d orbital of V. At the high base concentrations used within this study, all of the available orbitals are assumed to be useful in accepting electron pairs. This extra empty orbital allows Ti to accept twice as many electron pairs than V, increasing its acidic capabilities. The larger nuclear charge on the V contracts its empty orbital more than the empty orbitals on the Ti, again enhancing the acidity of Ti compared to V.

The crystal field effect also affects the acidity of the orbitals. With four d electrons, the empty orbital of V is the highest energy orbital, contributing the least to the stability of the alloy when bonding. With only three d electrons, Ti has two available orbitals for bonding. Not only is the highest energy orbital available for accepting electron pairs, but the second highest orbital is still available. The crystal field effect enhances the acidity of the Ti by allowing its orbitals, that are available to accept electron pairs, have a greater effect than the highest V orbital.

In accordance with the previous results cited in Table 1-1, the 4d elements have a greater acid-base effect than the 3d elements. The NbPd

alloys measured in this study consistantly have a lower Pd activity than the VPd alloys.

The data in this study confirms the qualitative factors effecting the acid-base reaction. Similar studies should be run to further verify these results. ZrPd alloy data would be helpful in describing the difference in the acid-base reaction in the cases where one or two accepting orbitals are present. ZrPd with two empty orbitals like Ti may follow the titration curve of TiPd with a drastic change in slope, unlike the more gradual curves of VPd and NbPd. The measurement of the quantitative difference between 3d and 4d alloys would also be possible with both the comparisons of NbPd with VPd and ZrPd with TiPd. With the high vapor pressure of Pd, and the sensitivity of the emission measurements, vapor pressure measurements of the 5d alloys may also be possible. The extension of the compositional range of the Rh alloy before the carbide formation, compared to Pd alloys, make them attractive for further study. Further investigations of new sample holder materials to prevent the formation of intermediate compounds, such as the carbide compounds in this study, would enable the investigation of a larger section of the titration curve.

The data from this vapor pressure study is described by a regular solution equation, see Table 4-15. The opposite sign of the cubic coefficient between the TiPd and VPd or NbPd alloys indicates a difference between these reactions at high base concentrations. Yet the large uncertainty of the Pd activity has to be considered when deriving any conclusions from the solution equations. Even if the regular

solution equations adequately describe the Pd activity at high Pd concentrations, the equations do not describe the activity at lower base metal concentrations. For example, the large positive cubic coefficients of VPd and NbPd alloys increase the Pd activity at lower Pd concentrations. The Pd activity would be greater than unity for alloys with atomic percents of Pd less than 61% Pd and 56% Pd for VPd and NbPd, respectively.

Hopefully, with more data, a solution equation will be developed to model the acid-base reaction. Thermodynamic investigations are needed throughout the whole composition range of the alloys. Because of the high refractory properties of the Engel-Brewer alloys, experimental methods are difficult and limited. The complimentary work of emf measurements, compound equilibration, vapor pressure measurements and calorimetry are needed to confirm the correct thermodynamic properties.

References

1 Nadler, M. R. and Kempter, C. P., J. Phys. Chem., 64, 1468 (1960)

2 D., A. S., Plat. Metals Rev., 8, (3), 101 (1964)

3 Raub, E. and Falkenburg, G., Z. Metallkd., 55, (4), 186 (1964)

4 Adelsberg, L. M. and Cadoff, L. H., J. Am. Ceram. Soc., 51, (4), 213 (1968)

5 Rudy, E., et al., Planseeber. Pulvermetall., 16, 3 (1968)

6 Carlson, N. O., et al., Bull. Alloy Phase Diag., 6, (2), 114, (1985)

7 Rudy, E., et al., "Ternary Phase Equilibria in Transition Metal-Boron-Carbon-Silicon Systems: Technical Report #AFML-TR-65-2, Part I, Vol. II", 7 (1965)

8 Bickerdike, R. L. and Hughes, G., J. Less-Common Met., 1, 42 (1959)

9 Cadoff, I. and Nielsen, J. P., J. Met., 5, (2), 248 (1953)

10 Kurnakov, N. N. and Troneva, M. Ya., Russ. J. Inorg. Chem., 6, (6), 690 (1961)

11 Murray, J. L., Bull. Alloy Phase Diag., 3, (3), 321 (1982)

12 Kubaschewski, O., in "Atomic Energy Review; Spec. Issue No. 9", Kubaschewski, O., ed. 137 (1983)

13 Raub, E. and Roeschel, E., Z. Metallkd., 59, (2), 112 (1968)

14 Koster, Von W. and Haehl, W-D., Z. Mettalkd., 49 (12), 647 (1958)

15 Giessen, B. C., et al., Met. Trans. A, 11A, 709 (1980)

16 Waterstrat, R. M. and Manuszewski, R. C., J. Less Common Met., 52, 293 (1977)

17 Alcock, C. B. and Hooper, G. W., Proc. Roy. Soc. (London), A254, 551 (1960); Dreger, L. H. and Margrave, J. L., J. Phys. Chem., 64, 1323 (1960); Haefling, J. F. and Daane, A. H., Trans. Met. Soc. AIME, 212, 115 (1958); Hampson, R. F. and Walker, R. F., J. Res. Natl. Bur. Std., 66A, 177 (1962); Norman, J. H., et al., J. Phys. Chem., 69, (4), 1373 (1965); Zavitsanos, P. D., J. Phys. Chem., 68, (10), 2899 (1964)

18 Taberko, A. V., et al., Russ. J. Phys. Chem., 51, (1), 164 (1977) Chegodaev, A. I., et al., Russ. J. Phys. Chem., 52, (8), 1229 (1978)

19 Cowan, R. D. and Deike, G. H., Rev. Mod. Phys., 20, (2), 418 (1948)

20 Corliss, C. and Bozman, W., NBS Monograph, #53 (1963)

21 Gibson, J. K., Ph.D. Thesis, Univ. of Cal., Berkeley, (1983)

22 Holleck, H., Metall., 37, (7), 703 (1983)

23 Choudary, U. V., et al., Met. Trans. A, 8A, 1487 (1977)

24 Cima, M., Ph.D. Thesis, Univ. of Cal., Berkeley, (1986)

25 Topor, L. and Kleppa, O. J., Z. Metallkd., 77, (10), 633 (1986)

26 Scatchard, G., Chem. Rev., 8, 321 (1931)

TABLE 4-1

Observed Eutectic Temperatures for the Pure Metals

Date	Observed Temperature (K)	Reference Temperature & Source	
Pd			
5/13/85	1788		
5/14	1804		
5/23	1783		
5/31	1768		
6/04	1788		
11/04	1788		
2/01/86	1783	1777 ±16	Ref. (1)
2/19	1793		
4/17	1778	1777 ±16	Ref. (2)
4/26	1768		
5/04	1783	1777 ±16	Ref. (3)
6/16	1786		
6/27	1779		
7/11	1780		
11/11	1781		
1/14/87	1778		
2/16	1773		
Rh			
		1967 ±17	Ref. (1)
10/9/86	1931 to 1940	1967 ±17	Ref. (2)
		1967 ±17	Ref. (3)
Ti			
		1918	Ref. (7)
2/4/86	1956	1923	Ref. (8)
		1973	Ref. (9)
V			
		1903	Ref. (4)
11/7/86	1941 to 1961	1923	Ref. (5)
		1923	Ref. (6)

TABLE 4-2

Observed Melting Points for the Binary Alloys

Alloy	Observed Temperature (K)	Reference Temperature & Source	
TiPd		Ref. (11)	Ref. (12)
94% Pd	1765 1766	1730 - 1750	1780 - 1800
88% Pd	1692 to 1732 1727	1680 - 1700	1727 - 1763
81% Pd	1721 1705	1700 - 1740	1710 - 1727
80% Pd	1737 to 1753	1720 - 1730	1725 - 1755
75% Pd	1820 to 1828 1808 to 1818	1810	1665 - 1754
70% Pd	1758 to 1824	1670 - 1770	1665 - 1760
65% Pd	1712 1685	1620 - 1690	1665 - 1782
55% Pd	1676 to 1681	1550 - 1590	1665 - 1719

VPd		Ref. (14)
95% Pd	1737 to 1747	1710 - 1735
90% Pd	1636 to 1737	1690 - 1700
85% Pd	1692 to 1699 1694	1670 - 1690
70% Pd	1702	1650 - 1670

TABLE 4-2 continued

Observed Melting Points for the Binary Alloys

Alloy	Observed Temperature (K)	References Temperature & Source
NbPd		Ref. (15)
94% Pd	1829 to 1841	1830 - 1850
89.5% Pd	1862	1860 - 1880
87.5% Pd	1895 to 1900	1850 - 1870
83% Pd	1907	1870 - 1890
77% Pd	1931 to 1950	1890
VRh		Ref. (16)
90% Rh	1950	2150 - 2180
80% Rh	1941	2010 - 2130
75% Rh	1900 to 1910	2010 - 2080
70% Rh	1880 to 1900	1930 - 2010
55% Rh	1808 to 1839	1830 - 1880

TABLE 4-3

Emission Intensities — Log of Relative Pressure

PURE PD

Wavelength 1	4087 Å	Wavelength 2	4212 Å
Energy Level	36181 Cm^{-1}	Energy Level	35451 Cm^{-1}
Degeneracy	3	Degeneracy	7

Date	Temperature K	1/T	Wavelength 1 Intensity (mV)	Wavelength 1 Log P (relative)	Wavelength 2 Intensity (mV)	Wavelength 2 Log P (relative)
3/17/86	1951	5.13	-	-	3	14.30
	2032	4.92	1.75	14.24	15	14.58
	2092	4.78	6.5	14.51	48	14.79
	2157	4.64	25	14.79	140	14.96
	2255	4.43	120	15.04	390	14.98
3/25/86	1966	5.09	-	-	4.5	14.40
	2036	4.91	2.0	14.28	17.5	14.63
	2136	4.68	16.5	14.70	102	14.91
	2225	4.49	85	15.02	315	15.01
	2347	4.26	390	15.19	960	15.02
4/7/86	1991	5.02	0.5	13.91	5	14.31
	2055	4.87	2.0	14.18	18.5	14.56
	2124	4.71	10	14.54	72	14.82
	2213	4.52	57	14.89	277	15.01
	2279	4.39	160	15.07	545	15.03
4/26/86	1952	5.12	-	-	2.5	14.22
	2043	4.98	2	14.24	20.5	14.66
	2135	4.69	12	14.57	96	14.89
	2228	4.49	64	14.88	350	15.05
5/4/86	1951	5.13	-	-	2	14.13
	2010	4.98	0.75	13.99	10	14.52
	2091	4.78	7	14.54	57	14.87
	2197	4.55	50	14.91	245	15.02
	2288	4.37	190	15.11	620	15.05
6/27/86	2012	4.97	1	14.10	13.5	14.64
	2114	4.73	12	14.67	93	14.98
	2185	4.58	48	14.94	230	15.05
	2279	4.39	200	15.17	670	15.12

TABLE 4-3 continued

Date	Temperature K	1/T	Wavelength 1 Intensity (mV)	Wavelength 1 Log P (relative)	Wavelength 2 Intensity (mV)	Wavelength 2 Log P (relative)
7/11/86	1983	5.04	0.5	13.95	6.5	14.47
	2058	4.86	3.5	14.41	33	14.79
	2137	4.68	18	14.74	118	14.97
	2205	4.54	60	14.95	260	15.02
11/11/86	1982	5.05	0.5	13.96	6.5	14.48
	2084	4.80	7	14.58	53	14.87
	2155	4.64	28	14.84	147	14.99
	2218	4.51	90	15.07	340	15.08
	2308	4.33	310	15.24	780	15.08
6/16/86	2009	4.98	-	-	12	14.60
	2087	4.79	5.5	14.46	47	14.80
	2174	4.60	37	14.88	190	15.01
	2234	4.48	85	14.98	380	15.06
	2312	4.33	285	15.51	860	15.10
1/14/87	1982	5.05	-	-	5	14.36
	2058	4.86	3	14.34	23	14.63
	2142	4.67	15	14.63	100	14.88
	2237	4.47	80	14.94	340	15.00
2/16/87	2066	4.84	2.5	14.22	24	14.61
	2159	4.63	15	14.55	108	14.83
	2249	4.45	65	14.80	300	14.89

TABLE 4-4

Emission Intensities — Log of Relative Pressure

TiPd Alloys

Wavelength 1	4087 Å	Wavelength 2	4212 Å
Energy Level	36181 Cm^{-1}	Energy Level	35451 Cm^{-1}
Degeneracy	3	Degeneracy	7

Alloy	Temperature K	1/T	Wavelength 1 Intensity (mV)	Wavelength 1 Log P (relative)	Wavelength 2 Intensity (mV)	Wavelength 2 Log P (relative)
94% Pd	2020	4.95	1	14.06	10	14.46
F-2,1	2116	4.73	7	14.42	57	14.75
	2191	4.57	21	14.56	150	14.84
	2284	4.38	86	14.78	420	14.90
F-2,2	1946	5.14	-	-	2	14.16
	2035	4.92	1.5	14.16	16	14.59
	2124	4.71	10	14.54	76	14.84
	2216	4.51	50	14.83	255	14.96
	2339	4.28	265	15.05	800	14.97
88% Pd	2031	4.93	2	14.30	17	14.64
F-4,1	2094	4.78	5	14.38	48	14.78
	2150	4.65	13	14.53	96	14.82
	2246	4.45	53	14.72	277	14.87
F-4,2	2044	4.89	3	14.41	27	14.77
	2144	4.67	15.5	14.64	105	14.87
	211	4.52	42	14.77	218	14.91
	2268	4.41	88	14.85	395	14.94
81% Pd	1993	5.02	-	-	2	13.91
F-5,1	2086	4.80	1.5	13.90	10	14.14
	2144	4.67	3	13.92	32	14.37
	2224	4.50	13	14.21	108	14.55
	2302	4.34	44	14.42	320	14.71
F-5,2	1938	5.16	-	-	1	13.90
	2005	4.99	-	-	2.5	13.94
	2105	4.75	1.5	13.81	16	14.25
	2196	4.55	9.5	14.19	83	14.56
	2323	4.31	61	14.48	390	14.72

TABLE 4-4 continued

Alloy	Temperature K	1/T	Wavelength 1 Intensity (mV)	Wavelength 1 Log P (relative)	Wavelength 2 Intensity (mV)	Wavelength 2 Log P (relative)
80% Pd	2035	4.92	-	-	2	13.69
J-2,1	2099	4.76	0.5	13.56	6	13.85
	2162	4.63	2.5	13.76	25	14.18
	2219	4.51	8	14.02	67	14.37
	2272	4.40	25	14.29	177	14.57
J-2,2	2104	4.75	1	13.64	9	14.01
	2194	4.56	7.5	14.10	56.5	14.40
	2249	4.45	17.5	14.23	137	14.55
	2331	4.29	91	14.62	445	14.74
75% Pd	2042	4.90	0.5	13.64	6	14.13
J-3,1	2105	4.75	2	13.93	20	14.35
	2192	4.56	4	13.83	40	14.26
	2287	4.37	20	14.13	160	14.47
J-3,2	1996	5.01	-	-	1.5	13.76
	2099	4.77	2	13.96	16	14.28
	2206	4.53	5	13.87	49	14.29
	2267	4.41	14	14.06	126	14.44
	2331	4.29	44	14.30	325	14.61

TABLE 4-5

Emission Intensities — Log of Relative Pressure

VPd Alloys

Wavelength 1	4087 Å	Wavelength 2	4212 Å
Energy Level	36181 Cm^{-1}	Energy Level	35451 Cm^{-1}
Degeneracy	3	Degeneracy	7

Alloy	Temperature K	1/T	Wavelength 1 Intensity (mV)	Wavelength 1 Log P (relative)	Wavelength 2 Intensity (mV)	Wavelength 2 Log P (relative)
95% Pd	2023	4.94	1	14.04	11	14.49
V-11,1	2056	4.80	3.5	14.42	34	14.81
	2155	4.64	13	14.51	94	14.79
	2240	4.47	54	14.76	275	14.89
90% Pd	1990	5.03	-	-	7	14.47
V-1,1	2092	4.78	-	-	36	14.66
	2152	4.65	11	14.45	76	14.71
	2235	4.48	42	14.67	235	14.85
85% Pd	1989	5.03	-	-	5	14.32
V-2,1	2079	4.81	2	14.06	19	14.45
	2175	4.60	11.5	14.37	120	14.81
	2265	4.41	51	14.63	335	14.88
V-2,2	1997	5.01	-	-	5.5	14.32
	2089	4.79	3	14.19	28	14.57
	2143	4.67	7	14.3	66	14.69
	2213	4.52	28	14.59	180	14.82
80% Pd	2044	4.89	-	-	7	14.19
V-3,1	2104	4.75	2	13.94	24.5	14.44
	2166	4.62	9	14.30	70	14.61
	2224	4.50	22	14.44	205	14.83

TABLE 4-6

Emission Intensities — Log of Relative Pressure

NbPd Alloys

Wavelength 1	4087 Å	Wavelength 2	4212 Å
Energy Level	36181 Cm^{-1}	Energy Level	35451 Cm^{-1}
Degeneracy	3	Degeneracy	7

Alloy	Temperature K	1/T	Wavelength 1 Intensity (mV)	Wavelength 1 Log P (relative)	Wavelength 2 Intensity (mV)	Wavelength 2 Log P (relative)
94% Pd	2043	4.90	1.5	14.11	16	14.55
N-1,1	2117	4.72	7	14.42	59	14.76
	2194	4.56	23	14.58	146	14.81
	2238	4.47	55	14.77	285	14.92
89.5% Pd	2035	4.92	0.5	13.68	7	14.23
N-2,1	2101	4.76	2.5	14.05	25	14.46
	2188	4.57	14	14.40	110	14.71
	2273	4.40	42	14.51	275	14.76
87.5% Pd	2095	4.77	1	13.68	11	14.14
N-3,1	2155	4.64	4	14.00	39	14.41
	2247	4.45	24	14.38	180	14.68
83% Pd	2020	4.95	-	-	9	14.42
N-5,1	2094	4.78	4	14.29	37	14.67
	2164	4.62	20	14.66	124	14.87
	2256	4.43	100	14.96	390	14.98
77% Pd	1982	5.05	-	-	2.5	14.06
N-7,1	2095	4.77	5.5	14.42	48	14.78
	2185	4.58	34	14.79	195	14.98
	2282	4.38	170	15.08	620	15.08

TABLE 4-7

Emission Intensities — Log of Relative Pressure

PURE Rh

Wavelength 1 3701 Å Wavelength 2 4375 Å

Date	Temperature K	1/T	Wavelength 1 Intensity (mV)	Wavelength 1 Log P (relative)	Wavelength 2 Intensity (mV)	Wavelength 2 Log P (relative)
10/11/86	2150	4.65	10	4.33	8	4.24
	2245	4.45	36	4.91	92	5.32
	2329	4.29	96	5.35	380	5.95
10/22/86	2038	4.91	0.5	3.01	1	3.31
	2104	4.75	4	3.93	4	3.93
	2206	4.53	19	4.62	32	4.85
	2262	4.42	54	5.09	94	5.33
	2318	4.31	72	5.22	260	5.78

TABLE 4-8

Emission Intensities — Log of Relative Pressure

VRh Alloys

Wavelength 1 3701 Å Wavelength 2 4375 Å

alloy	Temperature K	1/T	Wavelength 1 Intensity (mV)	Wavelength 1 Log P (relative)	Wavelength 2 Intensity (mV)	Wavelength 2 Log P (relative)
90% Rh	2114	4.73	5	4.02	6	4.10
VR-2,1	2247	4.45	30	4.83	66	5.17
	2339	4.28	74	5.24	250	5.77
80% Rh	2074	4.82	2.5	3.71	2.5	3.71
VR-4,1	2144	4.66	8.5	4.26	11	4.37
	2232	4.48	29	4.81	63	5.15
	2334	4.28	92	5.33	335	5.89
75% Rh	2089	4.79	2.5	3.72	2	3.62
VR-5,1	2181	4.59	13	4.45	18	4.59
	2249	4.45	30	4.83	68	5.18
	2303	4.34	56	5.11	170	5.59
70% Rh	2086	4.79	2	3.62	2	3.62
VR-6,1	2186	4.57	12	4.42	16	4.54
	2268	4.41	35	4.90	74	5.22
	2319	4.31	66	5.18	220	5.71
55% Rh	2129	4.70	1.5	3.50	1.5	3.50
VR-7,1	2211	4.52	6	4.12	5	4.04
	2329	4.29	34	4.90	45	5.02

TABLE 4-9

EDAX Results for Alloys After Vapor Pressure Measurements

TiPd

Alloy	R_{Ti}	Alloy	R_{Ti}
F-2,1A	0.036	F-2,2A	0.044
B	0.035	B	0.040
		C	0.040
		D	0.042
F-4,1A	0.076	F-4,2A	0.079
B	0.076	B	0.076
		C	0.078
		D	0.079
		E	0.080
F-5,1A	0.124	F-5,2A	0.101
B	0.119	B	0.100
C	0.108	C	0.126
		D	0.110
J-2,1A	0.122	J-2,2A	0.131
B	0.121	B	0.134
C	0.114	C	0.137
D	0.117	D	0.118
E	0.119	E	0.130
		F	0.125
J-3,1A	0.129	J-4,1A	0.161
B	0.132	B	0.286
C	0.133	C	0.577
D	0.706	D	0.156
E	0.140	E	0.154
F	0.508	F	0.152
G	0.142	G	0.151
H	0.850	H	1.000
J-5,1A	0.200	J-5,2A	0.202
B	0.990	B	0.188
C	0.161	C	0.176
D	0.179	D	0.378
E	0.212		
J-6,1A	0.145	J-6,2A	0.132
B	0.153	B	0.131
C	0.148	C	0.997

TABLE 4-10

EDAX Results for Alloys After Vapor Pressure Measurements

VPd

Alloys	R_V	Alloys	R_V
V-11,1A	0.049	V-1,1A	0.078
B	0.046	B	0.081
C	0.046	C	0.076
D	0.047		
V-2,1A	0.107	V-3,1A	0.111
B	0.103	B	0.114
C	0.103	C	0.110
D	0.102	D	0.327
E	0.098	E	0.110
F	0.097	F	0.886
G	0.099	G	0.107
V-5,1A	0.169		
B	0.112		
C	0.122		
D	1.000		
E	0.113		
F	0.114		
G	0.110		

TABLE 4-11

EDAX Results for Alloys After Vapor Pressure Measurements

NbPd

Alloy	R_{Nb}
N-2,1A	0.093
B	0.099
C	0.099
D	0.102
N-7,1A	0.932
B	0.148
C	0.144
D	0.141
E	0.154

TABLE 4-12

EDAX Results for Alloys After Vapor Pressure Measurements

VRh

Alloy	R_V
VR-2,1A	0.066
B	0.065
C	0.067
VR-7,1A	0.245
B	0.412
C	0.439
D	0.214
E	0.275

TABLE 4-13

Carbide Equilibration Results

Alloy	Atomic Percent Base Metal	Temperature (K)	Reference Source
TiPd	78.5%	2300	This Study
	75%	1300	Ref. (22)
VPd	81.5%	2300	This Study
	80%	1300	Ref. (22)
NbPd	84%	2300	This Study
	85%	2321	Ref. (21)
	84%	2268	Ref. (21)
	84%	2331	Ref. (21)
	85%	1300	Ref. (22)
VRh	68%	2300	This Study

TABLE 4-14

Base Metal Activity from Vapor Pressure Measurements

Alloy	Atomic Percent Base Metal	- log (α) Base Metal	Activity Base Metal	Activity Acid Metal	- log (γ) Base Metal
TiPd	94%	0.05	0.89		0.10
	88%	0.00	1.00		-0.05
	81%	0.68	0.21		0.59
	80%	0.84	0.14		0.74
	78.5%	0.99	0.10	2.3×10^{-4}	0.84
VPd	95%	0.09	0.81		0.06
	90%	0.23	0.59		0.18
	85%	0.41	0.39		0.34
	81.5%	0.50	0.32	6.0×10^{-3}	0.41
NbPd	94%	0.14	0.72		0.12
	89.5%	0.46	0.35		0.41
	87.5%	0.71	0.19	6.6×10^{-4}	0.64
VRh	90%	0.00	1.00		-0.04
	80%	0.00	1.00		-0.09
	75%	0.05	0.89		-0.07
	70%	0.16	0.69		0.01
	68%	0.62	0.24	6.0×10^{-3}	0.45

TABLE 4-15

Regular Solution Model

Alloy	b	c	Solution Equation
TiPd	3.7	-108	$\log_A \gamma = 3.7x^2 + -108x^3$
VPd	- 25.8	75	$\log_A \gamma = -25.8x^2 + 75x^3$
NbPd	- 47.0	112	$\log_A \gamma = -47x^2 + 112x^3$

Alloy	Percent Base Metal	- log (γ) (Vap. P.)	$w_{calc.}$ from γ	$w_{best\ fit}$ from Regular Solution Eq.	- log (γ)
TiPd	94%	0.02		-3	0.01
	88%	-0.05		-9	0.13
	81%	0.59	-16.3	-17	0.61
	80%	0.74	-18.5	-18	0.72
	78.5%	0.88	-19.0	-19.5	0.90
VPd	93%	0.06		-20.5	0.10
	90%	0.18	-18	-18	0.18
	85%	0.34	-15	-14.5	0.33
	81.5%	0.41	-12	-12	0.41
NbPd	94%	0.12	-48	-41.5	0.10
	89.5%	0.41	-34	-35	0.42
	87.5%	0.64	-33	-31	0.61
	84%			-29	0.74
	82%			-27	0.87

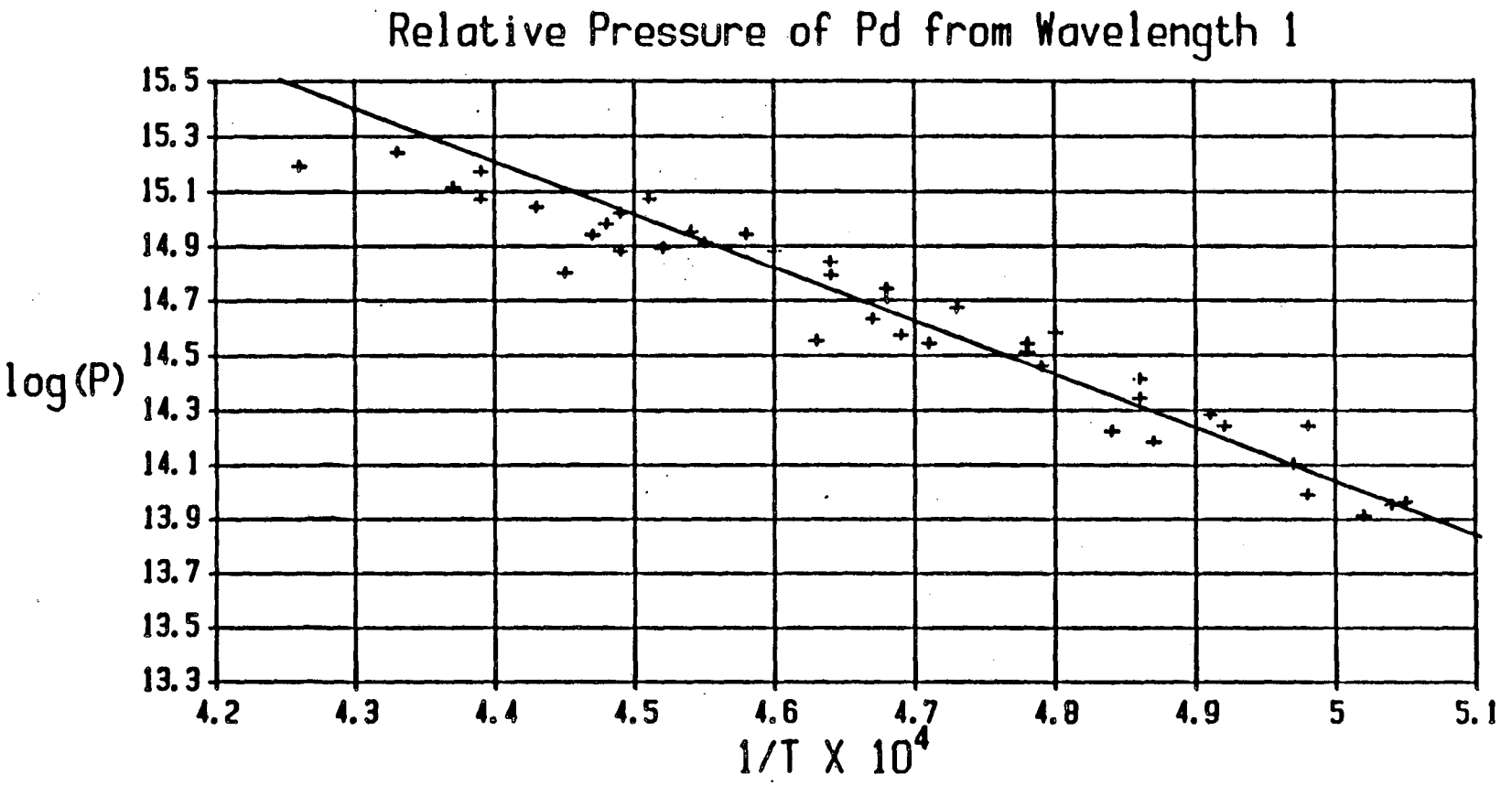

Figure 4-1

The relative pressure of Pd from emission data of wavelength 1, calculated by equation (2-12) is shown. The slope of the linear relation corresponds to an enthalpy of vaporization of 90 Kcal/mole.

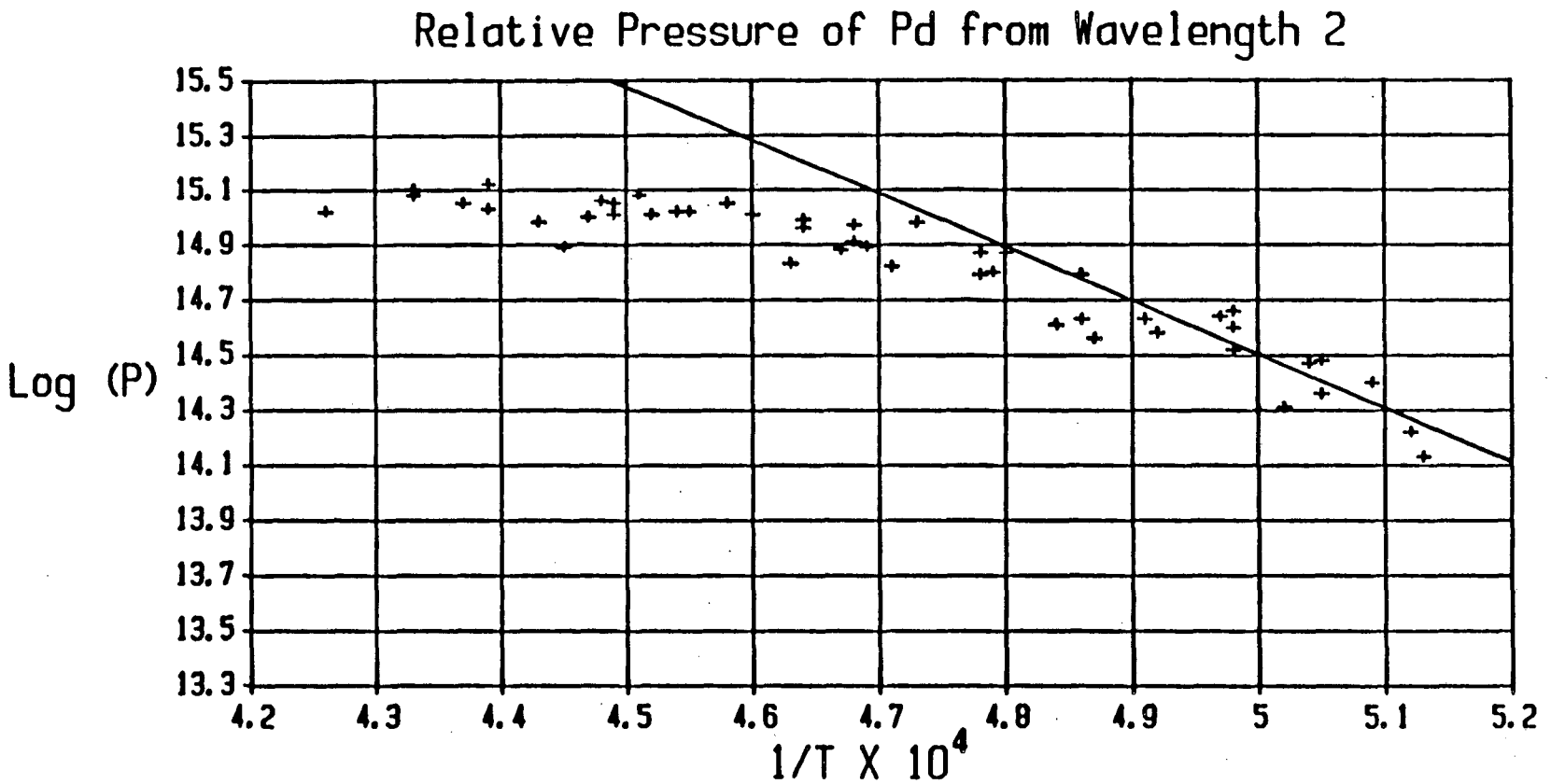

Figure 4-2

The relative pressure of Pd from emission data of wavelength 2, calculated by equation (2-12) is shown. The slope of the linear relation corresponds to an enthalpy of vaporization of 90 Kcal/mole.

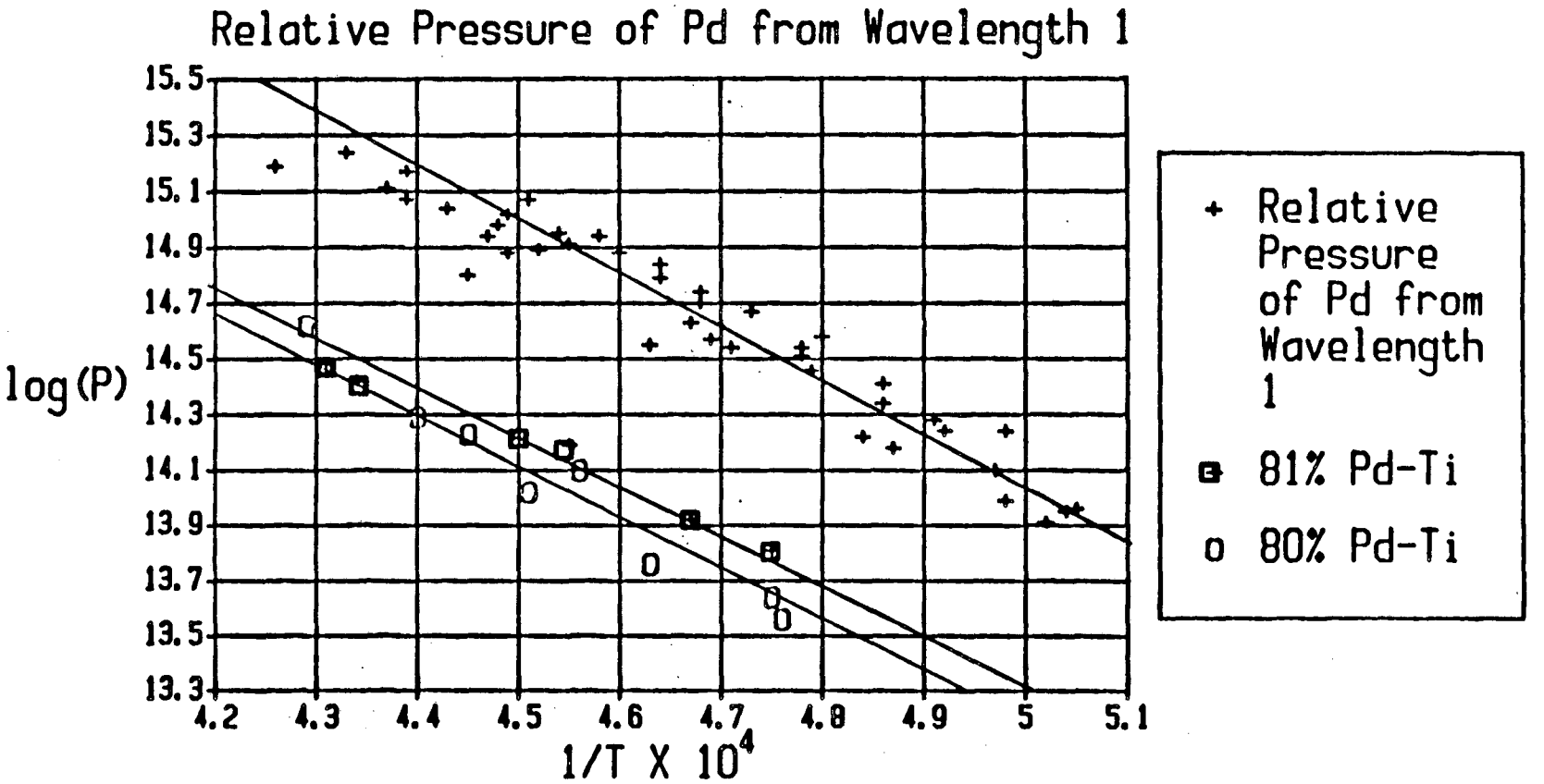

Figure 4-3

The relative vapor pressure of pure Pd is compared to TiPd alloys. The differences in the vapor pressures correspond to activities of 0.21 and 0.14 for 81% Pd and 80% Pd alloys, respectively.

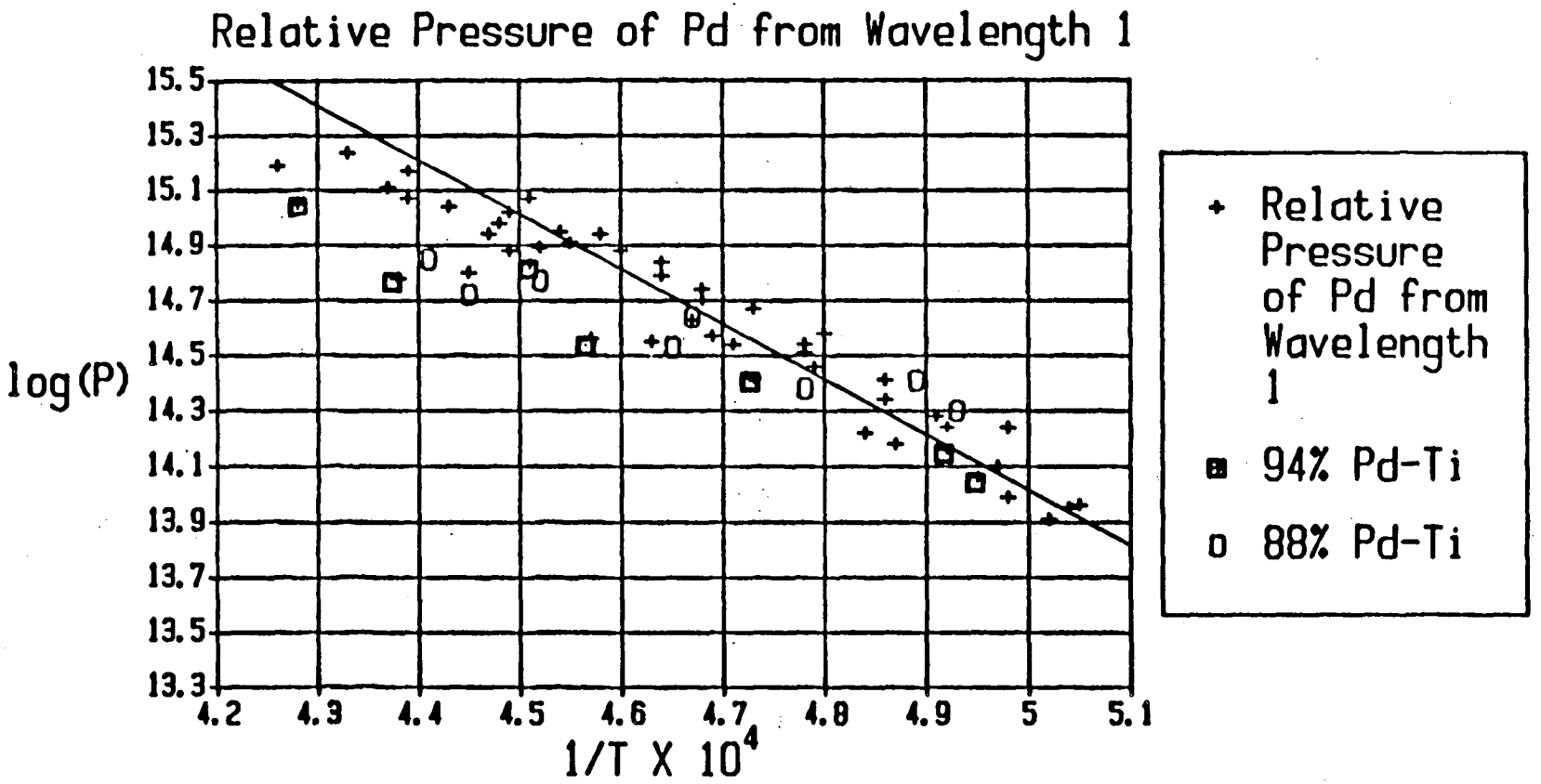

Figure 4-4

The relative vapor pressure of pure Pd is compared to TiPd alloys. The the vapor pressures of the 94% Pd and 88% Pd alloys lie within the uncertainty of the pure Pd values.

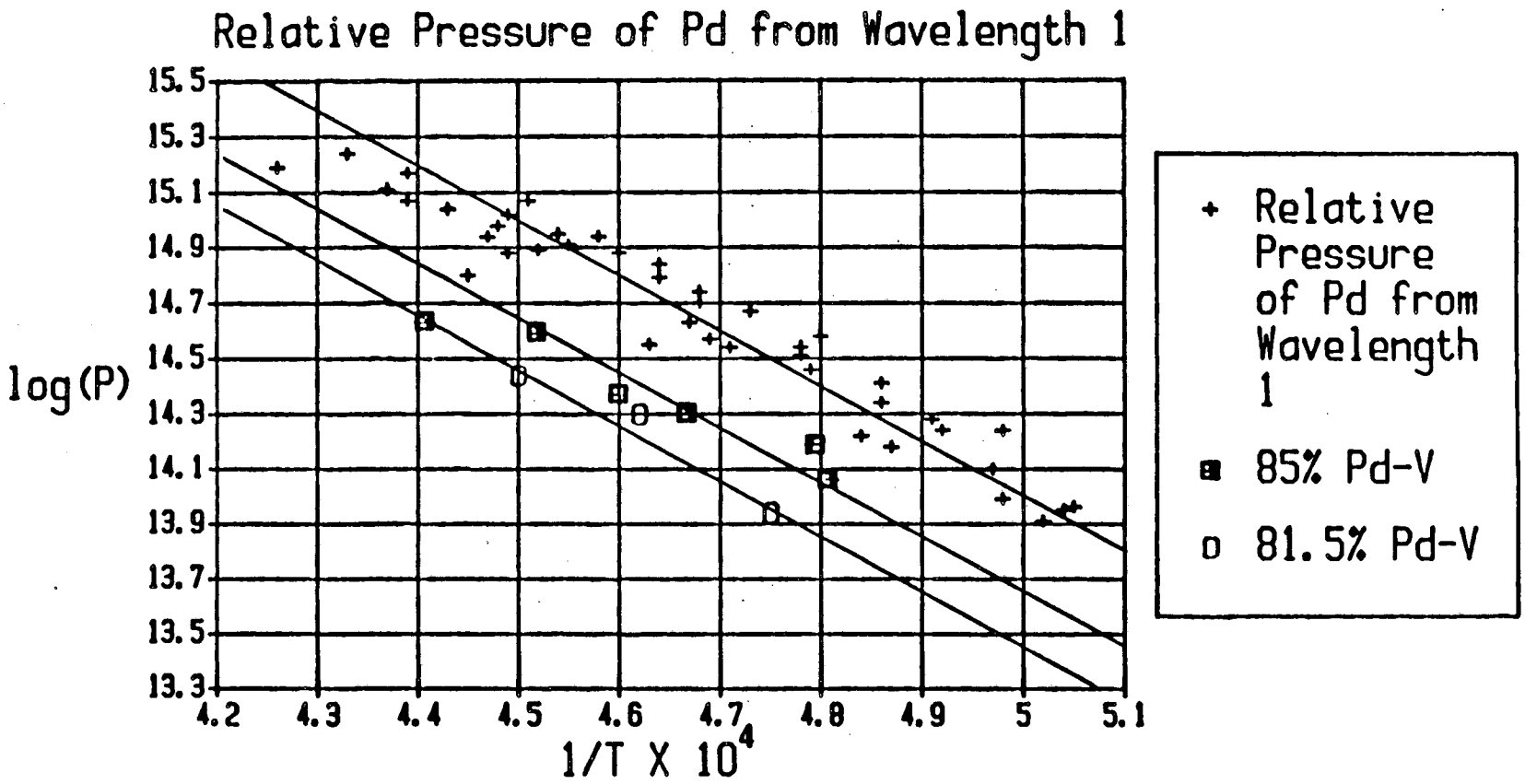

Figure 4-5

The relative vapor pressure of pure Pd is compared to a VPd alloys. The differences in the vapor pressures correspond to activities of 0.39 and 0.32 for the 85% Pd and 81.5% alloys, respectively.

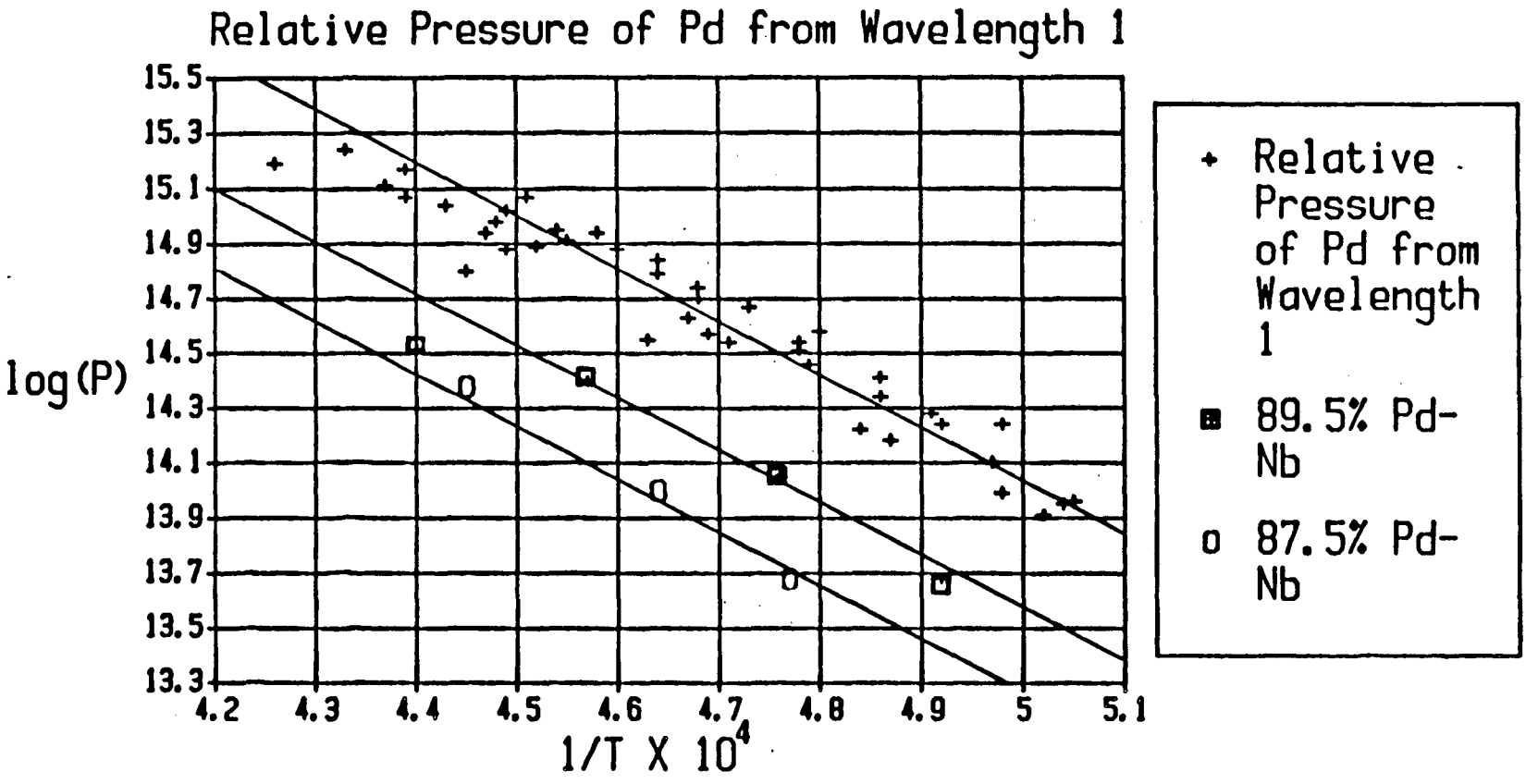

Figure 4-6

The relative vapor pressure of pure Pd is compared to NbPd alloys. The differences in the vapor pressures correspond to an activities of 0.19 and 0.35 for the 87.5% Pd and 89.5% Pd alloys, respectively.

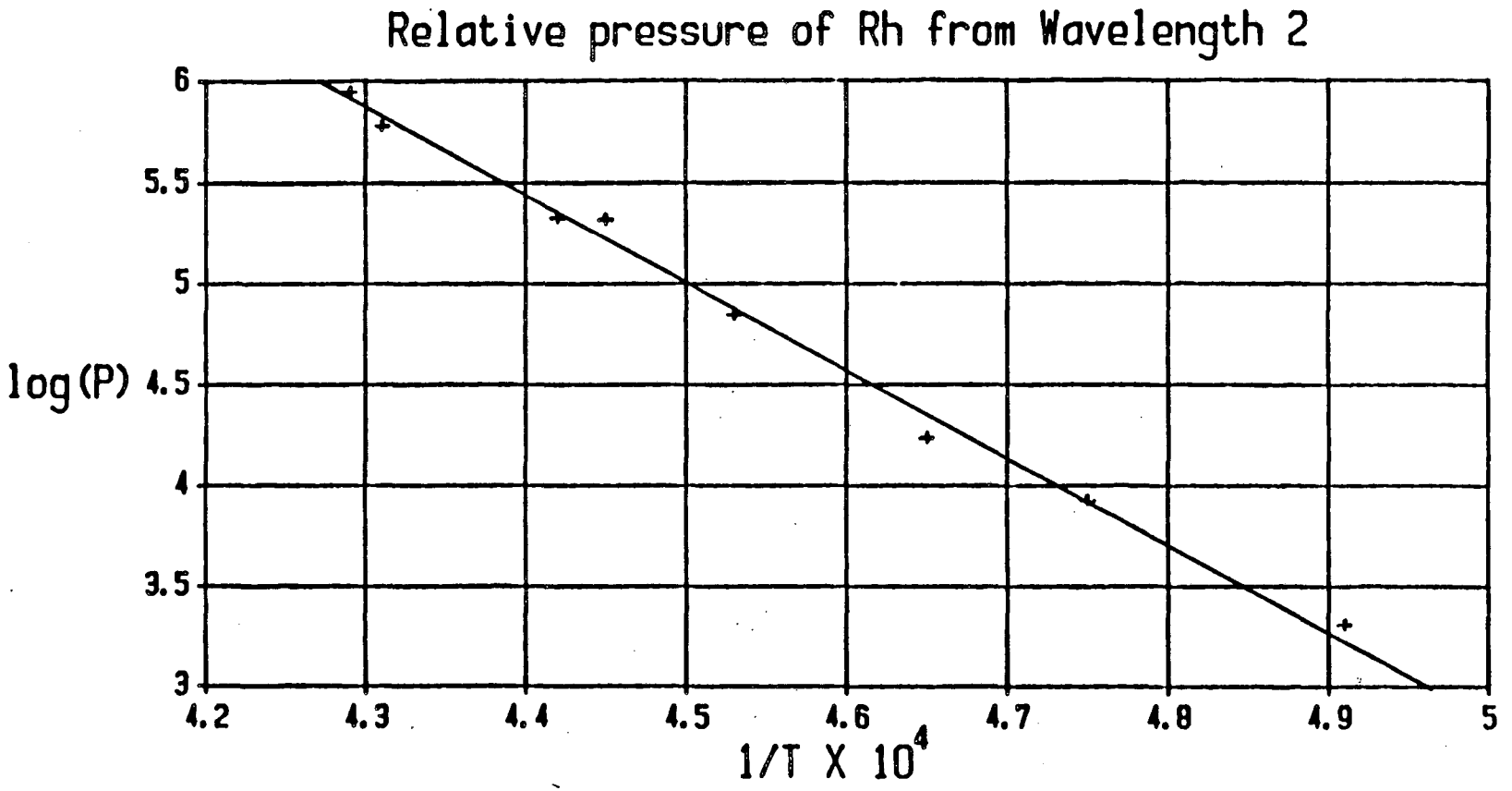

Figure 4-7

The relative pressure of Rh from emission data of wavelength 2, is shown.

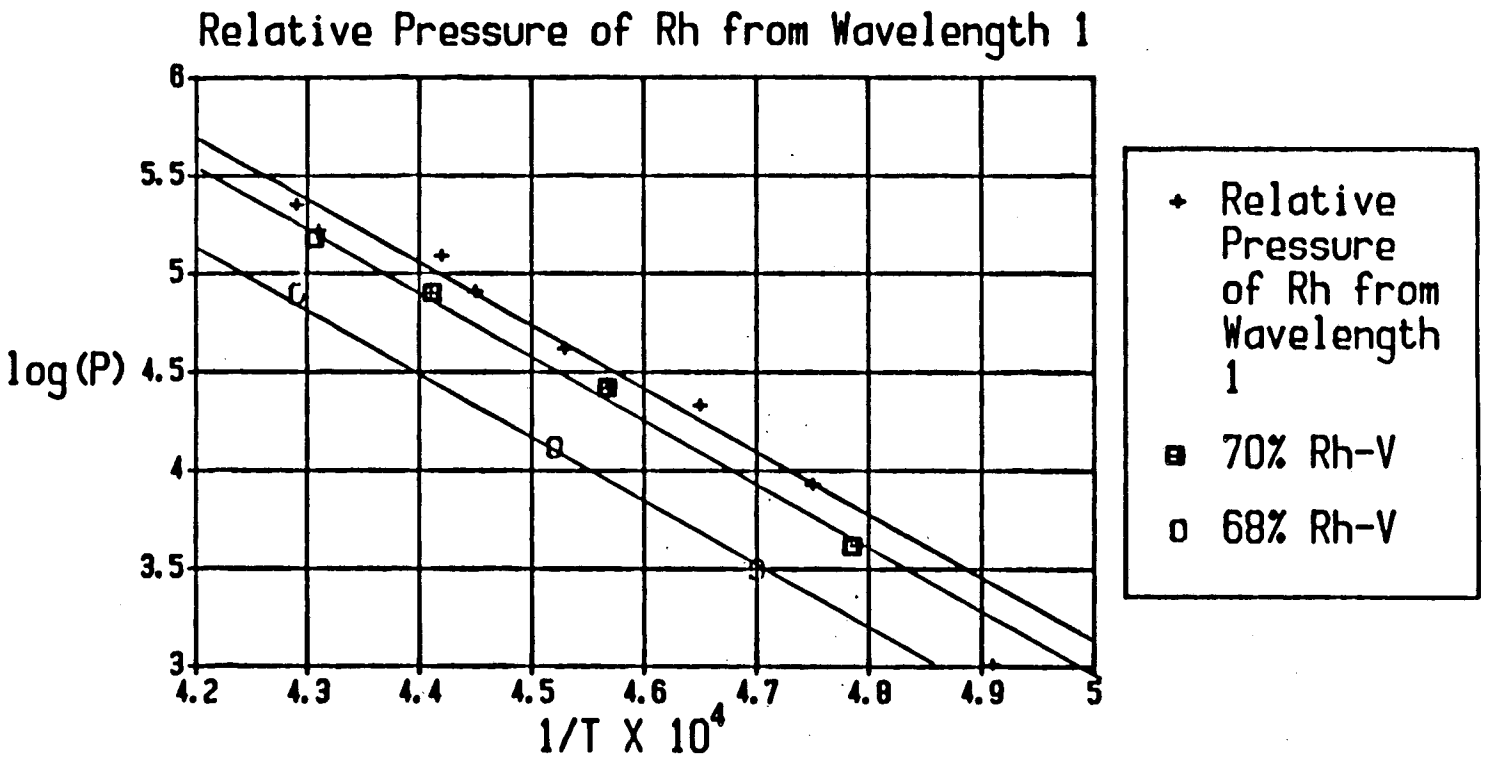

Figure 4-8

The relative vapor pressure of pure Rh is compared to VRh alloys. The difference in the vapor pressures correspond to activities of 0.69 and 0.24 for 70% Rh and 68% Rh (originally the 55% Rh alloy) alloys, respectively.

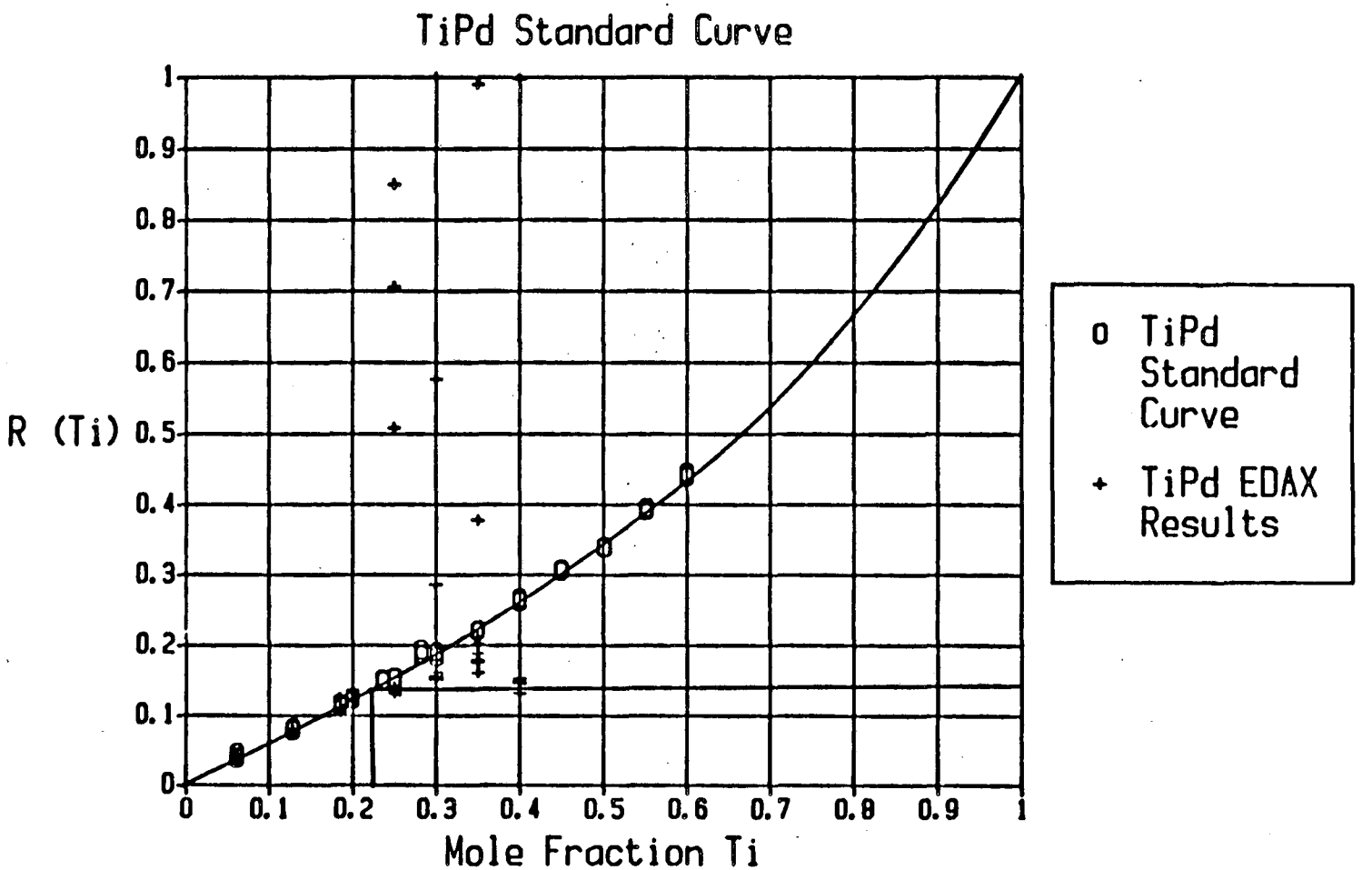

Figure 4-9

The relative X-ray emission intensity of the Ti (Kα) and Pd (Lα) peaks as a function of X_{Ti} in TiPd alloys.

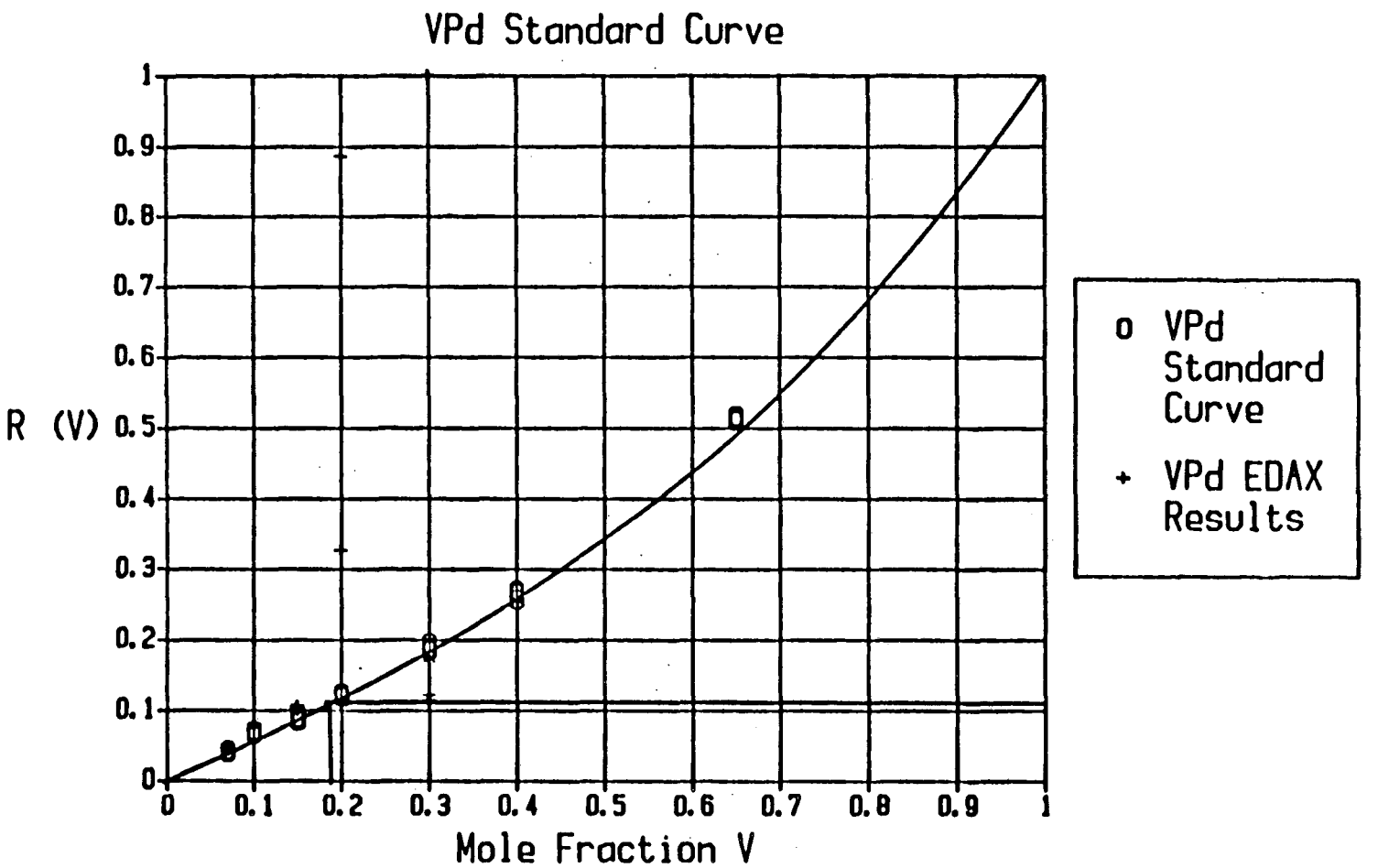

Figure 4-10

The relative X-ray emission intensity of the V (Kα) and Pd (Lα) peaks as a function of X_V in VPd alloys.

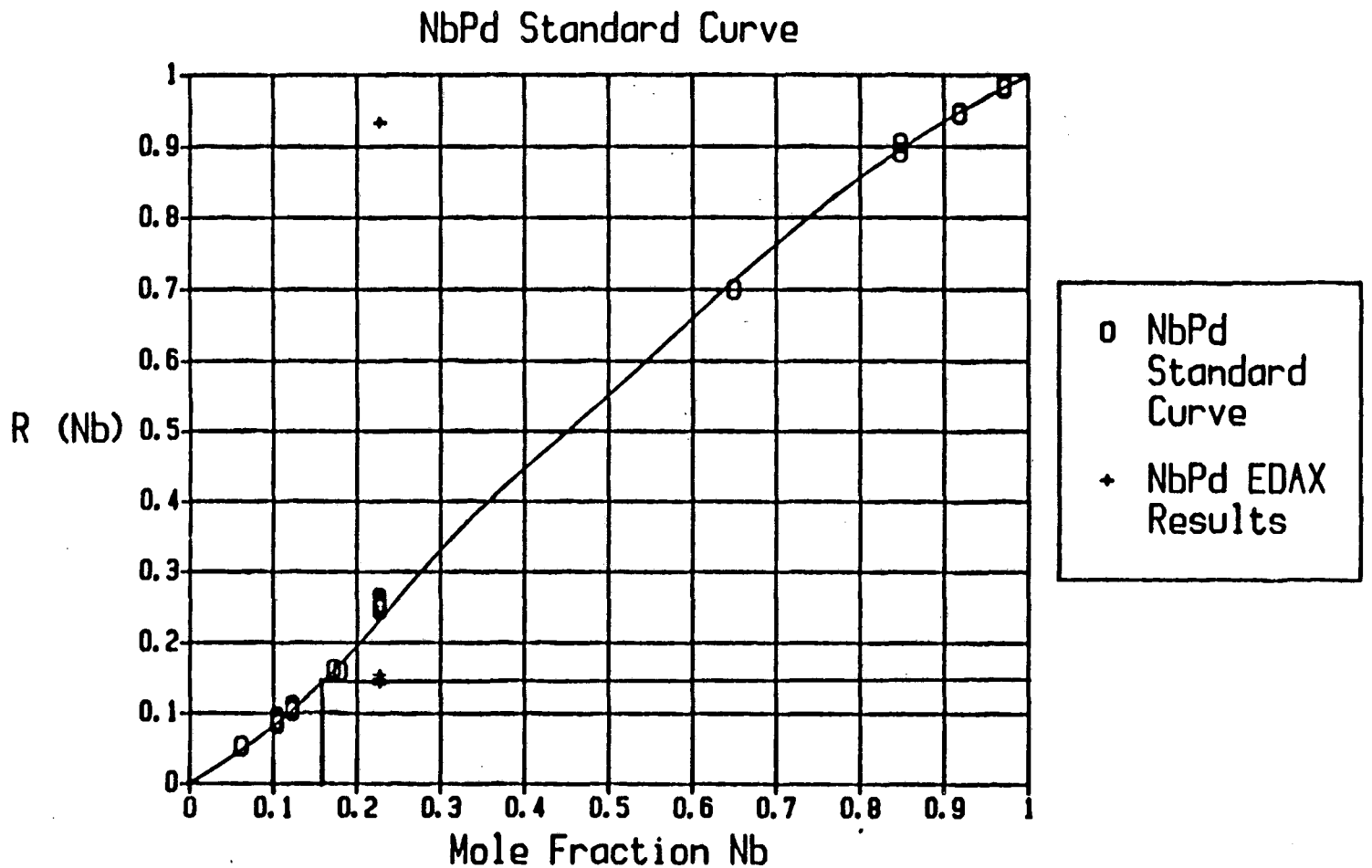

Figure 4-11

The relative X-ray emission intensity of the Nb (Lα) and Pd (Lα) peaks as a function of X_{Nb} in NbPd alloys.

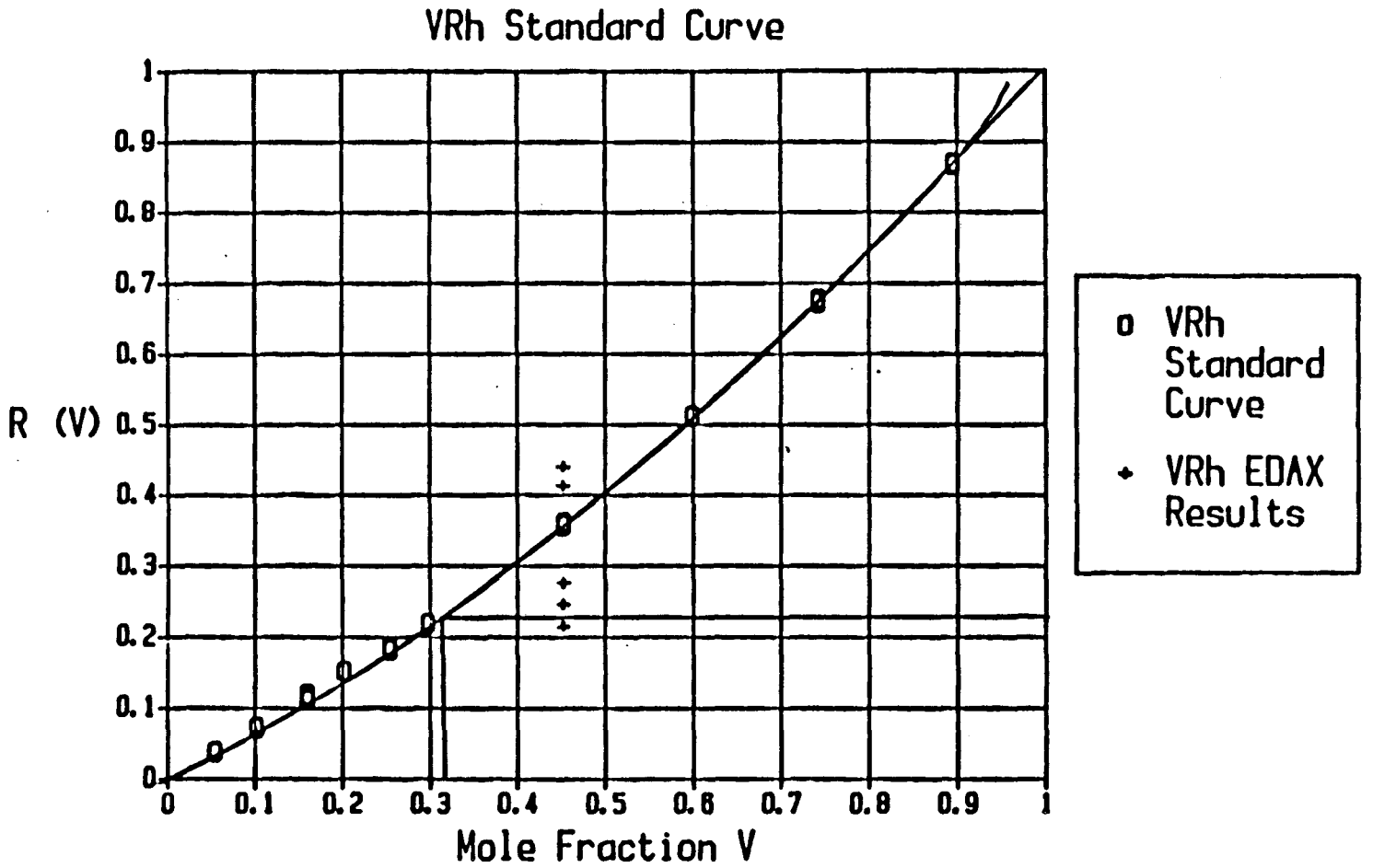

Figure 4-12

The relative X-ray emission intensity of the V (Kα) and Rh (Lα) peaks as a function of X_V in VRh alloys.

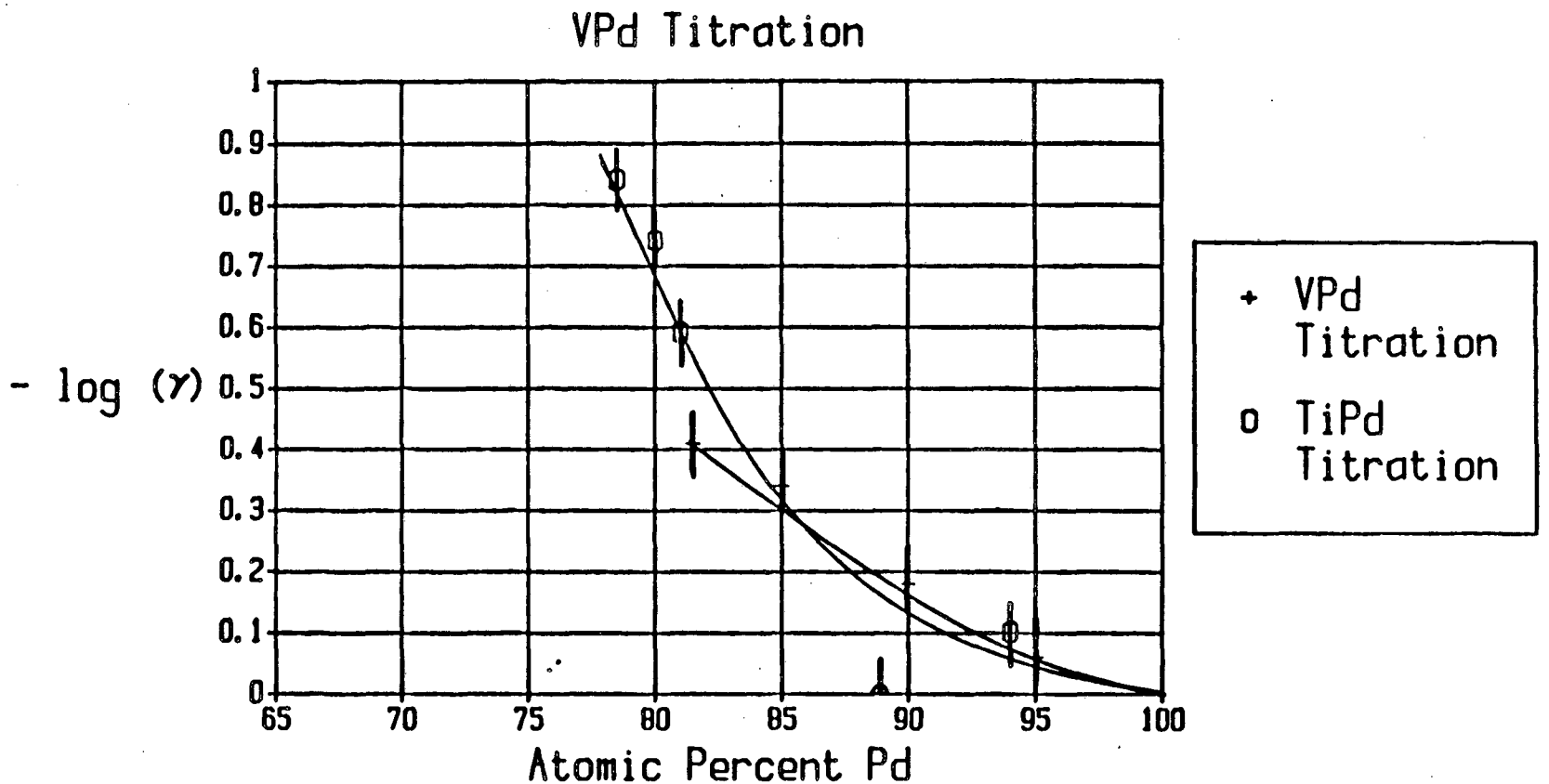

Figure 4-13

The titration curve of TiPd is compared to the titration curve of VPd. Ti is a better acid as the Pd concentration decreases.

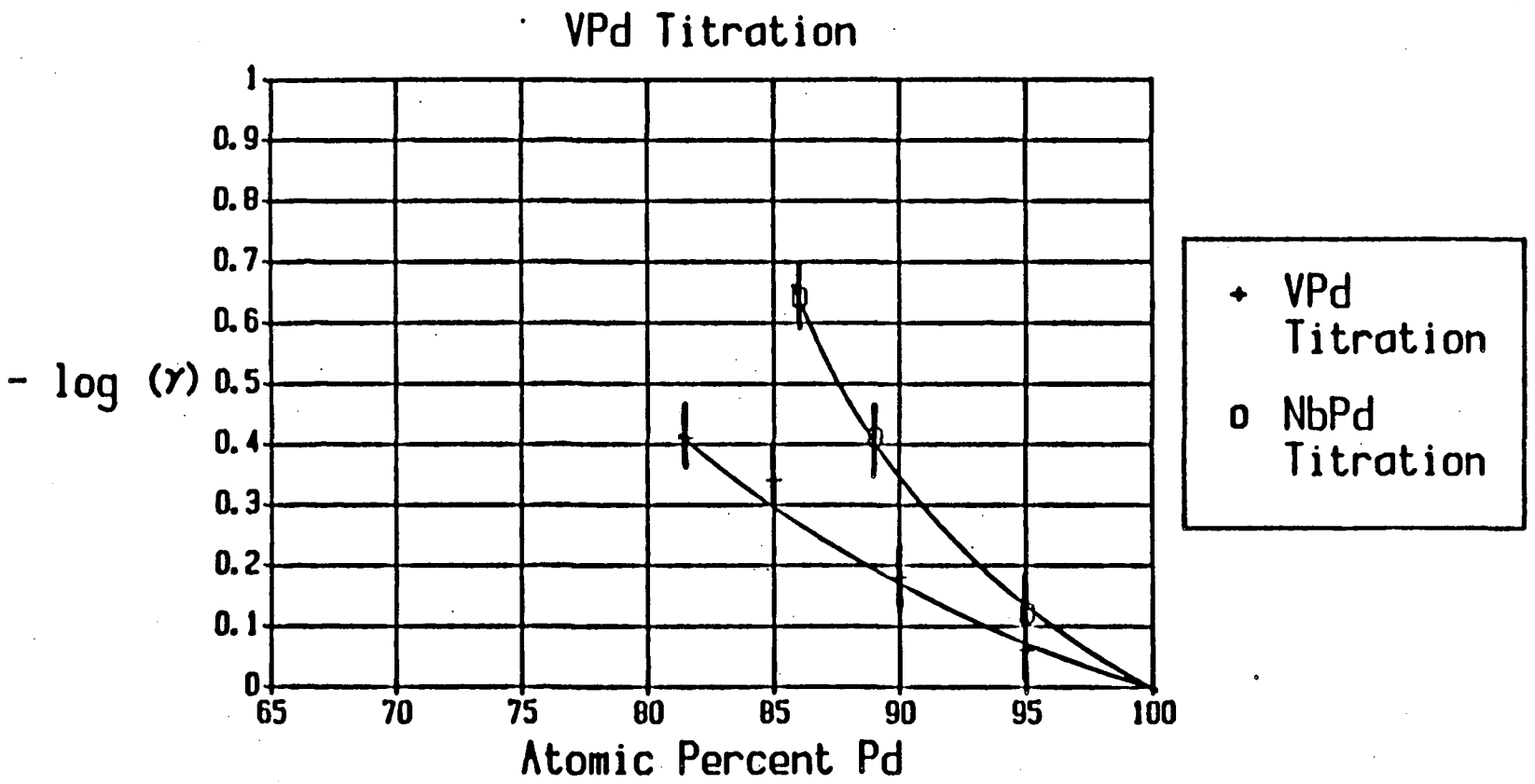

Figure 4-14

The titration curve of NbPd is compared to the titration curve of VPd. Nb is a better acid, demonstrating the increased acid-base effect of the 4d elements over the 3d elements.

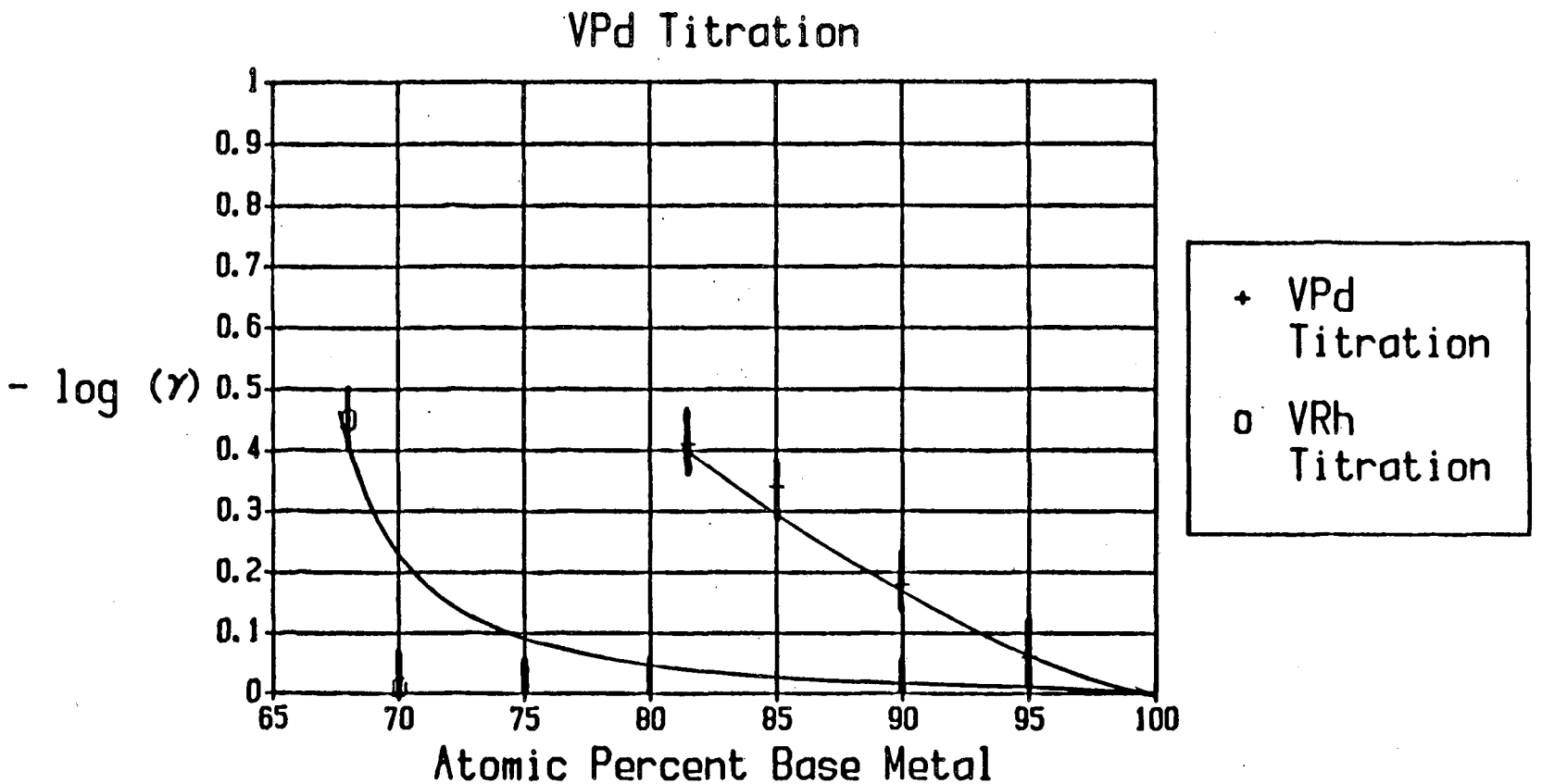

Figure 4-15

The titration curve of VRh is compared to the titration curve of VPd. Pd is a better base at high base metal concentrations. Rh is indicated to be a better base at lower base metal concentrations.

LAWRENCE BERKELEY LABORATORY
TECHNICAL INFORMATION DEPARTMENT
UNIVERSITY OF CALIFORNIA
BERKELEY, CALIFORNIA 94720